Msc Thesis

The study of corrosion on carbon steel and zinc under thin-film electrolyte

06/03/2022
3ME - Materials Science and Engineering
Metal science technology

Manlin Pan
5160227

Abstract

Atmospheric corrosion is one of the most widespread types of metal corrosion in the world. Commonly, atmospheric corrosion is affected by the electrochemical properties of the metal and environmental factors, such as humidity, temperature and the properties of the electrolyte on the metal surface. Currently, there still lack of laboratory studies which investigated the effect of changing electrolyte thickness on corrosion behaviours. In this study, a corrosion cell with adjustable electrolyte thickness was used to simulate the atmospheric corrosion process of carbon steel and zinc under thin-film sodium chloride electrolyte conditions. The effects of electrolyte thickness and chloride ion concentration on the atmospheric corrosion of these two metals were investigated by open circuit potential, polarization and galvanic coupling techniques. To perform the experiments under thin-film conditions a novel electrochemical cell was employed. Experiments confirmed the effect of electrolyte thickness on the corrosion rate of the metals. Particularly, it was established the role of oxygen transport in the kinetics of the process. At large electrolyte thickness (several hundred micrometers), oxygen is limited at the proximities of the metal, leading to corrosion rates comparable to the values under bulk electrolyte conditions. With the reduction of the electrolyte thickness, a higher concentration of oxygen is available, due to the faster oxygen equilibrium between air-electrolyte, leading to a substantial increase in both corrosion rate and the diffusion control limiting current. Corrosion current density under approximately 40μm thin-film electrolytes were two orders of magnitude higher than the currents measured for both carbon steel and zinc metals under immersed conditions (bulk electrolyte). The effect of chloride ion concentration on corrosion rate under thin-film electrolytes was also revealed. The higher solubility of oxygen on low chloride-concentration electrolytes showed also an acceleration of the process. Carbon steel and zinc metals presented the highest corrosion rates under 0.01M NaCl electrolyte with 40μm thickness.

Content

1 Introduction

The “corrosion” of metal materials generally refers to metal forming more chemically stable compounds through chemical or electrochemical reactions in the environment. The quantification of corrosion is usually expressed as a function of mass loss of the metal versus the time. [1] This mass loss on the metal surfaces can be homogenous, such as uniform corrosion, or highly localized crevice corrosion and pitting corrosion. [2] Corrosion generally occurs on the surfaces of metallic materials in contact with the liquid environment. In most cases, the corroded metal is not exposed to large amounts of electrolytes but an atmospheric environment. The degradation process of materials caused by exposure to air and air pollutants was called atmospheric corrosion. [3]

Atmospheric corrosion is the most extensive type of metal corrosion due to the high possibility for metal to be exposed in the atmospheric environment than in another environment. Many metals can be corroded only by exposure to moisture in the air, but this process can be strongly affected by certain substances in the atmosphere. The damages caused by atmospheric corrosion on infrastructure (such as bridges, architecture, and pipelines) , cultural heritage and electronic components are enormous. [4] In the last 100 years, the research on atmospheric corrosion has gradually become systematic and more scientific. Vernon studied the combined effect of relative humidity and sulfur dioxide and discovered the impact of critical relative humidity on atmospheric corrosion. [5] Subsequently, electrochemical techniques were used by scientists to explore the mechanism of atmospheric corrosion. The advanced surface analysis techniques, such as Auger electron spectroscopy, [6] scanning tunnelling microscopy [7] and X-ray photoelectron spectroscopy, [8] carried out a more accurate analysis of chemical composition and surface topography of corrosion products. Advanced characterization techniques allow the quantitative analysis of corrosion products which promotes the study of how different environmental factors influence corrosion. Recent research usually uses wet-dry cycling to change the electrolyte thickness in the experiment to study the effects of electrolyte thickness on the corrosion reaction. However, this method ignores the impact of changes in electrolyte concentration on corrosion during wet-dry cycling. [9] [10] It is necessary to figure out a new experimental approach to accurately control the thickness of the electrolyte without changing the electrolyte concentration during the electrochemical study. This will help to elucidate the effect of the electrolyte thickness on atmospheric corrosion under thin- film conditions.

This study will mainly focus on using novel electrochemical setup called LUNA cell to control the electrolyte thickness and chloride ion concentration during the thin film electrolyte atmospheric corrosion of carbon steel and zinc. The corrosion behaviour of both metals under thin film electrolyte down to 40μm thickness will be studied by potentiodynamic polarization experiments.

In this report, firstly the scientific literature focusing on the effect on the atmospheric corrosion of both environmental factors and metal properties will be reviewed and discussed. The electrochemical techniques which were used during this study will be

also discussed. The experimental setup and the results will be explained to reveal the effect of the electrolyte thickness and chloride ion concentration during thin film atmospheric corrosion. In the end, some feasible experimental improvements and research directions in the future will be mentioned.

2 Literature review

2.1 Environmental factors of atmospheric corrosion

Since this study mainly focuses on the atmospheric corrosion of carbon steel and zinc metal under thin-film electrolytes, understanding the fundaments of atmospheric corrosion is necessary. Atmospheric corrosion is affected by both environmental factors and the properties of the metal which undergoes the corrosion reaction. Main environmental factors include temperature, relative humidity, pollutant concentration, chloride and sulphate ions and hygroscopic salts. [11] [12] These environmental factors are not constant but will change continuously over time during atmospheric corrosion. It is necessary to establish an atmospheric corrosion model which considers the comprehensive effects of a dynamic corrosion environment.

Another thing to note is that each environmental factor does not act on the materials alone but depends on and influences each other. [13] [14] Overall, relative humidity has the most significant influence on corrosion, followed by temperature. Their accelerating corrosion rate is a non-linear effect. [15] [16] Sulfur dioxide and chloride are important environmental factors that will accelerate corrosion also. Both effects from these atmospheric pollutants are nonlinear and follow the power-law dose-response functions. Some major environmental factors will now be discussed.

Humidity

The relative humidity of the ambient environment largely determines atmospheric corrosion. It is generally believed that the corrosion rate positively correlates to the relative humidity. [17] [18] However, many pieces of literature report that under certain specific environmental conditions, carbon steel has almost no atmospheric corrosion when the relative humidity is below 80%-85%. [19] [20] This threshold humidity is usually expressed as critical relative humidity (CRH). Critical relative humidity indicates humidity, while the clean metal surface will not corrode when humidity is lower than this value. When the metal surface is covered with corrosion products, secondary critical humidity is usually found, and the corrosion rate increases significantly. The humidity of the material surface can be more stable when hygroscopic salts are present on the surface, thereby significantly reducing the CRH. [21] Outdoor environments usually have the most complex atmospheric corrosion conditions. In this case, the CRH is affected by various factors such as the material properties, corrosion product composition, atmospheric pollutant concentration, and hygroscopic salt deposition. [22]

Chloride and sulphate ions

The ionic concentration in the electrolyte determines the resistance of the electrolyte and will affect the corrosion rate. The general model of the environment's effect on

metal corrosion consists of three parts: dry deposition of sulfuric dioxide, dry deposition of chloride and the wet deposition of hydrogen ions. The current research has insufficient data on the impact of wet deposition, which explains why the research on atmospheric corrosion mainly focuses on the effects of sulfur dioxide and chloride. [23] Electrolytes with high chloride concentrations mostly appear in marine environments, and sulphate-enhanced corrosion is a typical industrial environment.

Studies have shown that sulfur dioxide can be oxidized in water to sulfate ions and generate hydrogen ions. [24] The acidity of the electrolyte increases with the dissolution of sulfate ions, which increases the corrosion rate and leads to the dissolution of corrosion products. Besides, when studying the accelerating effect of sulfur dioxide on carbon steel corrosion, researchers found that sulfur dioxide also causes a decrease in critical relative humidity. [25] Sulfur dioxide can also act as a catalyst such that one sulphate ion can catalyse the dissolution of more than 100 iron atoms. [26]

The deposition of chloride can significantly accelerate the atmospheric corrosion of both steel and zinc. [27] [28] Allam et al. believe that the chloride ions only considerably affect the atmospheric pollution in the initial stage. As the thickness of the rust layer increases, the supply of further chloride ions will gradually decrease and, therefore, slow down chloride formation. [29] In addition to corrosion rate, previous studies also found that the composition of corrosion products can be affected by chloride ion concentration. In the study of low carbon steel, researchers found that the rust layer's change in morphology and composition occurs when the chloride ion is above the critical concentration. [30] The corrosion rate calculated using polarization resistance together with FTIR analyses, indicating the β-FeOOH formation caused by chloride ions which is conflicts with the result from the classical method. [30]

Other pollutants

Besides the pollutant mentioned above, nitrogen compounds, carbon dioxide, ozone, organic acids, and saline particles can also deposit from the atmosphere in the electrolyte film, leading to the acceleration of the corrosion rate. [12] Carbon dioxide can strongly affect the corrosion process of both steel and zinc. Carbon dioxide gas dissolved in water will decompose to form bicarbonate and carbonate ions. This reaction will cause the pH of the electrolyte to deviate from neutral and aggravate the corrosion. [31]

$$CO_2\,(g) \leftrightarrow CO_2\,(aq) \tag{1}$$

$$CO_2\,(aq) + H_2O \leftrightarrow HCO_3^{2-} + H^+\,(pKa1 = 6.35) \tag{2}$$

$$HCO_3^{2-} \leftrightarrow H^+ + CO_3^{2-}\,(pKa2 = 10.33) \tag{3}$$

By using gases with different SO_2 and NO_2 concentrations, much research has already proved that NO_2 can increase the corrosion rate of many metals. [14] However, the mechanism of how NO_2 affect the corrosion rate is still under investigation in field exposures. This might be due to the complexity of the atmospheric environment in the field study. In the field environment, ozone will also present and act as an oxidant for metals during the photolysis of NO_2. The oxidation effect of ozone on metals might cause the effect of NO_2 cannot be quantified.

Hygroscopic salts can absorb water above the critical relative humidity and form an electrolyte solution at higher relative humidity. When hygroscopic salt is present on the metal surface, moisture will tend to remain on the surface and cause an increase in corrosion rate. [32] Common hygroscopic salts include the chlorides in soil and marine environment, which affect the corrosion of metals were shown in Table 1. [33-35]

Table 1. Deliquescence relative and crystallization relative humidities for different salts.[33-35]

Salt	*Deliquescence relative humidity (DRH) %*	*Crystallization relative humidity (CRH) %*
NaCl	75.28[a]	47[a]
Na_2SO_4	84.2[a]	57–59
$NaHSO_4$	52.0[a]	<5[a]
NH_4Cl	77.1[a]	47[a]
$(NH_4)_2SO_4$	79,97[a]	37–40
$NaNO_3$	74.5[a]	<5–30[a]
NH_4NO_3	61.83[a]	25–32[a]
$MgCl_2$	33[b], 15.2[c]	5.5[c]
$ZnCl_2$	<1	

Temperature

The influence of temperature on atmospheric corrosion can be shown in two aspects: directly affecting the corrosion reaction rate and affecting the formation of electrolyte film. Thermodynamically speaking, the reaction rate of most corrosion will increase with the increasing temperature. [16] [27] [36] On the other hand, higher temperatures will tend to dry the electrolyte layer on the metal surface quickly thereby reducing the time of wetting. [37] Atmospheric corrosion is considered as complicated wet-dry cycles during in-situ outdoor exposure. [13] The corrosion reaction only occurs when there is a layer of moisture covered on the metal surface. Therefore, the decrease of time of wetness(TOW) will result in the suspension of corrosion reaction. [32] Beside the drying of electrolyte, the obstruction of corrosion reaction from the temperature increases also include the reduce the solubility of various gases such as oxygen and sulfur dioxide.

Although temperature can affect the rate of corrosion in both positive and negative ways, it is generally believed that the corrosion rate is independent of ambient temperature from 10° to 25°C. Other studies also stated that the effect of temperature on atmospheric corrosion in the outdoor environment is minor and is only effective under continuous high humidity. The importance of temperature will be affected by other

environmental factors. Some experiments have proved that the corrosion rate of zinc and steel does not show a dependence on temperature with the presence of CO_2. [38]

2.2 Corrosion behaviours of steel and zinc alloys

2.2.1 Steels

2.2.1.1 Influence of steel composition

In addition to environmental factors, the chemical composition [39] [40] [41] and the microstructure [41] of the metals also has a great impact on corrosion. Different materials show different atmospheric corrosion behaviours and resistance. The most commonly used metal in nowadays world: steel, also has a large group of types including carbon steel, low-alloy steel and stainless steel. In a specific condition, the composition of the steel will largely affect its corrosion behaviour under atmospheric corrosion. The content of minor metal elements becomes the major effect of the difference in corrosion behaviour.

Carbon steel

Carbon steel is a type of steel which have carbon content higher than 0.05% and lower than 2% with very few other elements added. Carbon steel is widely used in automobiles, architecture, pipelines, and other urban and industrial environments because of its superior mechanical properties and weldability. In the polluted atmosphere, chloride and SO_2 are the most common pollutants that affect the corrosion of carbon steel. Besides these, it has been confirmed by research that both time of wetting (TOW), temperature and rainfall will all affect the corrosion of carbon steel. The chemical composition, structure, and joint design of the carbon steel itself are also considered important factors affecting atmospheric corrosion. Research on the corrosion of long-term outdoor espouses carbon steel found that, in all types of atmospheres, the corrosion rate decreased with the exposure time and will be stabilized after the first 4-6 years. [42]

Low-alloy steel

Low-alloy steel usually contains Cu, Cr, Ni, P, Si and Mn as alloying elements with less than 0.2 wt.% of carbon. Kamimura et al. compared the difference between the composition of corrosion products from carbon steel and low-alloy steel. XRD reveals that the amorphous substance in the rust layer for the carbon steel contains both maghemite (γ-Fe_2O_3) and goethite (α-FeOOH). However, only α-FeOOH was found for the low-alloy steel. The difference in the composition of corrosion products is

caused by minor elements in low alloy steel. [43] Although minor alloying elements affect corrosion products' composition, the effect on corrosion rate is considered to exist only under specific circumstances. Field studies show that the corrosion resistance effects of alloying elements in low-alloy steel seem to be limited to samples that experienced repeatedly wet-dry cycles. The corrosion sensitivity of low-alloy steels highly depends on the rate and morphology of the gradually formed rust layer. These rust layers, which are usually porous and crystalline, can hardly prevent the diffusion of electrolytes and therefore will not protect the metal surface efficiently. [44]

Weathering steel is a family of low alloy steel with an addition of the above-mentioned alloying elements in an amount between 1.0 wt.% and 5.0 wt.%, which have higher corrosion resistance and better strength and is often used in bridges, load-bearing structures and other buildings. [45] Unlike the corrosion of low-alloy steel, the corrosion of weathering steel will produce a more stable layer of rust, also called patina, that adheres to the metal substrate. This growing layer of rust is less porous and thus can form a protective barrier against the further entry of oxygen, moisture and other contaminants. The presence of this patina results in much lower corrosion rates compared to different types of steel.

Stainless steel

Compared to low-alloy steel, stainless steel has a chromium-rich passivation film which will significantly inhibit atmospheric corrosion. The corrosion on stainless steel generally exists as pitting corrosion to form crevices located around the inclusions on the passive layer. Therefore, the crevices and defect density on the passivation layer will affect the subsequent corrosion behaviour. The composition of the electrolyte solution, the quality of the passivation layer and the environmental factor will affect the atmospheric corrosion rate of stainless steel. The dissolution and re-passivation reaction will occur at the same time. The difference in the rate of these two reactions will determine whether the metal will be corroded. Boulton et al. reported the corrosion behaviours of stainless steel 304 welded plates, which have been placed in severe marine, urban-marine and geothermal atmospheric environments for three years. [46] The corrosion behaviours of stainless steel in each environment can be discussed from the study by Syed et al. [3]

2.2.1.2 Corrosion product under aqueous and chloride-containing environments

Oxides and Hydroxides

The development of corrosion layers on steel without atmospheric pollutants can be divided into three stages. The first step is forming an oxide/hydroxide film with a thickness of about 1-4 nanometers in a few seconds. This oxide/hydroxide layer is stable and passivate when there is no water present in the atmosphere. With the presence of H_2O_2, the passivation performance of this oxide/hydroxide layer will be enhanced.

After several hours of exposure in near-neutral aqueous environments, the oxide/hydroxide layer will transfer into $Fe^{2+}{}_2Fe^{3+}O_x(OH)_y$ and $Fe^{2+}Fe^{3+}O_x(OH)_y$. These intermediate products will then be transformed into the final oxide and hydroxide layer. The corrosion product γ-FeOOH, which indicates the beginning of the third stage, can be observed after two weeks or less. The composition of corrosion products will reach stability in a short time.

The study by Fuente et al. [11] also confirmed that the time factor under long-term exposure (more than years) can only change the ratio of each corrosion product or determine the presence and disappearance of some intermediate compounds, but not determine the final corrosion product. Several corrosion products are possibly formed during steel corrosion due to the presence and competition between Fe^{2+} and Fe^{3+} ions. During the three-stage transformation, iron is initially oxidized to Fe^{2+}. The intermediate corrosion products include both Fe^{2+} and Fe^{3+}, and the final corrosion products contain only Fe^{3+}. [11]

Fuente et al. studied the corrosion product in all four atmosphere environments. Lepidocrocite (γ-FeOOH) and goethite (α-FeOOH) are the two phases that are always present. In the marine atmosphere, magnetite (Fe_3O_4) and maghemite (γ-Fe_2O_3), which share similar crystal structures, are generally present in the corrosion product. Magnetite is usually found deep inside the corrosion layer, which is close to the metal substrate, where the lower oxygen concentration facilitates magnetite production. In the industrial atmosphere, hematite (α-Fe2O3) and ferrihydrite ($Fe_5HO_8{\cdot}4H_2O$) were also found [42]. Experiments showed that the corrosion products formed on the steel surface have a double-layer structure composed of an adhesive inner layer and a non-adhesive outer layer. As a result of ion migration, soluble salts (chlorides and sulfates) are usually concentrated in the adherent layer of the corrosion product.

Table 2. Potential iron/steel corrosion product according to Cornell's and Schwertmann's research. [47]

Type	Name	Formula
Oxides	Magnetite	Fe_3O_4
	Maghemite	γ-Fe_2O_3
	Hematite	α-Fe2O_3
Hydroxides	-	$Fe(OH)_2$
	Bernalite	$Fe(OH)_3$
	Green rusts	$Fe_x^{III}\,Fe_y^{II}\,(OH)_{3x+2y-z}\,(A-)_z$ where $A^- = Cl^-$; $½SO_4^{2-}$
	Ferrydrite	$Fe_5O_8H{\cdot}H_2O$
Oxyhydroxides	Goethite	α-FeOOH
	Lepidocrocite	γ-FeOOH
	Akaganeite	β-FeOOH
	Feroxyhite	δ-FeOOH
	Schwertmannite	$Fe_{16}O_{16}(OH)_y(SO_4)_z{\cdot}nH_2O$

Chlorides

The corrosion product is also affected by the type of pollutant ions in the solution. A relatively stable iron hydroxide layer will be formed in the absence of anions (such as Cl- or SO42-). However, these iron hydroxide layers will be more soluble and provide less protection in the presence of Cl^- or $SO4^{2-}$. The acceleration effect of chloride ions on the corrosion rate of steel has been proven in many studies in the marine atmosphere. [47] The research from Nishikata et al. has used AC impedance to measure the corrosion rate of steels covered with NaCl solution layer under wet-dry cycles. An acceleration of the corrosion rate from one cycle to another is observed, attributed to the increase in the concentration of chloride ions and the formation of electroactive material (i.e., FeOOH) during the drying process. These electroactive materials will act as oxidants during the wet phase. [48]

In chlorine-containing solutions such as marine environments, the presence of akageneite (β-FeOOH) is typically found in the corrosion product during atmospheric corrosion. The formation of akageneite is usually through the hydrolysis of $FeCl_3$ or oxidation of $FeCl_2$ during the early stage of corrosion. The researcher believes indetectable soluble compounds such as $FeCl_3$ and $FeSO_4$ exist in corrosion products. This might be due to the low concentration of soluble compounds below the instrument's detection limit or due to the complex structure of the double-layer corrosion products after prolonged exposure. As mentioned before, the soluble salt generally migrates on the adherent inner layer, making it more difficult to detect.

Table 3. Potential iron/steel corrosion product under Cl^- presented environment. [47]

Name	Formula
Ferrous chloride (lawrencite)	$FeCl_2$
Ferric chloride (molysite)	$FeCl_3$
Ferric oxychloride	FeOCl
Ferrous hydroxychloride	β-$Fe_2(OH)_3Cl$
Green rusts	GR1 (GR Cl)
β-oxihydroxide (akaganeite)	β-FeOOH

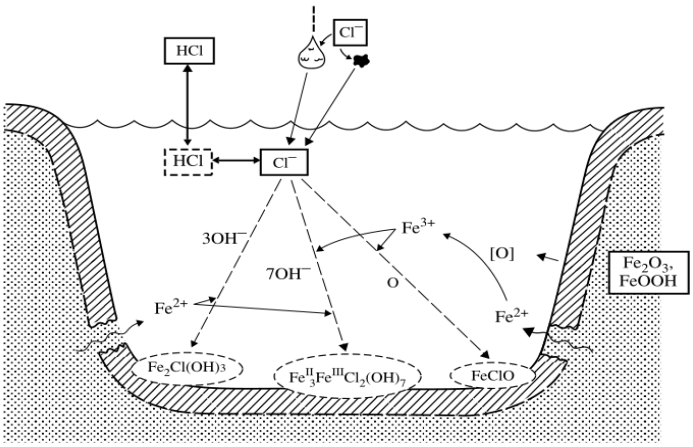

Figure 1. A schematic representation of the processes involved in forming chlorine-containing components during the atmospheric corrosion of iron and steels. The atmosphere is at the top of this diagram, a surface water layer is in the centre, and the corroding metal is at the bottom. [11]

2.2.2 Zinc

2.2.2.1 Corrosion product under chloride environment

Time of wetness, and the presence of carbon dioxide, sulfur, oxygen, and Cl^- ion in the atmosphere are the main factors that affect the atmospheric corrosion of zinc. Moisture has a significant influence on the corrosion of zinc in the atmosphere. The relative humidity and temperature mainly determine the amount of moisture adsorbed on the zinc surface. When the moisture layer evaporates, a thin film of zinc hydroxide will precipitate on the surface for hours or days, giving zinc a better corrosion resistance than most steel. This zinc hydroxide film will transform into various other atmospheric corrosion products during in-situ outdoor exposure. Possible corrosion products include ZnO, $ZnCO_3$(smithsonite), Zinc hydroxycarbonate, $Zn_4SO_4(OH)_6{\cdot}H_2O$ (zinc hydroxy sulphate), $Zn_5(OH)_8Cl_2{\cdot}H_2O$ (simonkolleite) and $NaZn_4Cl\ (OH)_6SO4{\cdot}6H_2O$ (sodium zinc chlorohydroxysulphate). The compounds of final corrosion products depend on the different respective characteristic anions in environments.

Researchers have conducted field studies on the oxides corrosion products on the exposed zinc surface under different typic environments and discovered the multi-layer structure of corrosion products. [49] [50] Subsequently, Thomas et al. used FIB-SEM and TEM to study the corrosion of pure zinc under low volume saline drop in the laboratory. Under this short time corrosion experiment, researchers also observed a multi-layer corrosion product structure and refined the understanding of layered structure. From an electrochemical study on the corrosion behaviour of zinc substrates in sodium chloride solution, Prestat et al. [51] observed a three-layer compact layer

structure (Figure 2.) which is similar to that under saline drop conditions. The upper layer of the corrosion product is a network of simonkolleite flakes, the middle layer is composed of porous ZnO, and the structure closest to the zinc substrate is the "interface layer" of a zinc-rich layer with oxygen. Electrochemical studies suggest that the sum of these layered structures is protective, which is consistent with the findings of Thomas et al. from the EIS study. [52]

The corrosion behaviour of zinc under the chloride environment is affected by other atmospheric pollutants, including Nitrogen dioxide, sulfur dioxide and carbon dioxide. [53] The presence of zinc hydroxycarbonate as the corrosion product under various atmospheric conditions proves that carbon dioxide plays an essential role in the atmospheric corrosion of zinc. Falk et al. observed the relation between CO_2 concentration and the composition of atmospheric corrosion products in laboratory studies. Besides, the experiment also shows that the corrosion rate of zinc is positively correlated with CO_2 concentration in the pure humid air. The enhanced effect of CO_2 on corrosion rate is due to the acidification of the surface electrolyte, which leads to an increase in surface conductivity and surface film solubility. [54] In their further study, Falk et al. found how CO_2 affects zinc corrosion under a sodium chloride environment. The presence of carbon dioxide reduces the degree of pitting corrosion caused by sodium chloride solution.

In the absence of CO_2, the corrosion product is a mixture of ZnO and simonkolleite. After four weeks, most of the added chloride is still in an insoluble form. However, the corrosion product will be a mixture of simonkolleite and zinc hydroxycarbonate for samples exposed to a CO_2 environment. [38] The absence of soluble chloride residues proves that CO_2 promotes the conversion of soluble chloride (NaCl) into simonkolleite during the neutralization of the surface electrolyte, as in Eq. (4). This insoluble $Zn_5(OH)_8Cl_2{\cdot}H2O$ protective layer explained the corrosion rate reduction with the presence of CO_2 in Figure 3.

$$5ZnO(s) + 2Cl^- + 6H_2O \leftrightarrow Zn_5(OH)_8Cl_2 \cdot H_2O + 2OH^- \quad (4)$$

[54]

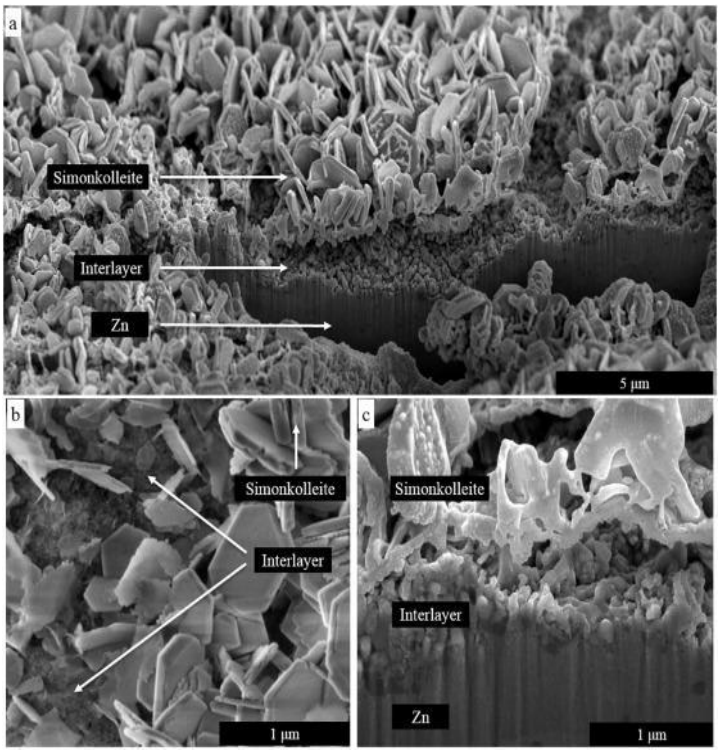

Figure 2. FIB-SEM analysis of the corrosion product of zinc under thin film sodium chloride electrolyte from Prestat's study. (a) Low-magnification tilted-view micrograph of the area around the FIB trench; (b) Top-view micrograph; (c) Zoom-in tilted-view micrograph at the trench edge. [51]

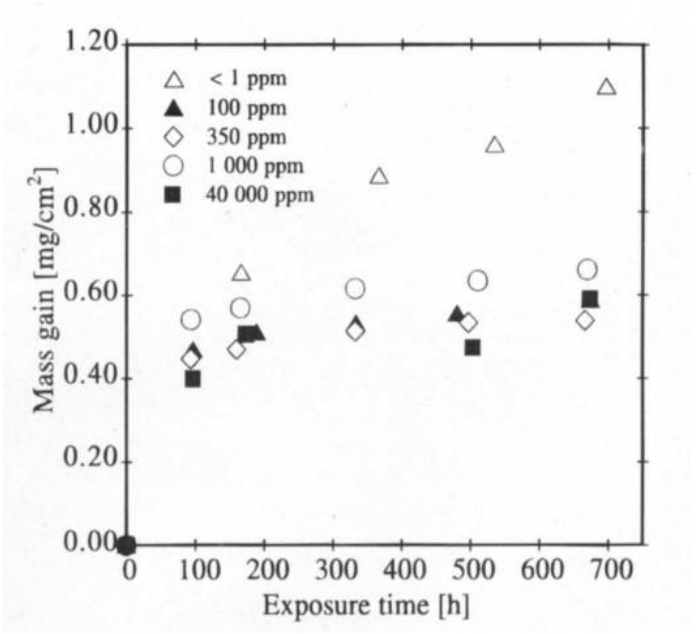

Figure 3. Mass gain vs. time for zinc samples exposed to different concentrations of CO_2. Prior to exposure, 70 µg/cm² NaCl was added to the samples. The scatter in mass gain is estimated to be ± 30 µg/cm². [55]

2.2.2.2 Corrosion of Zinc alloy

Zinc is usually alloyed with Al and Mg to modify its corrosion and mechanical properties; the most common method has covered the zinc with a magnesium-aluminium coating. A complex microstructure of the final coating will be formed by adding 0.2%-11% magnesium and 0.1%-3% aluminium to zinc. The final zinc magnesium-aluminium coating includes primary zinc, $MgZn_2$, binary eutectic $MgZn_2$-Zn, binary eutectic Zn-Al, and ternary eutectic. The effect of magnesium and aluminium can be explained by the following mechanisms: (1) To prevent the formation of ZnO as a corrosion product. Mg/Al and Zn/Al layered double hydroxide will form to inhibit oxygen reduction. [56] (2) Magnesium hydroxide will convert to soluble hydroxy carbonate and dissolved Mg, which can buffer the pH at cathodic sites. This reaction thermodynamically allows the precipitation of insoluble simonkolleite on the metal surface and delays the overall corrosion reaction rate. [57]

The researcher believes the exact mechanism and their combination effect largely depend on the exposure conditions. Recent experimental research shows the enhancement of corrosion properties of zinc magnesium aluminium coating in a chloride environment. The presence of Mg_2Zn_{11} and $MgZn_2$ as corrosion product film hinders the efficiency of oxygen reduction and limited the anodic reaction rate. [58] However, the poor protection effect of magnesium aluminium coating under carbon dioxide free environments and sulfur dioxide environments has also been mentioned in some research. This may be due to the extremely alkaline environment (carbon dioxide-free) or extremely acidic environment (sulfur dioxide presence) which will increase the dissolution of the zinc and aluminium rich phases. After field exposure, the corrosion of the zinc magnesium-aluminium coated material will be highly localized, and the binary or ternary eutectic will be most likely to be attacked. [17] [59]

2.2.2.3 The protective ability of zinc corrosion product

The stability of the corrosion product layer largely depends on environmental factors. Stable corrosion product films are favoured in neutral or near-neutral environments, while acidic or alkaline environments tend to dissolve these films and lead to further corrosion. The first formed zinc oxide and zinc hydroxide corrosion product layer can provide limited protection. [60] However, the transformation of the initially formed zinc hydroxide into the basic zinc carbonate begins as soon as the initial corrosion product forms. The low corrosion rate of zinc in a pure humid atmosphere is mainly due to this thin and dense basic zinc carbonate film. The solubility of basic zinc carbonate film in water is very low together with its dense structure can prevent the permeation and retention of oxygen and water.

Field research has confirmed that corrosion attacks on pure zinc in practical environments are not uniform but quite uneven and sometimes localized. [61] Pitting corrosion can be founded in both rural and urban environments after long-term exposure. In environments with high chloride concentration and low SO_x levels, such as marine environments, pitting corrosion is even more serious. The surface of zinc in the marine environment shows two clearly different subzones: a cracked inner sublayer

and an outer sublayer, accompanied by numerous microcracks and fine microscopic channels. These high defect density structures will cause further corrosion to penetrate deeper into the metal.

The protective ability of the corrosion product layer exposed to carbon dioxide and sulfur dioxide environment has also been studied. Falk et al. found that the zinc hydroxycarbonate layer formed on the surface of zinc has a slightly protective effect in pure air but plays no protective role in the humid SO_2 polluted air due to its instability in SO_2-contained air. [54] In a sulfur dioxide environment, alkaline zinc sulfate and zinc hydroxysulfate layers with corrosion-inhibiting effects will be formed. [53] However, since the moisture condensed in this type of atmosphere is acidic, the corrosion products will be dissolved into the moisture and been washed away rapidly. At long-term exposure to zinc, the protective effect of corrosion product layers is also considered ineffective. S. D. Cramer et al. studied the long-term corrosion of zinc on outdoor exposure and confirmed the corrosion rate is still at a level or rising even though the thickness of the corrosion layer continually increases. [62] In general, dense corrosion product layers have better corrosion inhibition effects. Those corrosion layers which are thick, bulky and with porous structures often have almost no inhibiting effect or even will enhance the corrosion reaction.

2.3 Effect of thin film electrolyte on atmospheric corrosion

In atmospheric corrosion, in addition to environmental factors and the property of the metal, the thickness of the solution film is also an important factor to determine the corrosion behaviours of the metal. In 1990, Stratmann proposed to use the Kelvin probe as a reference electrode to measure electrode potential. This method can simultaneously measure the electrode potential and corrosion rate, which allows researchers to derive the relationship between current density and electric potential. This relationship proves the correlation between electrode kinetic and electrolyte thickness. The researchers subsequently used Kelvin probes to measure the corrosion of pure iron and iron-copper alloys. Without touching the surface under investigation, the corrosion potential and corrosion rate of each metal were measured during several wet/dry transitions cycles. By changing the thickness of electrolyte layers, Stratmann's experiment proves that the change of the kinetics of the anodic and cathodic electrode reactions is determined by the thickness of the electrolyte layer, not by the time when the surface is kept visibly wet. [63] [64]

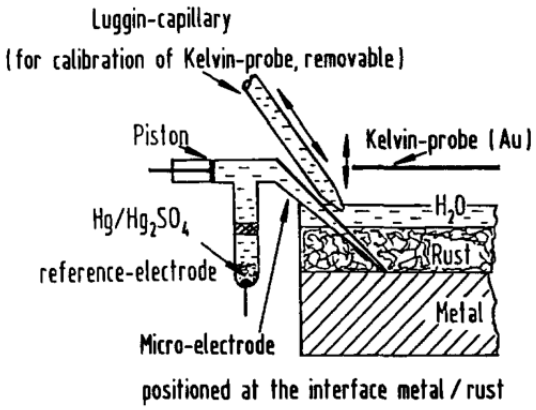

Figure 4. The configuration of the different electrodes used in Stratmann's study. [63]

To quantify the effect of electrolyte thickness on corrosion rates, the laboratory study and in-field study are both required. The salt spray test is generally used to simulate atmospheric corrosion under thin electrolyte film in the industrial study. Two methods are generally used to control electrolyte thickness in the laboratory. The micro-syringe method allows a predetermined amount of electrolyte to drop onto the metal surface to simulate different thicknesses without the change of concentration in the electrolyte. The other is a drying method that controls the thickness of the water layer with the change of concentration in the electrolyte. [65] Both methods have certain disadvantages in simulating the thin-film electrolyte condition. When the electrolyte is directly loaded on the surface of the metal using the microsyringe method, it is unable to guarantee the formation of an electrolyte film with uniform thickness. In the case of a thin electrolyte, the influence of electrolyte geometry on atmospheric corrosion will be even more significant. [66] The corrosion reaction will be highly affected by the geometry if the electrolyte forms droplets rather than thin films on the metal surface. [67] The corrosion will exhibit very non-uniform reaction rates at the different metal-droplet contact positions. The drying method requires precise control of the drying conditions to achieve the default electrolyte thickness which is also hard to accomplish in the laboratory.

The LUNA atmospheric test cell is an improvement on the traditional microsyringe method. A highly porous hydrophilic membrane is placed over the electrolyte to facilitate the formation of a homogeneous thin-film electrolyte on the metal surface. This may be an effective method to study the corrosion behaviour of metal under thin-film electrolytes. The structure and principle of the LUNA corrosion cell will be explained later.

Researchers from previous studies found that the thickness of the electrolyte can affect corrosion in three aspects: transportation of oxygen, accumulation of corrosion products, and the hydration of dissolved metal ions.

Firstly, the thickness of the electrolyte can determine the transport speed of oxygen. The corrosion rate of metal covered with thin-film electrolyte with a thickness equal to hundreds to dozens of microns is controlled by the oxygen reduction reaction on the

cathode. In the case of thin-film electrolytes, oxygen in the atmosphere can diffuse between the air-electrolyte interface and the electrolyte-metal interface, which is a concise path. Previous studies indicated that the thickness of the oxygen diffusion layer in pure water is about 300μm. When the thickness of the electrolyte is less than that of the oxygen diffusion layer, oxygen in the environment can enter the electrolyte and pass through the electrolyte to reach the metal surface and participate in the cathode reaction. Besides, since the oxygen reduction is diffusion-controlled, the reduction reaction is accelerated as the electrolyte layer gets thinner during the drying process. This explains why the corrosion rate increased rapidly during the drying process of the electrolytes film.

With the further decrease of the electrolyte thickness, the corrosion rate might decrease due to the accumulation of corrosion products. Stratmann et al. studied the corrosion behaviour of pure iron during wet-dry cycles. They observed the increase of corrosion potential and the decline of the anode reaction rate as the thickness of the electrolyte layer is further reduced. This is mainly due to two reasons: Firstly, the thin electrolyte layer generally has high alkalinity, which makes the iron surface easy to passivate; Secondly, when the solubility of iron in the electrolyte reaches the limit, iron ions immediately precipitated at the metal/electrolyte interface. The formation of these depositions blocked the metal surface and delayed the further dissolution of anode metal. [63]

The thickness of electrolytes can also affect the hydration of dissolved metal ions. When the thickness of the electrolyte layer has already been reduced below the critical thickness, further reduction in thickness continuously causes a decrease in the corrosion rate. Under ultra-thin electrolyte, the corrosion is controlled by the anode reaction and will be inhibited by reducing the thickness of the water layer. This leads to the passivation and the lack of water required for the hydration of to hydrate the dissolved metal ions. [48]

Besides these significant aspects, the solubility of atmospheric pollutants is also affected by the thickness of electrolytes. Compared with atmospheric corrosion in the case of bulk electrolytes, the concentration of atmospheric pollutants in the thin electrolyte film can also reach a higher value under thin-film electrolyte conditions. The concentration of dissolved salt determines the conductivity of the electrolyte, which affects the corrosion rate. Experiments have proved that the critical electrolyte thickness of the maximum corrosion rate changes with the increase of pollutant concentration, which indicates that the concentration of atmospheric pollutants is an essential determinant of the critical thickness. This enhancement effect especially happens in the case of alternating wet-dry cycles.

3 Experimental details and methods

3.1 Sample preparation

Carbon steel and pure zinc metal plates were used to study the corrosion behaviour under different electrolyte concentrations and electrolyte thicknesses. The metal plates were first been cut into pieces of 2.54 x 2.54 cm^2 with a thickness of 2 mm. A grinding machine processed the top surface of the metal plates to remove all scratches. 320-, 400-, 600-, 800- and 1200-grit SiC papers were used sequentially. The samples were not required to be polished to a mirror surface as the preparation process before the characterization experiments. These grinding processes were only to ensure the sample surface is without any scratches that might affect the uniform corrosion reaction. When scratches and cracks were present on the surface of the sample, a relatively severe corrosion reaction may occur at these crevice locations due to low oxygen and acidic conditions. The metal surface with more and deeper scratches generally has a larger surface area than a polished surface. The prepared samples were then rinsed sequentially with deionized water and ethanol to remove any abrasive particles detached from the samples and sandpapers. The residual liquid on the sample was dried with compressed air to avoid any corrosion reaction before the experiments. A piece of copper tape with an appropriate length was pasted on the back of each metal plate for further connection with the working electrode alligator clip of the potentiostat.

3.2 Bulk electrolyte

The bottom screw mount corrosion cell was used for carbon steel and zinc metal corrosion experiments under bulk NaCl electrolyte. The bottom mount corrosion cell is a stationary solution corrosion cell for conventional electrochemical measurements on thin metal plate specimens. In this study, the exposure area of the working electrode in each experiment was set to 3.14cm^2. This study used the Ag/AgCl, KCl(sat) reference electrode and platinum mesh counter electrode. During the bulk electrolyte corrosion experiments, it should be ensured that the tip of the reference electrode is close to the bottom of the glass chamber, where the working electrode is exposed to the electrolyte. Before each bulk electrolyte corrosion experiment, ensure that the inner of the corrosion cell is thoroughly cleaned and dry before pouring in 80mL sodium chloride electrolytes with different concentrations. The electrodes were then connected to the alligator clip to perform various electrochemical tests.

One of the advantages of the bottom mount corrosion cell is that it has low requirements on the dimension of the metal sample. The exposed area of the metal can be changed by changing the O-ring on the bottom casing to fit the experimental requirements and the sample dimension. The disadvantage of the base mount corrosion cell is that

although the electrolyte volume in the glass chamber is adjustable, the electrolyte thickness is still too thick for thin-film electrolyte experiments. In this study, the bottom mount corrosion cell was only used to measure the corrosion rate of metals under bulk electrolytes. When studying the effect of electrolyte thickness under thin-film electrolyte atmospheric corrosion (microns level), an experimental set-up called LUNA cell was used to reach the electrolyte thickness condition.

3.3 Thin-film electrolyte experiments: LUNA cell set-up

In recent years, an atmospheric test cell called LUNA Cell was proposed as a way to perform corrosion under thin-film electrolyte conditions. Due to the presence of atmospheric oxygen, the oxygen that can reach the metal surface under the thin-film electrolyte condition would be significantly higher than that in the experiments under the bulk electrolyte condition. The difference in oxygen supplement would lead to substantially higher corrosion rates under thin-film electrolyte conditions than under thick-film or bulk electrolyte conditions. Creating a uniform electrolyte layer with a specific thickness is the most critical step in quantifying the effect of electrolyte thickness on atmospheric corrosion. LUNA cell used in this study improves the microsyringe method, a traditional method used in the laboratory, to simulate the corrosion under thin-film electrolyte better. In the previous electrochemical studies that the microsyringe method was used; due to the existence of surface tension, it is difficult to form a thin film electrolyte with uniform thickness when the electrolyte is directly loaded on the working electrode surface. In the LUNA cell, however, the surface tension of the electrolyte droplet was disrupted by the highly porous hydrophilic membrane covered on the working electrode surface. By loading the electrolyte on the hydrophilic membrane, the thickness of the electrolyte was controlled by changing the thickness of the membrane and the loaded electrolyte volume. A uniform thin film electrolyte could be distributed on the surface of the working electrode to study electrolyte thickness effect on atmospheric corrosion.

The structure of the LUNA corrosion cell was very different from the bottom screw mount corrosion cell used in the bulk electrolyte corrosion study. A multi-layer stacking corrosion cell was built up by sequentially assembling electrode plates and the functional components on a stage consisting of four threaded rods and a square metal substrate. PTFE and silicone sheets were cut into different shapes and used as gaskets to separate and fix other assembly lines. The metal samples used in thin-film electrolyte experiments are the same as the working electrode used in corrosion experiments under bulk electrolyte. The upper surface of the working electrode needs to be completely parallel to the ground to prevent the uneven distribution of the electrolyte. The tilting and sag on the upper surface of the metal may lead to localized accumulation of the electrolyte. This inaccuracy of electrolyte thickness might affect the rate of corrosion reaction.

The thickness of the thin-film electrolyte is determined by the hydrophilic membrane covered on the working electrode and the loaded volume of the electrolyte. The atmospheric electrolyte membrane used in this LUNA cell is based on a highly porous woven glass fibre fabric. Because the hydrophilic membrane would break the surface tension of the aqueous electrolyte, the electrolyte could be evenly distributed on the surface to form a thin film with a thickness above 30μm. The thin-film electrolyte with a specific thickness could be created by controlling both the dimensions and thickness of the membranes. One typical setting for an atmospheric corrosion experiment was to use an 80μm membrane loaded with a 4μL/cm^2 aqueous solution. The volume of the loading solution in this setup approximately corresponds to a 40μm thick electrolyte membrane. The electrolyte should thoroughly and evenly wet the entire membrane also the area over the tape-masked off portions of the working electrode. A thicker electrolyte film could reach up to 320μm thickness by stacking the hydrophilic membrane and increasing the electrolyte volume.

Woven carbon fiber cloth with a Nafion post coating was used as the counter electrode material. This thin-film carbon cloth could establish high-density contact points with the electrolyte membrane and promote cathodic and anodic reactions. Using carbon cloth as the counter electrode includes good air permeability, conductivity, and inexpensiveness. Considering both electrolyte chemical properties and the size of the LUNA cell, a small Re-S1 Ag/AgCl reference electrode (52 mm in length and 4.5 mm outside diameter) was used in thin-film electrolyte experiments at room temperature (25 °C). A bridge tube with a 9.0mm outer diameter connected the reference electrode and the membrane loaded with electrolytes. The bridge tube was filled with the aqueous solution with the same composition and concentration as the membrane electrolyte to ensure it was isotonic with the membrane.

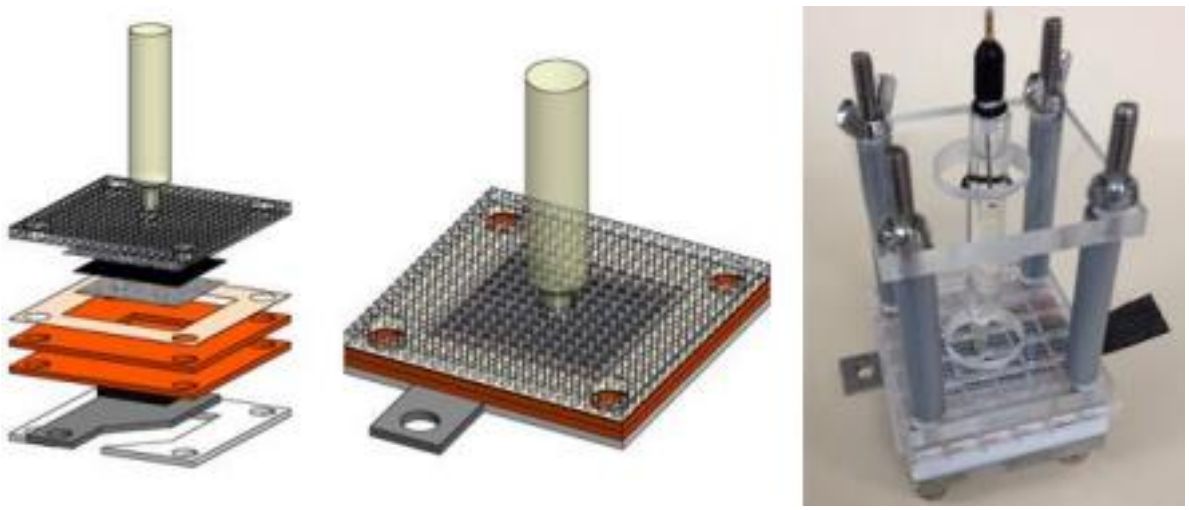

Figure 5. The multi-layer structure and the image of the fully assembled the LUNA cell.

For the galvanic coupling experiments, the carbon counter electrode in the electrochemical corrosion was exchanged for the metal in the couple with more positive open-circuit potential, the carbon steel. This affected the configuration of the LUNA

cell. The carbon steel sand zinc specimens with the same exposed area were placed abreast. The insulating property of the PTFE gasket itself was used to separate the two specimens with a one-millimeter gap. The current collector and counter electrode assembly were no longer necessary in these experiments. More detailed explanation of the LUNA Cell structure and the functions of each layer component are included in Annex.1.

3.4 Electrochemical experimental settings

A potentiostat from BioLogic instruments was used to process the electrochemical experiments in this study. Three electrochemical techniques were mainly used to study the corrosion behaviour of carbon steel and zinc under thin-film electrolyte: open circuit potential, polarization and galvanic current measurements.

Open circuit potential (OCP)

In this study, OCP measurements for 5 minutes were performed before each experiment.

Potentiotiodynamic Polarization experiments

The polarization measurements consisted of changing the applied potential on the working electrode and measuring the current as the response of the system.
During the measurement of the external circuit current, the potential-time history of the working electrode can be controlled by continuously or stepwise resetting the setpoint potential (the starting setpoint potential is generally set to corrosion potential E_{corr}). The anodic and cathodic polarization curves can be respectively generated with the continuously increasing (above E_{corr}) / decreasing (below E_{corr}) of setpoint potential. The cathodic potentiodynamic polarization was done right after OCP, the potential range of it was set from 0.015V to -0.800V vs. E_{OCP}. After the cathodic polarization, another 5 minutes of OCP was done as a resting. The anodic potentiodynamic polarization with the potential range set from -0.015V vs. E_{OCP} to 0.800V vs. E_{OCP} was done at the end. For each specimen, the scan rate was set to 2.0 mV/s.

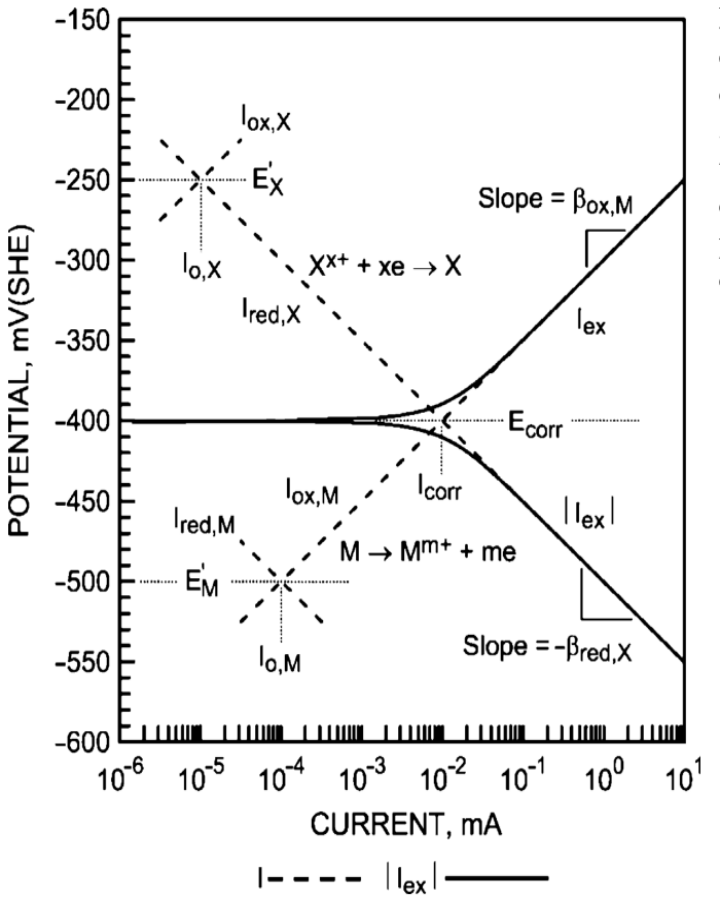

Figure 6. A schematic experimental polarization curves (solid curves) assuming Tafel behaviour for the individual oxidation, and cathodic-reactant reduction polarization curves (dashed curves). [68]

From the Tafel extrapolation (Figure 6), the corrosion current density, anodic beta coefficient and cathodic beta coefficient and the limiting current densities were obtained. The Tafel analysis was performed by extrapolating the linear segment of the logarithmic current/potential plot back to their intersection. For accurate extrapolation, a potential scan of at least 600 mV (300 mV, in the anodic direction and 300 mV, in the cathodic one) is required to obtain the linear segments with at least one decade of current change. The potential at the intersection is the corrosion potential, E_{corr}, and the value of the anodic current or cathodic current is the corrosion current density, I_{corr}. A higher corrosion current indicates a higher corrosion rate.

Galvanic current measurements

The zero-resistance ammeter (ZRA) method, a non-destructive corrosion technique, is normally used to measure the electrochemical noise in order to monitor the corrosion of galvanic couples. ZRA simulates the contact of two metals by applying zero volts between the working electrode and the counter electrode.

A small Re-S1 Ag/AgCl reference electrode with the bridge tube was placed on the top of the membrane and connected to the potentiostat. OCP was monitored for five

minutes before measuring the electrochemical signal. Zero volts were applied between the working electrode and the counter electrode for 5 minutes. The limiting current (IM) was set to 10,000 mA. The experiment will be stopped immediately if the corrosion current becomes higher than IM.

The test was performed within 0.5 seconds (tb=0.5s) after the start of the ZRA module to avoid current perturbations that may occur when zero volts were established. Both galvanic potential and current changes were recorded every 0.01 seconds. The potential range was set from -2.500V to 2.500V.

The current and potential (Ewe, Ece) versus the reference electrode were measured to examine the effects of coupling dissimilar metals (steel and zinc). The current sign determines which metal is more active and the magnitude of the current determines the activity of the galvanic couple. The currents involved in the ZRA measurement are generally down to microampere magnitude. The corrosion cells should be placed in a faraday cage to improve measurement quality by eliminating the environmental noise and other electrodynamic perturbations.

4 Results

4.1 Carbon steel

4.1.1 Bulk electrolyte experiments

The carbon steel samples were fully immersed in NaCl solutions with different concentrations: 1.0M, 0.1M and 0.01M. By comparing the change of corrosion current density and corrosion potential, the effect of chloride-ion concentration on bulk electrolyte corrosion is studied.

Figure 7 and Table 4 shows the corrosion of carbon steel under bulk electrolyte with different chloride ions concentration. The highest corrosion current density (9.3 uA/cm^2) was found at 1.0M NaCl bulk electrolyte. The decrease in current density can be observed by reducing chloride ion concentrations.

The diffusion limiting current density of carbon steel under bulk NaCl electrolyte was also measured at all three chloride ion concentrations. The curves in Figure 7 show how the corrosion current density changes with the changes in polarization potential. As the polarization potential decrease to a more negative region, the corrosion reaction should change from activation control to diffusion control. This change should appear on the curve as a segment perpendicular to the x-axis. The corrosion current density will no longer change with the decrease of polarization potential during the diffusion control region. According to the cathodic branch of the polarization curve shown in Figure 7c, the diffusion limiting current of carbon steel under 0.01M NaCl bulk electrolyte can be calculated. The cathodic branch curves in Figure 7 also revealed no complete diffusion control region for the corrosion process of carbon steel under 1.0M and 0.1M NaCl in the bulk electrolyte.

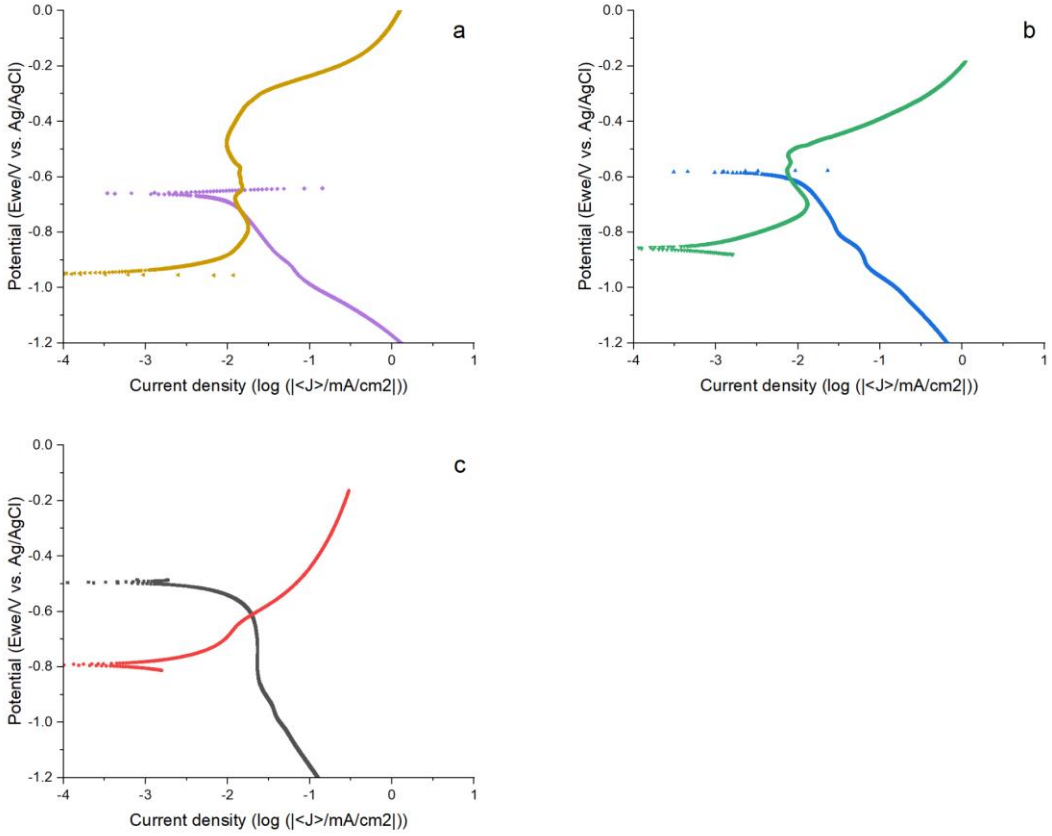

Figure 7. The polarization curves of carbon steel in (a) 1.0M, (b) 0.1M and (c) 0.01M NaCl when the electrolyte is a bulk solution. The anodic and cathodic branches were obtained separatel

Table 4. The potential and current density of carbon steel bulk electrolyte with different NaCl concentrations

	β_a (mV)	**β_c (mV)**	**Potential (mV)**	**Current density ($\mu A/cm^2$)**	**Limiting current density ($\mu A/cm^2$)**
1.0 M	/	115±6	-937±17	9.3±0.7	NaN
0.1 M	/	141±7	-889±20	6.7±2.5	NaN
0.01 M	221±26	193±19	-798±15	2.9±0	16.7±3.7

4.1.2 Thin-film electrolyte experiments

320 µm-thickness electrolyte

Figure 8 and Table 5 shows the corrosion of carbon steel in 320µm NaCl electrolyte with different chloride ions concentration. The corrosion current density of carbon steel under 0.01M NaCl electrolyte increased from 2.9 to 12.5 µA/cm^2 by changing electrolyte thickness from bulk to 320µm.

The change from activation control to diffusion control was observed at all three chloride ion concentrations, indicating the presence of a diffusion limiting current. At 320µm electrolyte thickness, the difference in corrosion behaviour between electrolytes with different chloride ion concentrations is relatively small. The corrosion rate and the diffusion limiting corrosion rate showed only minor differences.

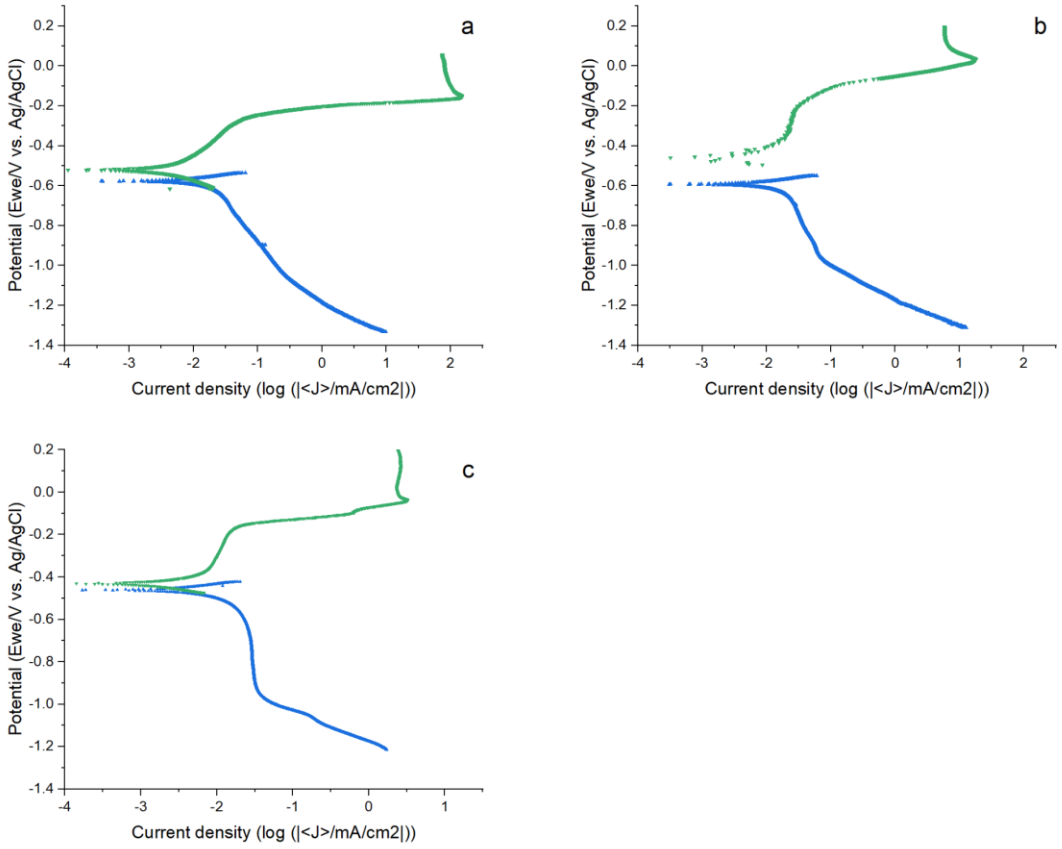

Figure 8. The anodic and cathodic polarization curves of carbon steel in (a) 1.0M, (b) 0.1M and (c) 0.01M NaCl when the electrolyte thickness is 320µm. The anodic and cathodic branches are polarized separately, except for experiments under 0.01M NaCl.

Table 5. The potential and current density of carbon steel exposed to 320μm-thickness electrolyte with different NaCl concentration

	β_a (mV)	**β_c (mV)**	**Potential (mV)**	**Current density ($\mu A/cm^2$)**	**Limiting current density ($\mu A/cm^2$)**
1.0 M	/	392±22	-465±27	7.4±1.8	30.2±3.2
0.1 M	/	/	-328±59	8.9±0.3	32.6±4.9
0.01 M	/	/	-289±68	12.5±3	31.9±5.2

160 μm-thickness electrolyte

Figure 9 and Table 6 shows the corrosion of carbon steel in 160μm NaCl electrolyte with different chloride ions concentration. A significant increase in corrosion rate and diffusion limiting current density was observed with a further reduction in electrolyte thickness under all three chloride ion concentrations. At 160μm thick electrolyte, the corrosion rate was observed to be inversely proportional to the chloride ions concentration with the highest corrosion rate observed in 0.01M NaCl electrolyte.

A change from activation-controlled to diffusion-controlled was observed at all three chloride ion concentrations, suggesting the existence of a diffusion-limited current. The highest diffusion limiting current density was observed in carbon steel under 0.01M NaCl electrolyte due to more vacancies available for oxygen transport in the electrolyte at low concentrations.

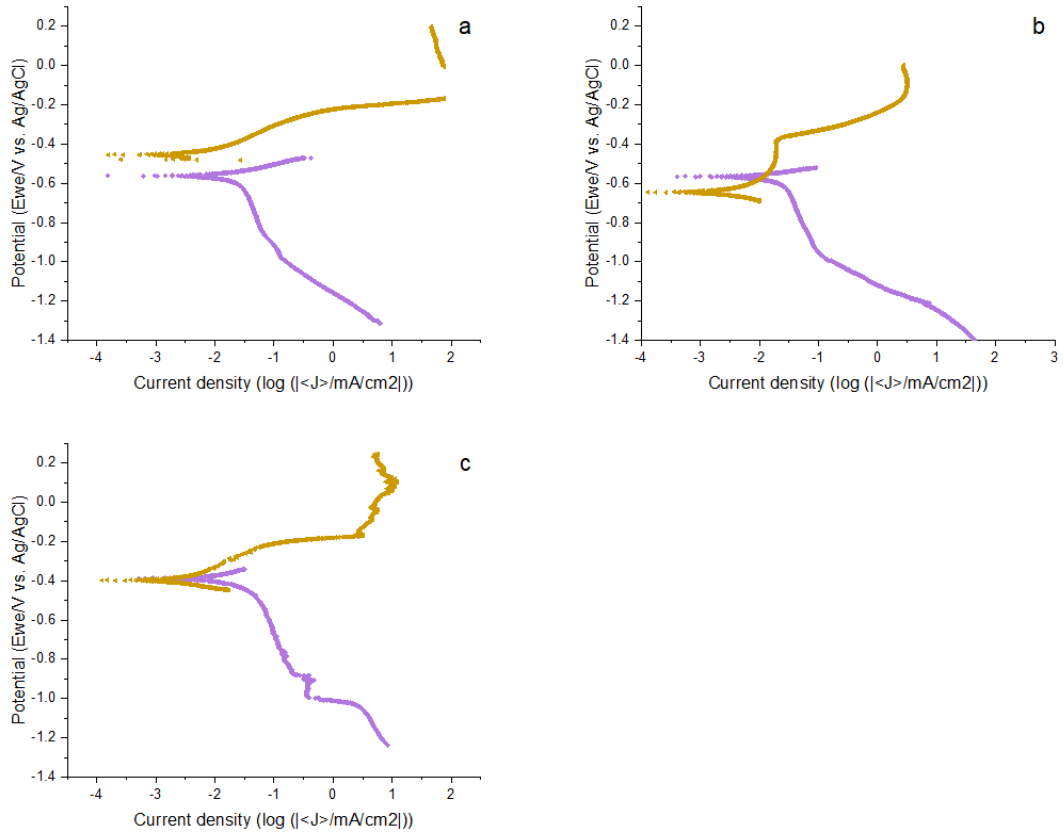

Figure 9. The anodic and cathodic polarization curves of carbon steel in (a) 1.0M, (b) 0.1M and (c) 0.01M NaCl when the electrolyte thickness is 160 μm. The anodic and cathodic branches are polarized separately.

Table 6. The potential and current density of carbon steel exposed to 160μm-thickness electrolyte with with different NaCl concentration

	β_a (mV)	**β_c (mV)**	**Potential (mV)**	**Current density (μA/cm^2)**	**Limiting current density (μA/cm^2)**
1.0 M	121±15	/	-407±19	12.6±2.1	46.3±5.7
0.1 M	274±81	472±150	-555±18	18.5±2.1	61.9±8.7
0.01 M	133±31	/	-267±43	25.7±2.8	96.1±24.1

40μm-thickness electrolyte

Figure 10 and Table 7 show the corrosion rate in 40μm thin-film electrolyte experiments. Since the thickness of the electrolyte is significantly lower than the thickness of the oxygen dissolving layer, oxygen in the air can easily pass through the electrolyte to reach the surface of the metal and participate in the cathode reaction. Significantly accelerated corrosion rates were observed at all three chloride ion concentrations compared to other electrolyte thickness conditions. The corrosion rate in 40μm 1.0M NaCl electrolyte increased by 385% compared with the bulk condition. However, since the corrosion rate under bulk electrolytes is small, this significant increase does not mean the metal is experiencing rapid corrosion. The increase in corrosion rate and diffusion limiting current is more obviously pronounced with the decrease in electrolyte concentration. When the carbon steel surface was covered with 40μm 0.01M NaCl electrolyte, the corrosion rate and diffusion limiting current bhowed their highest value among all experimental results.

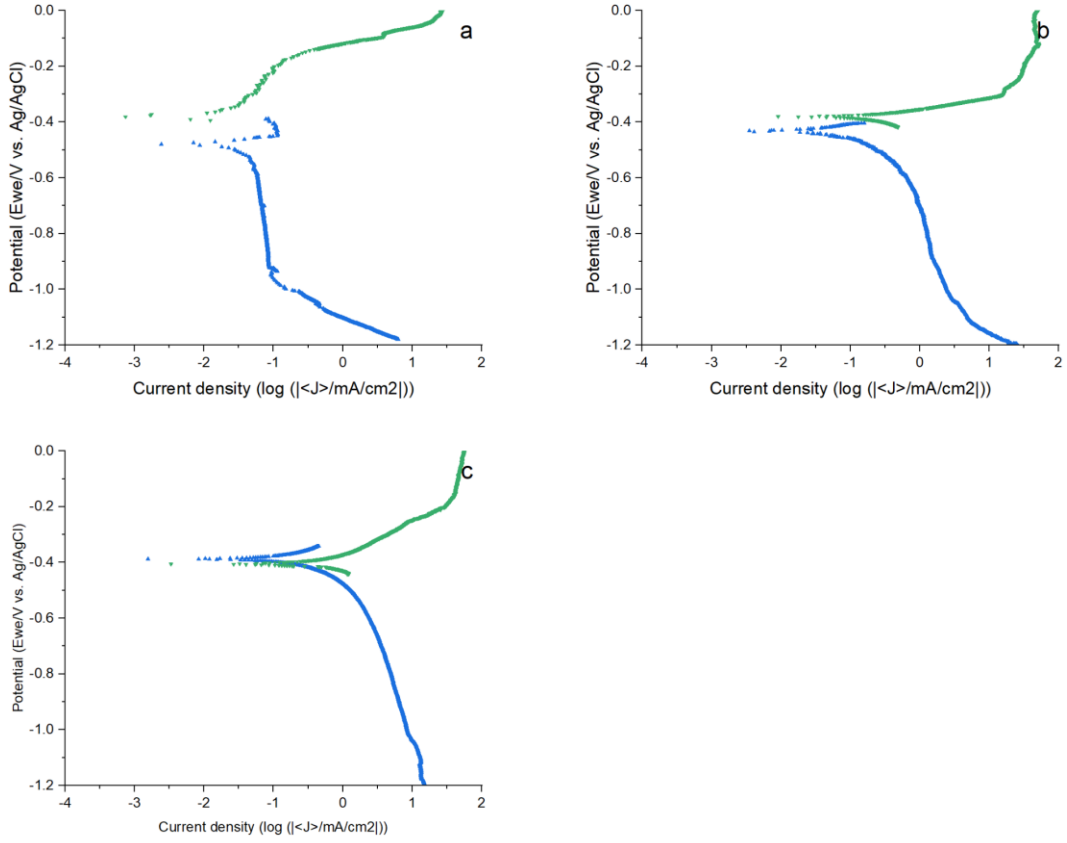

Figure 10. The anodic and cathodic polarization curves of carbon steel in (a) 1.0M, (b) 0.1M and (c) 0.01M NaCl when the electrolyte thickness is 40μm. The anodic and cathodic branches are polarized separately.

Table 7. The potential and current density of carbon steel exposed to 40 μm-thickness electrolytes with different NaCl concentrations.

	β_a (mV)	**β_c (mV)**	**Potential (mV)**	**Current density ($\mu A/cm^2$)**	**Limiting current density ($\mu A/cm^2$)**
1.0 M	143±59.1	/	-316±12	45.1±8.5	83.2±22.3
0.1 M	78±42	461±133	-402±35	233.7±37.8	1264.8±12.4
0.01 M	175±86	479±33	-390±21	813.3±58.5	4312.2±205.4

4.2 Zinc

4.2.1 Bulk electrolyte experiments

The zinc samples were also immersed under bulk NaCl solution with 1.0M, 0.1M and 0.01M ions concentrations. The potentiodynamic polarization was done to measure the corrosion potential and the corrosion current density to study the effect of ion concentration on zinc corrosion.

Figure 11 and Table 8 shows the corrosion of zinc under bulk electrolyte with different chloride ions concentration. Similar to the corrosion of carbon steel under bulk electrolyte conditions, low corrosion rates were observed at all three chloride ion concentrations. However, due to the more rapid redox reaction of zinc in the chloride environment, the corrosion rates of zinc are found to be higher than the corrosion rate of carbon steel at every chloride concentration. The highest corrosion rate (26.72 uA/cm^2) occurs in the 1.0M NaCl bulk electrolyte. A decrease in corrosion rate can be observed as the chloride ion concentration decreases. The diffusion control region was not observed in the corrosion reaction of zinc with bulk NaCl electrolyte, no matter the change of chloride ion concentrations.

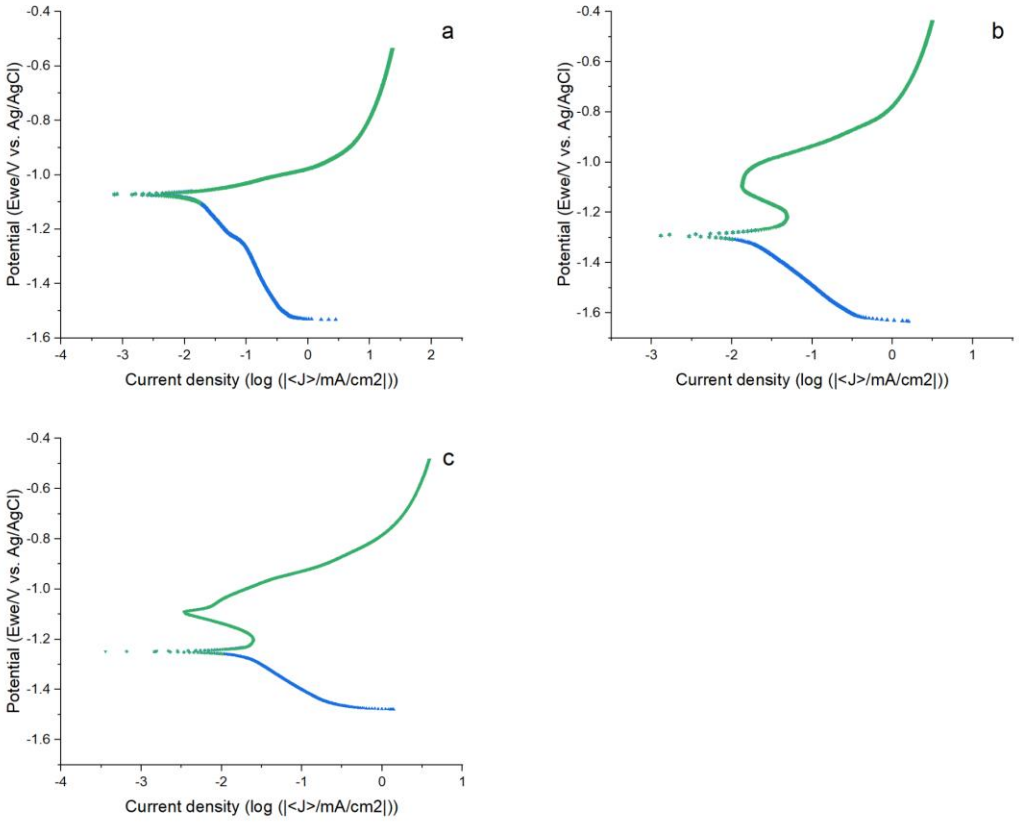

Figure 11. The polarization curves of zinc in (a) 1.0M, (b) 0.1M and (c) 0.01M NaCl when the electrolyte is bulk solution. The anodic and cathodic branches are polarized separately.

Table 8. The potential and current density of zinc in 1.0/0.1/0.01M NaCl bulk electrolyte.

	β_a (mV)	**β_c (mV)**	**Potential (mV)**	**Current density ($\mu A/cm^2$)**	**Limiting current density ($\mu A/cm^2$)**
1.0M	104±15	301±35	-1119±25	26.7±1.2	NaN
0.1M	/	225±36	-1197±32	9.7±1.9	NaN
0.01M	/	197±10	-1142±33	4.8±1.1	NaN

4.2.2 Thin-film electrolyte experiments

40μm thickness electrolyte

Figure 12 and Table 9 show the corrosion rate of zinc in a 40μm thin-film NaCl electrolyte with three different chloride ion concentrations. An increase in corrosion rate was observed at all three chloride ion concentrations.

Diffusion control regions were observed on the cathodic branch, and diffusion limiting current density was measured under all three chloride ion concentrations. The highest limiting current density was observed under 0.01M NaCl electrolyte since more oxygen could pass through the thin electrolyte to the metal surface. Under the thin electrolyte condition, the relationship between the corrosion rate of zinc and the chloride ion concentration is in the same direction as that relationship of carbon steel but with a clear difference in the growth rate. The corrosion of carbon steel under thin-film electrolyte is greatly affected by chloride ion concentration; the corrosion rate and diffusion limiting current density both changed significantly. By reducing the chloride ion concentration from 1.0M to 0.01M, the corrosion rate increased from 45.1 to 813.3 $\mu A/cm^2$. Compared to carbon steel, the increase in the corrosion rate of zinc with the decrease of chloride ion concentration is significantly lower under thin electrolytes. The corrosion rate increased from 159.6 to 363.2 $\mu A/cm^2$ and the diffusion limiting current density also only increased from 276.3 to 823.0 $\mu A/cm^2$. Compared with the polarization curve of the carbon steel corrosion process, the shape of the zinc polarization curve is more complicated, and the differences between each experiment is also more apparent. This is due to the rapid oxidation of zinc in air and its higher activity in the chloride ion aqueous environment.

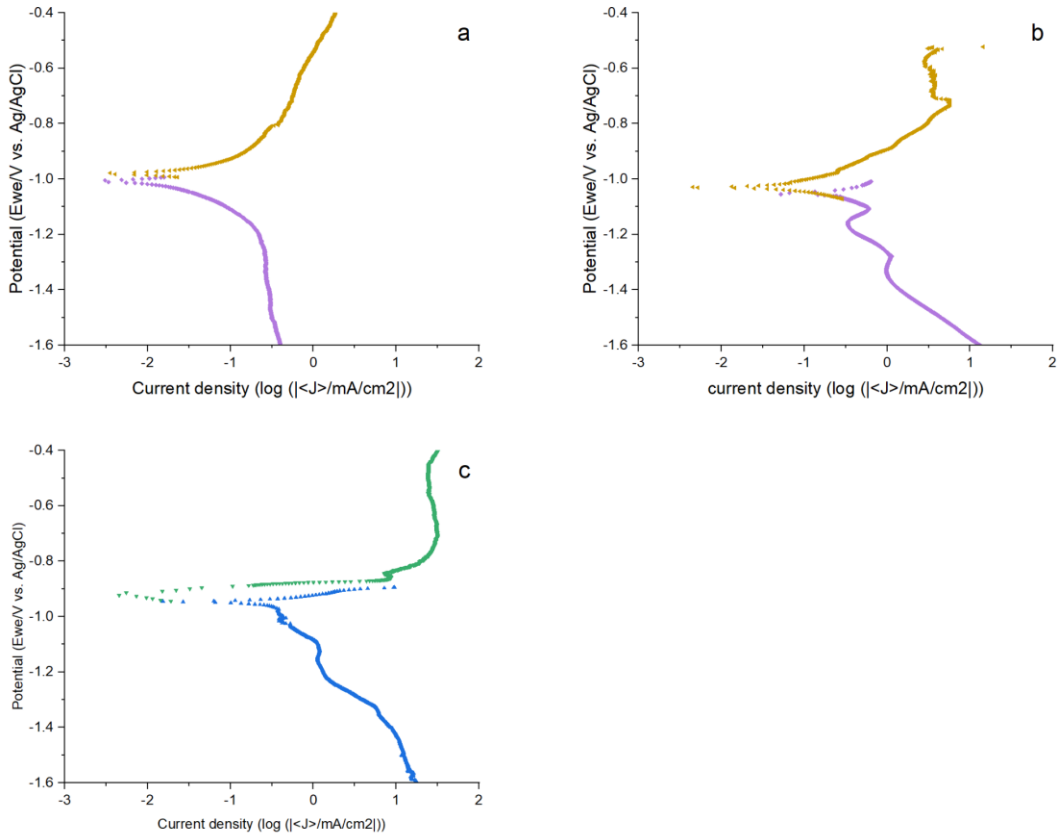

Figure 12. The anodic and cathodic polarization curves of zinc in (a) 1.0M, (b) 0.1M and (c) 0.01M NaCl when the electrolyte thickness is 40μm. The anodic and cathodic branches are polarized separately.

Table 9. The potential and current density of zinc in 40μm 1.0/0.1/0.01M NaCl electrolyte.

	β_a (mV)	**β_c (mV)**	**Potential (mV)**	**Current density ($\mu A/cm^2$)**	**Limiting current density ($\mu A/cm^2$)**
1.0 M	631±51	/	-991±11	159.6±75.9	276.3±88.4
0.1 M	377±92	581±160	-1002±58	247.9±21.2	435±79.6
0.01 M	107±50	478±64	-923±6	363.2±60.1	823.0±298.6

4.3 Galvanic couple: carbon steel and zinc

The galvanic current was measured under both bulk electrolyte and 40μm thin-film electrolyte to study the effect of electrolyte thickness on the galvanic corrosion behaviour of carbon steel and zinc couple. The experimental results showed a higher galvanic coupling current under the bulk electrolyte than the thin-film electrolyte was observed. At the same time, the galvanic coupling current shown in Table 10 was observed to decrease with the decrease of chloride ion concentrations in both bulk and thin electrolytes.

Table 10. The galvanic coupling current (μA) of the Zinc - Steel couple under bulk/40μm NaCl electrolyte with different chloride ion concentrations.

	1.0M	**0.1M**	**0.01M**
Bulk electrolyte	183.3±50.3	162.1±14.0	75.5±4.2
40μm electrolyte	123.3±10.5	73.5±7.4	23.7±0.8

5 Discussion

5.1 Effect of chloride-ion concentration

5.1.1 Oxidation reaction

The presence of chloride ions will affect the alkalinity of the solution and determine the metal dissolution reaction on the anode. The chloride can affect the metal corrosion process by changing the structure of the double electric layer and directly participating in the electrode reaction with a particular reaction order. The influence of chloride ions on the anode reaction includes First, as a surface-active substance, the adsorption occurs on the surface of the electrode and affects the corrosion potential. Second, activate the dissolution process of the anode. The chemical affinity of metal for chloride ions is greater than the chemical affinity of metal for oxygen, which destroys the structure of the oxide layer on the metal surface and promotes the occurrence of anode dissolution. The amount of chloride ion will also affect the ionic concentration in the electrolyte and determine the resistance of the electrolyte.

The anodic reaction that happened during the corrosion of carbon steel and zinc under sodium chloride solution should be:

For carbon steel:

$$Fe \rightarrow Fe^{2+}+2e^{-}$$

$$Fe^{2+} \rightarrow Fe^{3+}+e^{-}$$

For Zinc:

$$Zn \rightarrow Zn^{2+}+2e^{-}$$

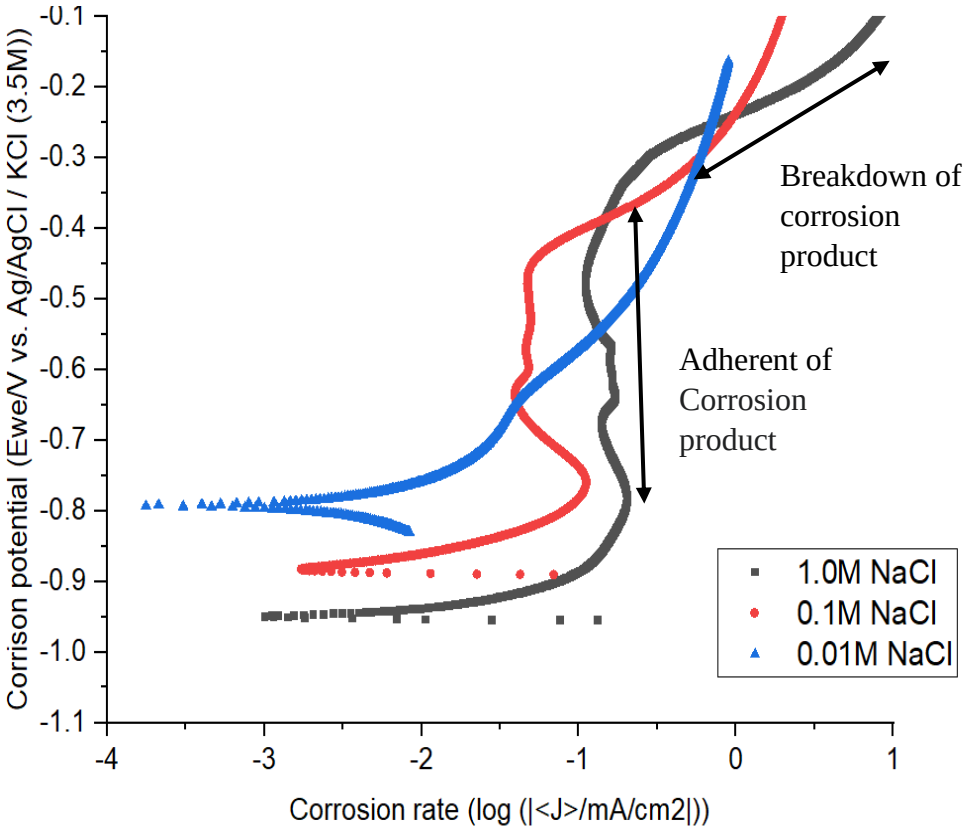

Figure 13. The anodic branch of the polarization curve of Carbon Steel under bulk NaCl electrolyte with different chloride ion concentrations

Figure 13. shows how chloride ions affect the structure of the oxide layer and promote the occurrence of anode dissolution. For the 1.0M and 0.1M chloride concentration experiments, with the increase of anodic polarization potential, a steady rise in anode corrosion current is observed. The anode potential shifted from OCP to values between -0.80V and -0.75V.

For 0.01M NaCl, this steady increase of anode corrosion current is observed at this anode potential region. During this stage, $Fe(OH)_2$, the corrosion product of carbon steel under a chloride environment, is formed with the metal dissolution process. The "mass loss" during the corrosion process not only causes the dissolution of metal ions into solution but may also cause the aggregation of ions to form solid corrosion products at the metal/solution interface, usually metal hydroxides or oxides. If the solid corrosion products adhered to the metal surface with a non-porous structure and had high electron and/or ion transport resistibility, the formation of corrosion products would significantly reduce the metal corrosion rate. As shown in Figure 13, with the further increase of potential, the anodic current density decreases drastically due to the existence of adhered corrosion products. This decrease in anodic current density indicates that critical anodic current densities of carbon steel under 1.0M and 0.01M NaCl environment were observed at -0.80 and -0.75V, respectively. The corrosion

products adhered to the metal surface, isolating the internal metal from the chloride ion to prevent further corrosion. This explains why the corrosion current density remains constant in the potential range of (-0.75V, -0.45V) and (-0.65V, -0.45V) under 1.0M and 0.1M sodium chloride solutions. The range of this polarization potential-independent stage depends on the thickness of the adhered corrosion product. The protection provided by corrosion product layers during this independent stage is determined by its thickness, porosity, and specific surface area. Under the 1.0M sodium chloride solution, because more corrosion products are formed and adhered to the surface of the carbon steel rapidly, the range of the independent stage is wider than that of the solution with low chloride ion concentration. Due to the poor stability and low density of the corrosion products, as the polarization potential increases above -0.45V, the dissolution of $Fe(OH)_2$, together with the exposure of carbon steel in electrolyte, again results in a high anodic current density. The corrosion in this region can be shown either uniformly (trans-passive behaviour) or non-uniformly (localized pitting or crevice corrosion).

When carbon steel is immersed in 0.01M sodium chloride solution, low chloride ion concentration results in a slow reaction rate, and the anodic branch maintains. The anodic branch maintains almost the same slope during the entire anodic polarization. A small step was observed in the (-0.75V, -0.65V) interval, but then the anodic slope recovered to a normal level. No potential independent stage caused by the adhesion of corrosion products is observed. To explain this anodic branch shape which is different from the 1.0M/0.1M experiments, both the effect of corrosion rate and the corrosion product composition should be considered. In the absence of anions (such as Cl^- or $SO4^{2-}$), lepidocrocite (γ-FeOOH) will be formed as a corrosion product. Yamashita et al. studied the atmospheric corrosion products on carbon steel exposed in a low-chloride environment, determined that lepidocrocite typically occurs in the outer layers of the rust layer and generally forms loosely aggregated particles with relatively large average diameters. [69] However, as the previous discussion about the effect of chloride ions on corrosion product composition, the chloride ion concentration of the electrolyte in atmospheric corrosion will favour the formation of oxyhydroxide akaganeite (β-FeOOH) instead of lepidocrocite as shown in Figure 15. When the NaCl concentration exceeds 0.05wt%, the weight ratio of akaganeite/lepidocrocite increases significantly. [47] Figure 14. shows the weight ratio of β-FeOOH to γ-FeOOH as a function of NaCl concentration. [47] [70] When the chloride ion concentration was 0.01M (0.058wt.%), the weight ratio of akaganeite/lepidocrocite was 10. However, by increasing the chloride ion concentration to 0.1M (0.58wt.%) and 1.0M (5.8wt.%), the weight ratios of akaganeite/lepidocrocite increased to 120 and 150, respectively. The significantly higher content of loosely lepidocrocite particles with large average diameters in 0.01M NaCl solution may explain the inconsistency of the adhesion behaviour of corrosion products on carbon steel surface compared to that at high NaCl concentrations. This may result in insufficient protection provided to the metal surface, thus manifesting as the absence of a potential independent stage on the anodic branch.

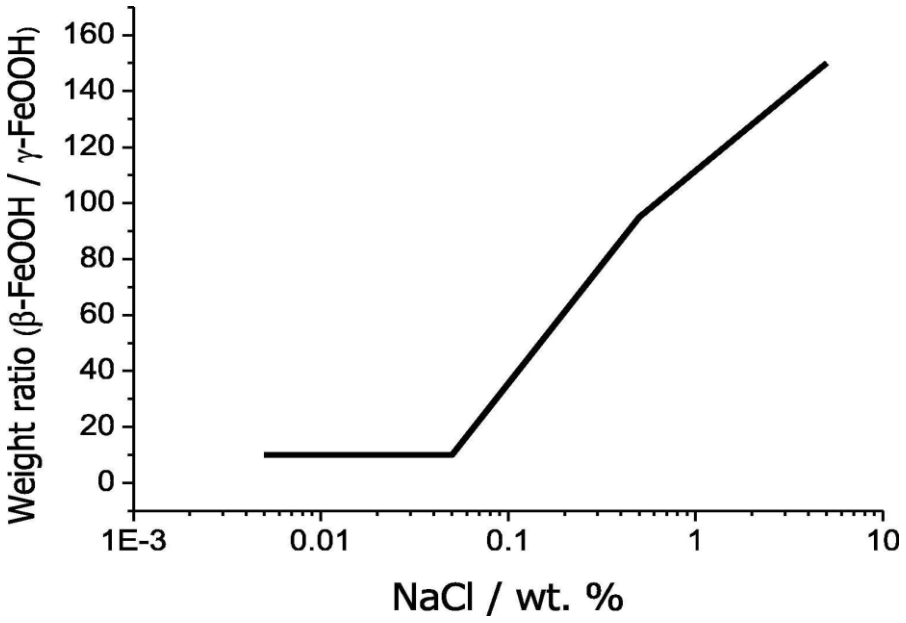

Figure 14. Weight ratio of β-FeOOH to γ-FeOOH as a function of NaCl concentration. [47] [70]

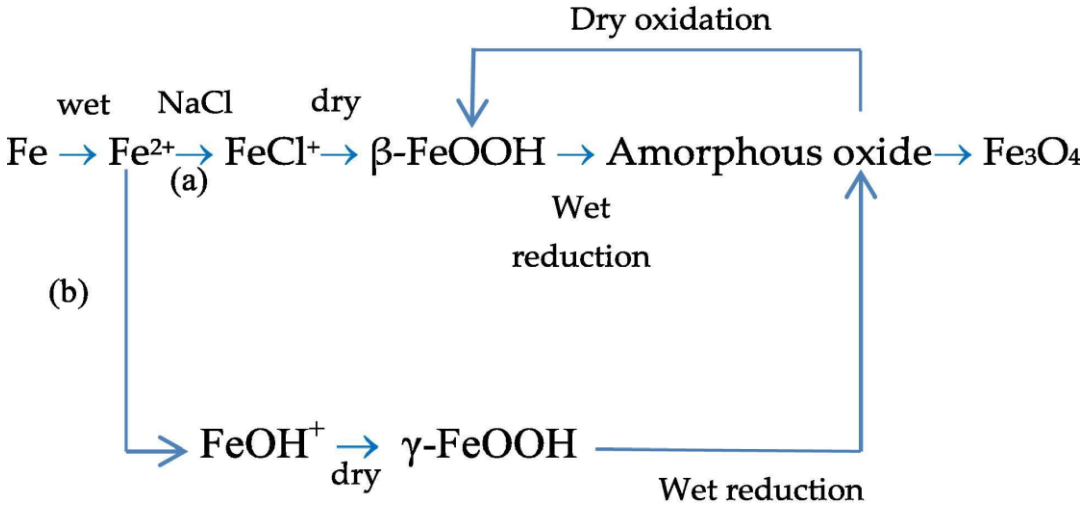

Figure 15. Rusting iron model in wet and dry corrosion condition containing NaCl (a) route for high Cl– concentration; (b) route for low Cl– concentration. [47] [70]

The polarization curves of zinc show the passivation of metal and the effect of chloride ions on passivation. At the potential nobler than E_{corr}, zinc first experiences an anodic dissolution and then re-passivated over a small voltage range. In the passivation region, the formation and dissolution of the passivation film reach an equilibrium state. The passivation state remains stable, and the corrosion current is no longer related to the potential over a small voltage. This behaviour is only observed under 0.1M and 0.01M NaCl electrolytes. The Tafel plot in figure 16 reveals that the effect of chloride ions on

zinc prevents the metal from passivation instead of increasing the possibility of passive layer rupture.

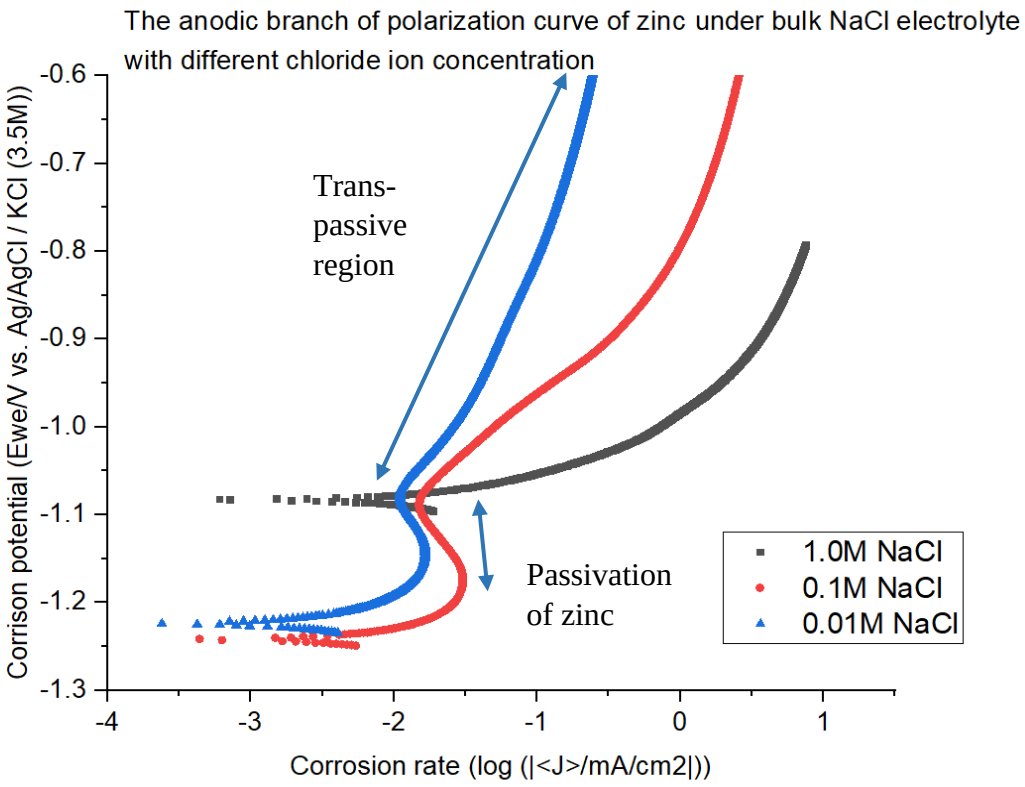

Figure 16. The anodic branch of the polarization curve of Zinc under bulk NaCl electrolyte with different chloride ion concentrations.

For experiments under low chloride ion concentration electrolytes (both 0.1M and 0.01M in this study), as the anode potential continues to increase to -1.1V, the passive film breakdown. The trans-passive region is reached, and the corrosion current density increases again. Two main reactions occur in this region and lead to an increase in the corrosion rate: firstly, the re-exposure and dissolution of the metal substrate, and secondly, the oxidation of low-valent ions of the metal to high-valent ions (for example, Fe^{2+} has been oxidized to Fe^{3+}). During the corrosion of zinc, the dissolution rate of the metal determines the region of trans-passive. However, in the corrosion of carbon steel, the dissolution of carbon steel and the oxidation of metal ions happened jointly and together to affect the trans-passive region.

The relationship between chloride ions and anodic reaction rate under bulk electrolyte can be shown from the anodic branch slope β_a in Table 4 and Table 8. Theoretically, a higher chloride concentration should lead to a more severe anodic reaction and result in a steeper anodic branch of the polarization curve, as we have seen in the corrosion of carbon steel. A similar conclusion can also be drawn by comparing the slope of the anodic branch for zinc corrosion under thin-film electrolyte experiments, as shown in

Table 9. However, it is impossible to extract an accurate anode curve slope from the Tafel plot in many cases. For example, in the bulk electrolyte experiment of zinc, the anode branch shows complex response as the potential increases from -1.2 to -1.0V. A linear segment with at least one decade of current change is necessary for accurate extrapolation; however, due to the presence of a passive region at this region, it is impossible to find such a linear segment for accurate anodic branch slope extraction. Only under 1.0 M NaCl solution, the formation and protection of ZnO were prevented due to the high chloride ions concentration and resulted in the absence of passive regions. This makes it possible to extract the anodic branch slope from the Tafel plot. However, the curve from the 1.0M NaCl condition seems to be the smoothest curve. The anodic curve consistently presents on the right side of the x-axis, which indicates a higher corrosion rate than the curve from lower chloride ions concentration experiments.

Besides the effect of the passive region and potential-independent stage on the anodic polarization curve, it must be acknowledged that the shapes of anodic polarization curves under thin-film electrolyte themselves are usually complicated. Compared with the anodic corrosion curves under bulk electrolytes, these curves show more severe fluctuation and irreproducibility. This is because metal ions can migrate parallel to the metal surface under thin-film electrolyte conditions during anodic polarization. The anode current density is not uniform across the entire working electrode but can be concentrated at the edge of the metal. [71] This unevenly distribution of anode current density may cause errors in anodic polarization results. The reproducibility of anodic polarization curves under thin-film electrolytes is poor, according to the study by Huang et al., so measuring the slope of the anodic curve is not a precise method to evaluate the anodic reaction. [72] It should be cautious when using the shape of the anode polarization curve to assess the corrosion reaction under thin-film electrolyte. A more scientific method to evaluate the anodic reaction is still by studying the changes in corrosion rate and corrosion potential when controlling all other variables but changing the ion concentration of the electrolyte.

5.1.2 Oxygen solubility and transport

The presence of chloride ions will affect the anodic corrosion by changing the alkalinity of the solution and affect the cathodic reaction by affecting oxygen solubility in electrolytes. The oxygen dissolved in the aqueous solution is a prime oxidant in most metal corrosion processes. The concentration of oxygen in the aqueous solution significantly impacts the corrosion kinetics, mainly when the corrosion process is limited by the oxidant mass transfer. By controlling variables such as the temperature T, the partial pressure of oxygen in the gas phase PO_2, and the inorganic electrolyte solute I, the quantification of oxygen solubility is feasible.

In this study, the temperature and partial pressure of oxygen in the gas phase are controlled to be constant under each experiment condition. The addition of an inorganic electrolyte solute will form an ionic conductive solution and reduce the solubility of O_2 in the solution. The solubility behaviour of O_2 in ionic conductive solutions is complicated and largely depends on the concentration and composition of the inorganic electrolyte solute I.

The presence of inorganic electrolyte solute mainly affects the solubility of oxygen from two aspects. First, electrolyte solvents occupying the voids in the solution will cause fewer voids to be occupied by oxygen. Second, complex interactions between the polar water molecules and the ionic components of the inorganic electrolyte solute will happen in ionic conductive solutions. The overall average spacing between H_2O molecules changes under these interactions and changes the partial molar volume of the water component V_{app} compared to the partial molar volume of pure water V_{H2O}.

$$V_{\mathrm{app}} = \left\{\left(\frac{1000 + C_I M_I}{d_s}\right) - C_I V_I\right\}\frac{M_{\mathrm{H_2O}}}{1000} \quad [73]$$

In this equation, the C_I is the molar concentration of solute, M_I and M_{H2O} represent the molecular weight for solute and H_2O, d_s is the density of the solution, and V_I is the molar volume of dry solute. The V_I, M_I and M_{H2O} are constant for a specific solute, and the partial molar volume will decrease with the increase of inorganic electrolyte solute concentration C_I. The decrease of V_{app} will provide less volume for oxygen to occupy and "squeeze" the oxygen out from the solution. [73]

For some single-component electrolytes, the effect of electrolytes on O_2 solubility can be simplified by the equation proposed by Sechenov et al. [74], which has proved its accuracy by experimental data.

$$\log\left(\frac{C^{\circ}_{O_2}}{C_{O_2}}\right) = KC_{\mathrm{el}} \quad [74]$$

In this equation, C_{O2} represents the oxygen solubility in an electrolyte solution with a concentration of C_{el} and C^0_{O2} is the oxygen solubility in pure water. K represents the O_2 solubility constant which is different for each electrolyte. From previous studies, the relation between the solubility of oxygen with the NaCl concentrations in the electrolyte has been calculated and experimentally confirmed, as shown in Table 11. The cathodic reaction that happened during the corrosion of both carbon steel and zinc under sodium chloride solution should be:

$O_2 + H_2O + 4e^- \rightarrow 4\ OH^-$ *Under alkaline solution*

The relationship between chloride ion concentration and oxygen solubility proves why chloride ion concentration can indirectly affect the oxygen reduction reaction on the cathode. Under bulk electrolyte conditions, the H_2O supply is considered sufficient, so oxygen becomes the only determinate reactant for the corrosion reaction rate. Under the 0.01M NaCl solution condition, the aqueous solution has the maximum oxygen solubility due to less ion-water interaction and fewer voids occupation. With the increase of inorganic electrolyte solute concentration, the oxygen solubility decreases and should decrease oxygen reduction reaction on the cathodic branch. The slope of the cathodic branch β_c in bulk electrolyte experiments is most suitable for verifying the theory proposed. The slope of carbon steel increases with the decrease of the concentration of chloride ions.

Besides the change of β_c, the corrosion rate is also suitable for studying the effects of chloride ions on cathodic reaction. Although the higher oxygen solubility in electrolytes with low chloride ion concentration will contribute to cathodic corrosion, the increase in corrosion rate is still observed with the increased alkalinity of the solution under bulk electrolyte conditions. The corrosion rate of carbon steel significantly decreased under 0.01M NaCl solution compared to 1.0M NaCl. At the same time, for zinc, the corrosion rate is even reduced by the order of magnitude with the decrease of the chloride ions concentration. The limited supply of oxygen can explain this under bulk electrolyte conditions. The thickness of the diffusion layer of oxygen in pure water is about 300μm. Since the thickness of the bulk electrolyte in this study is much higher than 300μm, the oxygen concentration at the metal surface will be very low. The change in corrosion rate indicates that the contribution of different dissolved amounts of oxygen to varying concentrations in the bulk electrolytes to the corrosion rate is relatively low. The corrosion reaction is dominated by the dissolution speed of the metal on the anode electrode.

Table 11. Solubility of oxygen in NaCl solutions as a function of concentration under 25 Celsius degrees. [75]

Molality of NaCl (M)	**Solubility of oxygen (μmol/Kg)**
0	258.9
0.1589	248.0
0.3034	238.3
0.5161	223.3
0.7857	206.7
0.9694	195.9
1.5151	169.8

The effect of chloride ion concentration on cathodic reduction reaction is more critical under thin-film electrolyte experiments. In all 320μm, 160μm and 40μm thin-film electrolyte experiments on carbon steel, the maximum corrosion rate is always found under 0.01M NaCl, and the minimum corrosion rate is always observed under 1.0M NaCl electrolyte. The difference between corrosion rates caused by different chloride ions concentrations is at its smallest in 320μm thickness and the largest in 40μm thickness.

In 320μm electrolyte thickness, although the slope of both anodic and cathodic branches in Table 9. significantly changed, the effect of chloride ion concentrations on the cathodic reaction was not very notably. The corrosion rate and diffusion limiting current density were the same under three different chloride ion concentrations. The similar diffusion limiting current density indicates that oxygen is still unable to pass through the electrolyte and reach the metal surface to participate in the cathode reaction at this thickness of the electrolyte. A significant increase in the slope of cathodic branch β_c with the decrease of chloride ion concentrations was observed. This is due to the more pronounced diffusion control region observed at low chloride ion concentration. A segment on the curve which is entirely perpendicular to the x-axis affects the value of the slope of the cathodic branch. By comparing the shape of the cathodic curves under three different chloride ion concentrations, it can be found that the corrosion reaction is still partially under activation control until the polarization potential is reduced to -400mV of OCP under high chloride ion concentration. The corrosion current density and the diffusion limiting current density are still the relatively better method to study the effect of chloride ion concentration in 160μm thickness of electrolyte. The corrosion rate and diffusion limiting current density negatively correlated with the chloride ion concentration. More oxygen passes through the oxygen diffusion layer in the electrolyte and reaches the metal surface. The high oxygen solubility in the electrolyte with low chloride ion concentration on the cathodic reaction becomes apparent.

For experiments in 40μm NaCl electrolyte, the concentration of chloride ions now significantly affects the corrosion rate. This is due to the very low thickness of the electrolyte compared to the thickness of the oxygen diffusion layer. The oxygen in the surrounding atmosphere can easily be transported through the membrane and electrolyte. As mentioned earlier, higher chloride ion concentration means fewer vacancies available in the electrolyte for oxygen transportation and resulting in low oxygen solubility. This finding is the same as that in some previous studies. At high chloride ions concentrations, the metal surface tends to adsorb chloride ions than adsorb oxygen which has been explained as competitive adsorption by Marqui. [76] Similar situations have been found and described in salt spray experiments and immersion experiments. [77] Under low chloride ions concentration conditions, high oxygen solubility enables a more rapid cathodic reduction reaction. More oxygen participating in the cathodic reaction allows a more extended activation control stage on the cathode

branch, which can be shown by comparing the diffusion limiting current density. Under both 320μm and 160μm electrolyte thickness, the effect of different chloride ion concentrations on the diffusion limiting current density is relatively small. However, when the electrolyte thickness was further reduced to 40μm, it is evident from comparing Table 5-7 that the diffusion limiting current density is much higher than other concentrations at lower chloride ion concentrations. This can be explained by looking into the following equation:

$$\textit{Limiting current density } i_{lim} = nFDC/\delta$$

Where D is the effective diffusion coefficient that considers the contributions from transport by migration, C is the oxygen concentration at the metal surface, n is the apparent dissolution valence, F is the Faraday constant, and δ is the electrolyte thickness. [78] The thinner the electrolyte, the smaller the δ, and the more significant impact of concentration change from 1.0M to 0.01M on limiting current density. Considering only electrolyte thickness and oxygen concentration as the variables, reducing the electrolyte concentration from 1.0 to 0.01M in 40μm electrolyte experiments will result in eight times Δi_{lim} compare to when concentration change is 320μm electrolyte experiments.

Because the cathodic reaction of zinc under thin-film NaCl electrolyte is similar to that of carbon steel, it is speculated that changing the chloride ion concentration on the corrosion rate will be consistent with the effect of changing the chloride ion concentration on carbon steel. Experiments show that the highest corrosion rate and corrosion potential are observed when zinc metal is corroded under a 40μm thin-film NaCl electrolyte with a 0.01 M concentration. The experimental results proved that since the primary cathodic reaction was not changed, the contribution of chloride ion concentration to corrosion will also be in the same trend by only changing the corroded metal from carbon steel to zinc. When the electrolyte is thin enough for the oxygen diffusion in the electrolyte, the fast oxygen transport brought by reducing the chloride ion concentration will significantly increase the corrosion rate. However, unlike the corrosion of carbon steel in sodium chloride solution, under the atmospheric corrosion of zinc, only partial oxygen was involved in the reduction reaction at the cathode. As an electrochemically active metal, zinc will preferentially undergo an oxidation reaction and form an oxide film on the metal surface when it contacts an aqueous electrolyte. The rate of this oxidation reaction is also affected by the thickness of the electrolyte. In the case of thin-film electrolytes, the oxygen in the environment passes through the electrolyte to reach the surface of the zinc, which can not only participate in the reduction reaction of the cathode but also other combines with the zinc metal to form zincite (ZnO). From Cui et al. [49] and many recent studies, without other atmospheric pollutants presented, zinc is most likely to form a protective simonkolleite ($Zn_5Cl_2[OH]_8 \cdot H_2O$) under Sodium chloride electrolyte. Due to less aggressive ions in the low chloride ion concentration electrolyte, the corrosion product films would not rupture but hinder the transport of electroactive species and resist further corrosion. This supposition also fits with the multi-layer structure observed by Prestat et al. [51]

from the FIB-SEM figures of the microstructure of zinc corrosion under sodium chloride electrolyte. The complicated heterostructure formed because of oxidation of zinc in sodium chloride, including a simonkolleite network on the top, a nanoporous ZnO layer in the middle and the Zn-rich film covering the metal surface, which shows the "barrier effect". This might explain why zinc exhibits a lower corrosion rate than carbon steel's corrosion rate under the same 40μm 0.01M NaCl electrolyte condition.

In conclusion, the effect of chloride ion concentration on the cathodic reaction mainly affects the solubility of oxygen to change the cathodic reduction reaction rate. The impact of chloride will not be evident in the case of bulk electrolytes due to the high electrolyte thickness compared to the oxygen diffusion layer in an aqueous solution. However, as the electrolyte thickness decreases, oxygen will have a greater possibility of passing through the electrolyte and reaching the metal surface to participate in the reaction. The effect of oxygen solubility begins to emerge when the electrolyte thickness decreases to 160μm. Under low electrolyte thickness conditions, oxygen supply will dominate the corrosion reaction rate and highly affect the corrosion rate of carbon steel and zinc.

5.2 Effect of electrolyte thickness

As early as 1964, Tomashov et al. already pointed out in his research that, by changing the electrolyte from liquid to thin film (atmospheric corrosion), the operating condition for both anodic and cathodic process will be completely changed. [79] A higher corrosion rate should be observed in atmospheric corrosion for almost all types of metal compared to in bulk liquid electrolyte. The most intuitive way to verify is to compare the current density of metal during polarization. The current densities of carbon steel and zinc specimens in 1.0/0.1/0.01M NaCl electrolyte were recorded. The atmospheric corrosion condition was achieved by reducing the electrolyte thickness from bulk to 40μm, as shown in Table 12, significant increase in current density can be observed in all three chloride ion concentrations.

Table 12. The current density (uA/cm^2) of carbon steel and zinc in bulk/40μm electrolyte with 1.0/0.1/0.01M NaCl concentration.

	Carbon steel Bulk	**Carbon steel 40μm**	**Zinc Bulk**	**Zinc 40μm**
1.0M	9.3±0.7	**45.1±8.5**	26.7±1.2	**159.6±75.9**
0.1M	6.7±2.5	**233.7±37.8**	9.7±1.9	**247.9±21.2**
0.01M	2.9±0	**813.3±58.5**	4.8±1.1	**363.2±60.1**

According to the model proposed by Tomashov, the corrosion mechanism can be distinguished according to the thickness δ of the moisture layer. The metal undergoes dry atmospheric corrosion when δ is less than 10nm. When the thickness of the water layer is in between 10nm and 1μm, the metal is under moist atmospheric corrosion. Further increasing the thickness of the water layer to 1mm is considered to be wet corrosion, and the corrosion with a δ greater than 1mm is called complete immersion. The particularly discrimination in corrosion factor is the difference in mechanism and rate of oxygen penetration. In complete immersion corrosion, the access of oxygen to the metal surface is primarily determined by stirring conditions so it is very limited for stationary bulk electrolyte. However, in the wet atmospheric conditions, the oxygen supply is mainly determined by the thickness of moisture film which will highly affect the reaction rate. Both previous experiments and theoretical research believe, the cathodic reaction rate is enhanced with a decreasing electrolyte thickness as oxygen diffusion through the layer is promoted.[80] In fact, the change of electrolyte thickness will affect many processes during the metal corrosion, not only the mass transport of the dissolved oxygen but also the accumulation of corrosion products and hydration of dissolved metal ions. [48] In order to verify the conclusion proposed by Tomashov, combining with the corrosion data from polarization curves, the effects of changing electrolyte thickness on both anodic and cathodic reactions under wet atmospheric corrosion conditions will be explained separately.

The polarization curves of carbon steel under 1.0M/0.1M/0.01M NaCl electrolyte with different electrolyte thicknesses are shown in Figure 17 to discuss the relation between electrolyte thickness and corrosion rate. By reading the anodic branch shape together with the anodic slope in Table 13, it can be learned that the anodic corrosion reaction will only be minorly changed with the change of electrolyte thickness under 1.0M NaCl electrolyte. This is because the metal dissolution reaction entirely depends on the properties of the metal and the chloride ion concentration but will not be affected by the oxygen supplements. The anodic polarization was first under the active control region and showed an increase in polarization current until the potential reached -0.2V. The anodic polarization curve shows a plateau stage, the current density continued to increase with a low anodic branch slope for about two decades of corrosion current density.

For carbon steel under 0.1M NaCl electrolyte, the difference in anodic polarization curve under different electrolyte thicknesses is more prominent and affects the further corrosion rate calculation. For carbon steel in 320μm thick electrolyte, a shape similar to the anode branch of carbon steel under 1.0M is also found. The anodic curve first increases at a high slope and then shows a plateau stage for about two decades of current density. The corrosion current density will finally become independent of the potential increase under a high polarization potential. This plateau stage was not observed in bulk electrolytes experiments, but common appears in thin-film electrolytes experiments. The shape of the anodic branch clearly shows the occurrence of pitting corrosion. This

pitting corrosion can occur at all chloride-ion concentrations, which is consistent with the conclusion from Han et al. based on their field exposure and laboratory simulation of carbon steel under wet-dry cycles. The filiform corrosion and pitting can be observed even at very low chloride levels and can appear in the very early stages of the atmospheric corrosion. [81] Corrosion experiments on pure magnesium under thin-film electrolyte layers was done by Zhang et al. which also indicated that the corrosion in thin-film electrolyte layers was more localized compared to in bulk solutions. [82]

In addition to pitting corrosion, a particular anodic polarization curve was observed from the sample in 160μm thick 0.1M NaCl electrolyte. Similar curves were also observed in 320μm 0.01M NaCl electrolyte experiments. Kelly [83] mentioned this anodic polarization curve shape in his book, which is because some metals and alloys can spontaneously passivate in the presence of oxidizing species (such as dissolved oxygen in electrolytes). This spontaneously passivate was shown in the Tafel plot as the absence of an active region. The intersection of the anode curve and the cathode curve appeared in the passive region because of the oxidant. The polarization curves have not exhibited the characteristics of an active-passive transition. The anodic branches of carbon steel in 40μm thick electrolyte do not show a similar shape. The slope of the anode branch is continually maintained at a low value. The anodic branch shape of the 40μm experiment, which is unique from other curves, maybe because of the extremely low electrolyte concentration and volumes.

The anodic branch of carbon steel under 0.01M is similar to that of carbon steel under 0.1M. The 320μm thickness experiments showed the absence of an active region. The 40μm thickness electrolyte experiments showed the continuous increase of corrosion current density with increased polarization potential. The slope of the anodic branch in the 40μm electrolyte remains the same until an extreme high polarization potential is reached. The carbon steel in 160μm thick electrolyte exhibited an anodic reaction intermediate between these two corrosion models.

Overall, as shown in Figure 17, it can be observed that the shape of the anodic branch of the polarization curve is not significantly affected by the thickness of the electrolyte under each specific electrolyte concentration. But the potential at which the anode curve is located can be very different due to the variation of open circuit potential with the change of electrolyte thickness. By reducing the thickness of the electrolyte from bulk electrolyte to thin-film electrolyte, both the anodic branch and cathodic branch are observed to move to the upper right side of the coordinate axis in Figure 17. The shift of the curves indicates a significant increase in corrosion potential and a corrosion rate by changing the electrolyte thickness. The presence of a plateau stage was observed on the anodic curve, suggesting that the corrosion under the thin-film electrolyte is more localized compared to the bulk solution. Theoretically, the reduction of electrolyte thickness will also affect the hydration of dissolved metal ions. When the required water for the hydration of the dissolved metal ions is insufficient, the corrosion is controlled by the anode reaction and will be inhibited because of the occur of passivation. However, this will only happen when

the thickness of the electrolyte layer has already been reduced below the critical thickness. Since the minimum electrolyte thickness in the experiments was set to 40μm, which was significantly higher than the critical electrolyte thickness of wet atmospheric corrosion for both carbon steel and zinc, no effect on hydration of dissolved metal ions was observed.

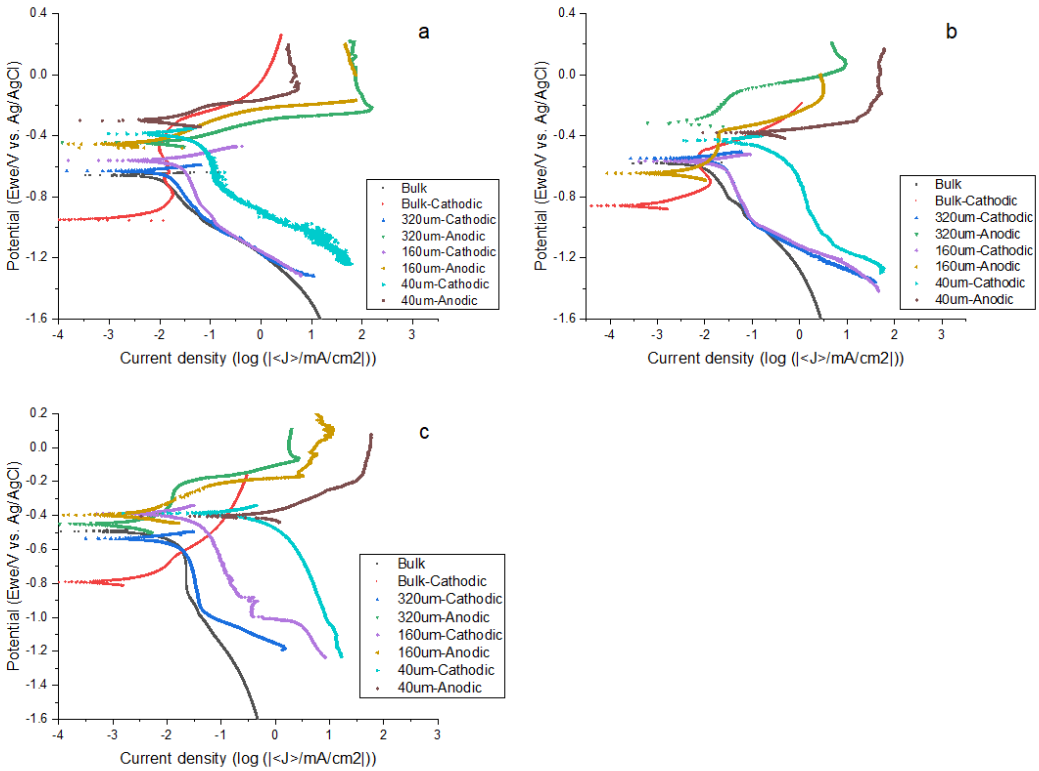

Figure 17. The anodic and cathodic polarization curves of carbon steel in (a) 1.0M, (b) 0.1M and (c) 0.01M NaCl when the electrolyte thickness is bulk/320/160/40μm. The anodic and cathodic branches are polarized separately, except for experiments in 320μm thickness 0.01M NaCl.

Table 13. The corrosion potential and corrosion rate of carbon steel under bulk/320/160/40μm of 1.0M NaCl electrolyte

	β_a (mV)	**β_c (mV)**	**Potential (mV)**	**Current density (μA/cm^2)**	**Limiting current density (μA/cm^2)**
bulk	/	115±6	-937±17	9.3±0.7	NaN
320 μm	146±60	392±22	-465±27	7.4±1.8	30.2±3.2
160 μm	121±15	/	-407±19	12.6±2.1	46.3±5.7
40 μm	143±59	/	-316±12	45.1±8.5	83.2±22.3

Table 14. The corrosion potential and corrosion rate of carbon steel under bulk/320/160/40μm of 0.1M NaCl electrolyte

	β_a (mV)	β_c (mV)	Potential (mV)	Current density (μA/cm^2)	Limiting current density (μA/cm^2)
bulk	/	141±7	-889±20	6.7±2.5	NaN
320 μm	216±18	/	-328±59	8.9±0.3	32.6±4.9
160 μm	274±81	472±150	-555±18	18.5±2.1	61.9±8.7
40 μm	78±42	461±133	-402±35	233.7±37.8	1264.8±12.4

Table 15. The corrosion potential and corrosion rate of carbon steel under bulk/320/160/40μm of 0.01M NaCl electrolyte

	β_a (mV)	β_c (mV)	Potential (mV)	Current density (μA/cm^2)	Limiting current density (μA/cm^2)
bulk	221±26	193±19	-798±15	2.9±0	16.7±3.7
320 μm	/	/	-289±68	12.5±3	31.9±5.2
160 μm	133±31	/	-267±43	25.7±2.8	96.1±24.1
40 μm	175±86	479±33	-390±21	813.3±58.5	4312.2±205.4

Based on previous research, some of the metals such as magnesium [82], aluminium alloy [84] [71], zinc [85] [28], galvanized steel [10] [86] and magnesium alloy [87] experienced an significantly increase in cathodic current density with the decrease of thin film electrolyte thickness when the thickness of electrolyte layer is more than 40 μm. However, in the vast majority of these experiments, either the influence of electrolyte thickness and electrolyte concentration could not be distinguished due to the use of wet-dry cycle method, or the influence of electrolyte shape on the corrosion reaction was not considered during the experimental design. Now, LUNA cell is used to accurately simulate the wet atmospheric corrosion under uniform thin film electrolyte. The cathodic polarization curves of carbon steel corrosion in Figure 17 are useful to reveal the effect of electrolyte thickness on atmospheric corrosion. Compared to the corrosion under bulk electrolyte, the corrosion rate is highly affected by the oxygen transmission under thin-film electrolyte. Under bulk electrolyte conditions, when the oxygen near the electrolyte-metal interface is consumed, there is no extra oxygen can reach the interface. As shown in Table 13, the cathodic slope of bulk electrolyte under 1.0M concentration is lower than the thin electrolyte experiments due to this lack of oxygen supplement. The insufficient oxygen supplement limited the cathodic reaction and was shown as a low cathodic slope in the Tafel plot. As the decrease of the

electrolyte thickness, the cathodic slope of 320 and 160μm under 1.0M concentration was shown under a similar level. This is because of the lack of vacancies in the 1.0M NaCl electrolyte for oxygen to dissolve and transport. Under high NaCl concentration, most of the positions between water molecules are taken by sodium and chloride ions, leading to low oxygen solubility. Even though the reduction of the electrolyte thickness allows the oxygen exchange between the atmosphere and the electrolyte, there are few positions for oxygen to be dissolved in. The electrolyte is also more favourable to adsorb chloride ions than the adsorption of oxygen molecules. The corrosion rate can also prove this result. With the decrease of electrolytes, the corrosion rate only increased from 7.4 to 12.6 μA/cm^2. When the electrolyte thickness decreases to 40μm, the effect on corrosion is more pronounced. The void density in the thin electrolyte is the same as the void density under a thicker electrolyte, but less distance is needed to be passed through. A thin electrolyte means the oxygen takes less time and is more easily moved to the metal surface to participate in the oxygen reduction reaction. At the same time, since we consider the amount of oxygen in the air to be sufficient, both the supply and transition of oxygen will no longer limit the cathodic reaction. The reduction reaction rate will be accelerated with a faster consumption of oxygen. The rapid increase of corrosion rate to 45.1 μA/cm^2 compared with the corrosion rate under thicker electrolyte (from 7.4 μA/cm^2 increase to 12.6 μA/cm^2) successfully proved the above mechanism. Under a 40μm thick 1.0M NaCl electrolyte thin film, the cathodic corrosion reaction of carbon steel is highly controlled by the oxygen supply under low polarization potential.

When the polarization potential decreases to 100mV negative to OCP, the cathodic reaction rate will soon be under diffusion control. The diffusion limiting current for carbon steel under 1.0M NaCl electrolyte will be small. The diffusion control region will appear close to the area used to calculate the cathodic slope. Under diffusion control, the corrosion rate was independent of the potential change and resulted in a rapid increase of the cathodic branch slope. In 40μm 1.0M NaCl electrolyte, the cathodic branch slope that we observed will be either overestimated or even too high to be measured out. It will be meaningless to compare the slope of the cathodic branch under this condition with the slope results from the experiments with different electrolyte thicknesses.

The effect of electrolyte thickness can be studied by both the cathodic polarization curve and the corrosion current density. The impact of electrolyte thickness on the cathodic branch shape of 0.1 and 0.01M experiments results was more apparent compared to the experiments under high chloride concentration. Under thin-film electrolyte with low chloride ions concentrations, the increase of cathodic slope was also observed compared to that under bulk electrolyte conditions. However, for both 0.1 and 0.01M, β_c was not continuously increased with the decrease of the electrolyte thickness from 320μm to 40μm but showed the opposite tendency. The reduction of cathodic slope does not indicate the decrease of cathodic reaction rate but shows the change of diffusion limiting current density. The oxygen solubility in 0.1M and 0.01M NaCl electrolytes is much higher than in 1.0M NaCl. This increased solubility allows

more oxygen to be transported through the electrolyte. With the decrease of the electrolyte thickness, the distance that needs to be passed is decreased, and the oxygen can reach the metal surface and precipitate the corrosion reaction quicker. When the polarization potential decreases to a more negative level (-200mV to OCP), the oxygen transport speed is still quick enough. The electrode potential still determines the reaction rate and allows the reaction to be under activation control. The experiments indicate that the diffusion control region will appear at a lower polarization potential with the decrease of electrolyte thickness. The vertical line segment of the diffusion control region will be far away from the region used to calculate the cathodic slope. With less affected by diffusion control regions, the cathodic slope was decreased but more accurately showed the cathodic reduction reaction speed.

The corrosion current density under different conditions was also compared to show the effect of electrolyte thickness. The corrosion rate under both 0.1M and 0.01M NaCl electrolyte increases with the decrease of electrolyte thickness as we observed in the 1.0M condition, but with different growth rates. The corrosion rate for 0.1M NaCl risen from 6.7 to 233.7 $\mu A/cm^2$ by changing the bulk electrolyte to a 40μm thick electrolyte thin film. With the constant solution concentration, the increase in the corrosion rate can be considered entirely dependent on the thickness of the solution. With the same change of electrolyte thickness, the corrosion rate for 0.01M NaCl increased from 2.9 to 813.3 $\mu A/cm^2$. As the thickness of the electrolyte decreases, the corrosion reaction rate at all three concentrations has increased. Among them, the corrosion rate at a concentration of 0.01M increases the most, followed by 0.1M, and the corrosion rate at a concentration of 1.0M increases the least. The relationship between the increase in corrosion rate and the electrolyte thickness conforms with the expectations based on the effect of oxygen concentration on the reaction. Combining the data from Table 11, and the equation of oxygen solubility, the oxygen solubility in 1.0M/0.1M/0.01M NaCl electrolyte were calculated as 196.7, 250.3 and 255.7 μmol/Kg. The lower the chloride ion concentration, the higher oxygen solubility in the electrolyte. Because of the highest oxygen solubility in 0.01M NaCl electrolyte, the oxygen concentration (C) at the metal surface will also be the highest. Considering only electrolyte thickness and oxygen concentration as the variables, reducing the electrolyte thickness from 320 to 40μm in 0.01M electrolyte will result in a highest Δi_{lim} compared to when the electrolyte concentration is 1.0M.

Overall, under all three chloride ion concentration conditions, the cathodic polarization curve was affected by the thickness of the electrolyte, indicating that the oxygen supplement will directly affect the cathodic reduction reaction. It is also observed that the corrosion rate increases with the decrease of electrolyte thickness. The increase in corrosion rate from the bulk solution to 160μm thick electrolyte is limited. However, further reducing the thickness of the electrolyte from 160 to 40μm will significantly increase the corrosion rate.

5.2.1 Effect on diffusion limiting corrosion rate

In addition to the corrosion rate, the diffusion limiting current is also essential to study the effect of electrolyte thickness on atmospheric corrosion. When a very negative polarization potential has been applied to the LUNA cell, The surface of the carbon steel will accumulate additional negative charges. The cathodic reaction on carbon steel is shown in the equation below; the supplement of negative charge will allow more oxygen to participate in the cathodic reaction.

$$O_{2.} + H_2O + 4e^- \rightarrow 4OH^- \qquad \textit{Under alkaline solution}$$

As the polarization potential has been decreased to a more negative region, the supply of negative charge and water molecules are considered in excess, and the rate of oxygen transport will only determine the rate of the overall cathodic reaction. By comparing the diffusion limiting current rate, the influence of changing the electrolyte thickness on oxygen transport and cathode reaction can be observed intuitively.

No significant diffusion limiting current was observed for carbon steel immersed in a bulk electrolyte of 1.0 M NaCl. When the thickness of the electrolyte was reduced to 320 μm, a segment of the cathodic curve perpendicular to the x-axis was observed for the first time. At this stage, the corrosion rate did not change with the continuous decrease of the potential to more negative regions, meaning that the supplement of oxygen completely controlled the rate of cathodic reaction. The corrosion rate density when this vertical line segment appears is the diffusion limiting current. As can be seen from Table 13, as the thickness of the electrolyte continues to decrease, the oxygen diffusion limiting appears at a higher current density.

This trend can also be observed in the 0.1M and 0.01M NaCl experiments. The diffusion limiting current at 320μm was nearly the same for all three chloride ions concentrations. Same as the corrosion rate at 320μm for all three chloride ions concentrations, since the thickness of the electrolyte is higher than the thickness of the oxygen diffusion layer in water, the external oxygen in the air cannot reach the metal surface to participate in the reaction. Under this electrolyte thickness, the change of chloride ion concentration only affects the oxygen solubility inside the electrolyte but does not substantially allow more oxygen transport from the environment. This explains why the change in chloride ion concentration did not affect the corrosion rate in 320μm thickness electrolyte.

When the thickness of the electrolyte is further reduced to 160μm, oxygen can pass through the electrolyte through the vacancies in the electrolyte to reach the metal surface. The increase in diffusion limiting current was observed at all three concentrations due to more oxygen participating in the cathodic reaction. Since the thickness of the electrolyte is the same, different chloride ion concentrations mean different vacancy concentrations for oxygen to transport. This difference will lead to a different increase in diffusion limiting current. As shown in Table 8, as the chloride ion

concentration decreases, there is more space in the electrolyte for oxygen to accommodate and participate in the cathode reaction at a 160μm thick electrolyte. The diffusion limiting current density under 1.0, 0.1 and 0.01M NaCl electrolyte increased by 16.1, 29.3 and 64.5 uA/cm^2. Since the diffusion limiting current of carbon steel in 320μm electrolyte is almost the same under three electrolyte concentrations, comparing the increase of the diffusion limiting current is meaningful.

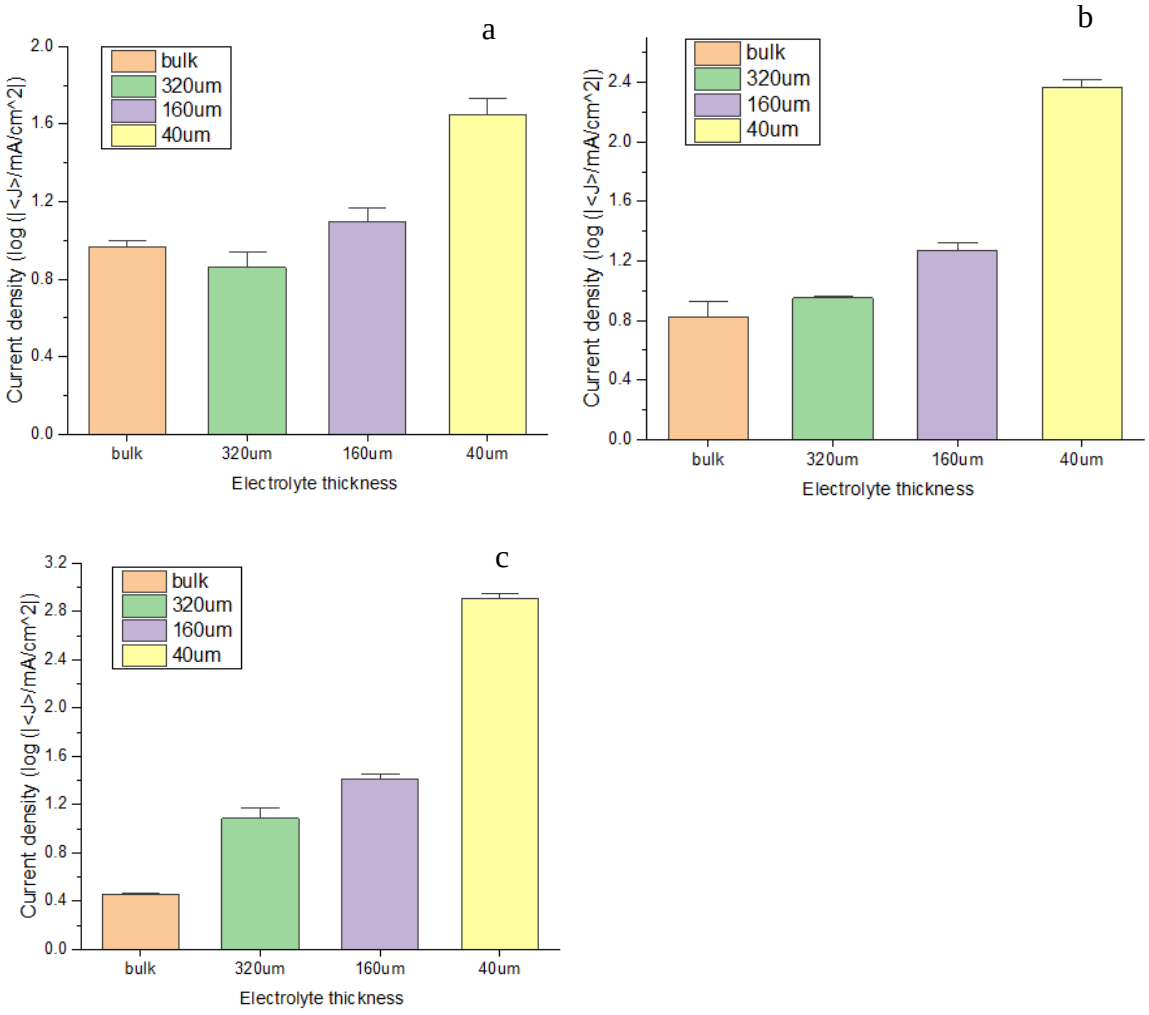

Figure 18. The histogram of the change of current density with the change of electrolyte thickness under (a) 1.0M, (b) 0.1M and (c) 0.01M NaCl solution.

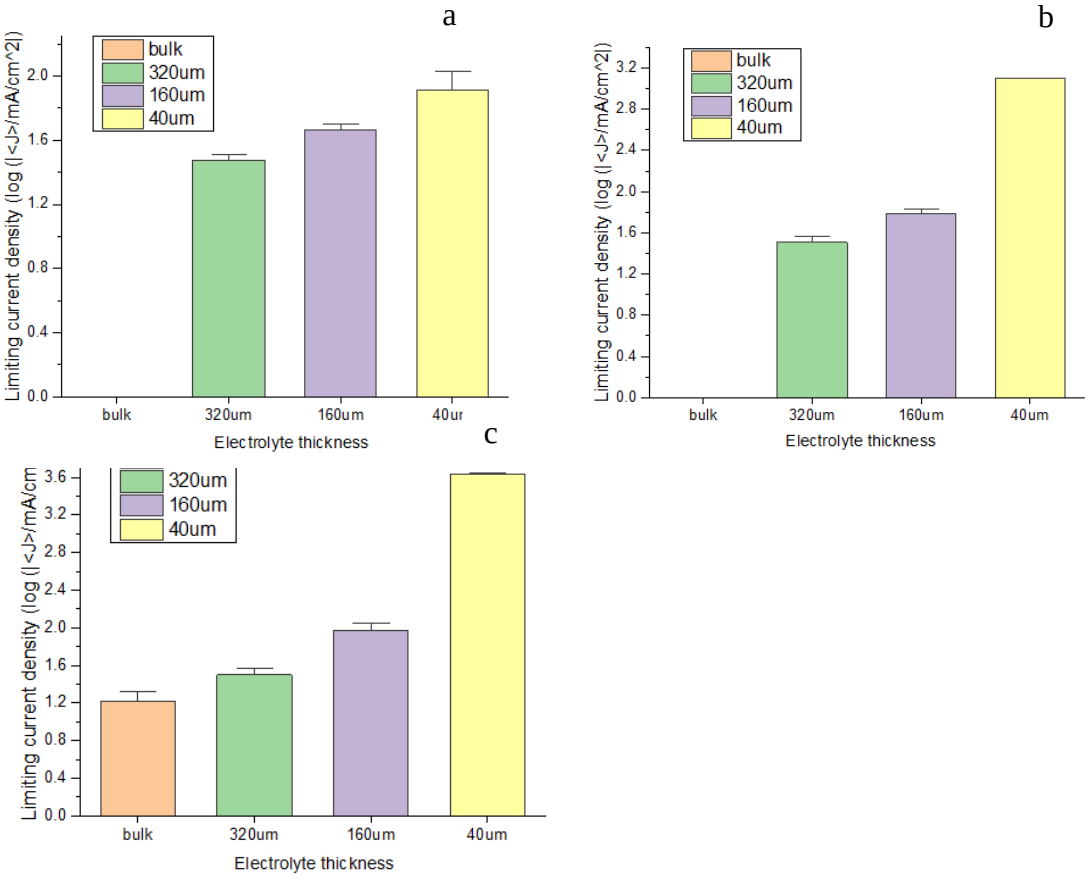

Figure 19. The histogram of the change of limiting current density with the change of electrolyte thickness under (a) 1.0M, (b) 0.1M and (c) 0.01M NaCl solution.

When the thickness of the electrolyte is further reduced to 40μm, a more noticeable change in diffusion limiting current can be observed. First, a significant increase in the diffusion limiting current is observed for all three electrolytes. However, the electrolyte thickness only changed by 120μm (from 160μm to 40μm) compared to the electrolyte thickness changed by 160μm when it was reduced from 320μm to 160μm. This shows that the increase of the diffusion limiting current does not change linearly with the thickness of the electrolyte. With thinner electrolytes, the diffusion limiting current will increase substantially.

There are two possible reasons for this rapid increase in diffusion limiting current. The first is that the relationship between electrolyte thickness and limiting current density is not linear. As shown in the equation of the limiting current density, if we consider only the electrolyte thickness and oxygen concentration as the variables, reducing the electrolyte thickness from 320μm to 160μm will double the limiting current density, but further reducing the thickness from 160μm to 40μm will quadruple the limiting current density. When the electrolyte thickness was controlled to be 40μm for all concentrations because the highest oxygen concentration (C) at the metal surface for

the experiment in 0.01M NaCl electrolyte, the calculated limiting current density will be the highest.

The second reason is the change in the membrane thickness, as we mentioned before. For the experiments in 160μm thickness, the thickness of the membrane was set to 320μm to support the electrolyte's surface tension. For the experiments in 40μm, only an 80um thick membrane is required to maintain the surface tension. In studying the effect of thickness on diffusion limiting current, the material and structure of the membrane are the same to avoid any influence. In the 160μm thickness experiments, the same membrane used in 40μm thickness experiments is now used to stack on each other to achieve a 320μm membrane thickness. In 160μm thickness experiments, the membranes stacked on top of each other can complicate the path of oxygen transport. This might prevent a portion of oxygen transport or cost more time for the oxygen to the electrolyte, finally resulting in a slower rate of oxygen reaching the metal surface to participate in the cathodic reaction.

Overall, because of the higher oxygen concentration at the metal surface to participate in the cathodic reaction with the decrease of electrolyte thickness, an increase in the diffusion limiting current is observed under each chloride ion concentration. Decreasing the electrolyte from 320 to 160μm has a limited effect on the diffusion limiting current, but when the electrolyte was further reduced to 40μm, a rapid increase in the diffusion limiting current was observed under each chloride ion concentration. The increase of diffusion limiting current with electrolyte thickness is negatively correlated with chloride ion concentration. Since the low chloride ion concentration means higher oxygen solubility, the highest diffusion limiting current was observed in 0.01M NaCl compared to the other two chloride ion concentrations.

5.2.2 Galvanic coupling experiments

Galvanizing is a common rust prevention method by applying metallic zinc to iron or steel surfaces since zinc has higher oxygen activity and is easier to be corroded under environment. When combined with iron/steel to form a galvanic coupling, zinc as a anode can provide cathodic protection to iron and steel. The experimental results section used the zero resistance ammeter technique to measure the electrochemical noise of the steel-zinc galvanic couple. The experimental results showed a higher galvanic coupling current under the bulk electrolyte than thin-film electrolyte was observed. At the same time, the galvanic coupling current shown in Table 10 was observed to decrease with the decrease of chloride ion concentrations in both bulk and thin electrolytes. These results seem to contradict the result from potentiodynamic polarization experiments. Here are the possible reasons that can be used to explain this contradictory result: First, the connection between the carbon steel-zinc couple and the

reference electrode during the experiment is different from the connection between the working electrode and reference electrode.

During the potentiodynamic polarization experiments, the reference electrode was placed directly on the top of the wetted membrane which covered the working electrode (carbon steel or zinc). However, during the galvanic coupling experiment, the anode (zinc) and the cathode (carbon steel) were separated by an insulating material and covered with a wetted membrane. The reference electrode will be placed on top of that insulating material. Also, under thin-film electrolyte experimental conditions, localised drying of the membrane is possible due to the rapid drying process of the electrolyte. Due to the height differences between carbon steel samples, zinc samples and the insulating material, electrolytes may accumulate in the gap between the insulating material and anode/cathode metal. And the thickness of the electrolyte on the insulating material is less than 40μm. Eventually, this uneven distribution of the electrolyte will result in electrolyte thickness localized below 40μm on the insulating material. When the thickness of the electrolyte is less than 30μm, the thickness of the electrolyte will be positively related to the corrosion rate. The decrease of the electrolyte thickness will no longer increase the corrosion rate but lower the corrosion rate instead. In addition to the effect on the corrosion rate, too thin electrolyte layers may also increase the possibility of poor connection with the reference electrode and lead to failed measurements.

5.2.3 The critical electrolyte thickness

By analysing the corrosion rates of carbon steel and zinc under thin-film electrolytes, we have already confirmed that the thin film electrolytes covered on the metal surface can lead to more severe corrosion. We refer to the thickness at which the corrosion rate is the first time observed to increase significantly compared to the corrosion rate under bulk electrolyte conditions as the critical electrolyte thickness. Under the electrolyte with a constant chloride ion concentration, the rate of the corrosion reaction should be dominated by the oxygen involved in the cathodic reaction. Therefore, the critical electrolyte thickness is expected to be close to the theoretical oxygen diffusion layer thickness.

For carbon steel under 1.0M and 0.1M NaCl electrolyte, the corrosion rate under bulk electrolyte and 320μm electrolyte show very similar results, 9.3 and 7.4, 6.7 and 8.9 $\mu A/cm^2$, respectively. But with a further decrease of the electrolyte thickness down to 160μm, the corrosion rate significantly increases. This shows that under 1.0 and 0.1M NaCl electrolyte, with the solution concentration remaining constant, reducing the electrolyte thickness from bulk to 320μm does not affect oxygen transport very much. As we mentioned before, the oxygen diffusion layer in an aqueous solution is about 300μm. This very little change in corrosion rate may prove that the critical electrolyte

thickness is lower than or close to 320μm. For carbon steel under 0.01M NaCl electrolyte, due to the high vacancy rate brought about by the low chloride ion concentration, the corrosion rate in 320μm electrolyte also shows an increase compared to the bulk electrolyte (2.9 uA/cm^2 to 13.5 uA/cm^2). Another possible reason is that the electrolyte layer dries too quickly during the experiment, which causes the actual electrolyte thickness to be thinner than the oxygen diffusion layer under specific experimental conditions.

When the thickness of the electrolyte layer is larger than that of the diffusion layer, the corrosion rate is not controlled by the diffusion-limiting current density of oxygen. But if the electrolyte layer is thinner than the diffusion layer, the oxygen diffusion rate increases and thus the corrosion rate increases. In fact, this critical electrolyte thickness of the metal surface is not a constant but depends on the chemical composition of the electrolyte and the properties of the metal. Chung et al. found that for very thin electrolyte layer, the critical thickness for the maximum corrosion rate is also changed by the concentration accumulation which indicates that the concentration accumulation is also an important factor in determining the critical thickness. [65] This result matches with what we observed from the different critical electrolyte thickness from corrosion in1.0M/0.1M NaCl and in 0.01M NaCl. Dubuisson et al. study the atmospheric corrosion of galvanised steel in a micrometric electrolyte droplet and found that the corrosion rate of galvanized steel will not change significantly when the electrolyte droplets is above 500 μm. [80] Zhou et al. have studied the atmospheric corrosion of aluminum alloy 7075 and found the highest corrosion rate in 110 μm thin film electrolyte. [84] These results all illustrate that for each atmospheric corrosion experiment, the maximum corrosion rate should be determined individually according to the corrosion reaction conditions.

5.2.4 Advantages and disadvantages of LUNA Cell

Salt spray tests are generally used to simulate atmospheric corrosion under thin electrolytes in industrial research. The laboratory uses typically the microsyringe method to directly load a predetermined amount of electrolyte droplets on the metal surface. When studying atmospheric corrosion under low electrolyte thicknesses, these two traditional methods cannot fully meet the following requirements. First, precisely controlling the thickness of the electrolyte layer. Second, form a complete and uniform thin film electrolyte on the surface of working electrodes.

<u>Creating a uniform thin film electrolyte</u>

Compared with the conventional electrochemical methods, the LUNA cell required the electrolyte to be loaded on the hydrophilic membrane rather than directly on the metal surface. The hydrophilic membrane helps the electrolyte to form a uniform and

continuous film by breaking the surface tension of the droplets. Compared with the salt spray method, the thickness of the studied electrolyte was controlled more precisely using the LUNA cell. Compared with the microsyringe method, the effect of droplet geometry on corrosion can be minimized by the presence of the hydrophilic membrane.

High oxygen transmission rate

The hydrophilic membranes and carbon cloth counter electrodes used in this study both have a porous structure that facilitates the penetration and transmission of oxygen. The presence of the fine plastic mesh and coarse plastic mesh applied a uniform compression across the back of the counter electrode without creating obstructions in the path of oxygen transmission from the surrounding environment to the metal surface.

Feasibility and cost

The layered structure of the LUNA cell allows it to simulate the corrosion of thin electrolytes in a small space, which facilitates multiple tests at the same time. At the same time, since the materials used to set up the LUNA cell (including the PTFE plate, silicon gasket and carbon cloth counter electrode etc.) are inexpensive and easy to obtain, the operability and repeatability of this experiment are possible. LUNA cells can also simulate many different atmospheric corrosion scenarios by changing the electrolyte composition, electrode metal selection, and surrounding environmental factors.

At the same time, there are still some imperfections in using LUNA cells to simulate thin-film electrolyte conditions. Since the LUNA cell is essentially a multi-layer structure by stacking the components on the z-axis, the presence of the counter electrode, plastic mesh andReducing brackets will still affect the efficiency of oxygen reaching the metal surface, which may lead to less participation in the cathode oxygen reduction. A reduction in the amount of oxygen for the reaction will eventually cause an inaccurate corrosion rate compared to the actual corrosion rate under thin-film electrolyte atmospheric conditions.

6 Conclusions and Recommendations

Atmospheric corrosion is a complex and interdisciplinary research area. It requires a thorough understanding of solid materials, atmosphere, liquid films, and the changing of the atmospheric environment. One of the problems in atmospheric corrosion research is that it is difficult to quantify the effect of every single factor separately. This is because atmospheric corrosion is a system that is affected by many factors; these factors not only influence the corrosion behaviour but also influence each other. It is almost impossible to control a single aspect, especially in in-situ outdoor exposure. Another problem is that the atmospheric environment at different sites is often distinctive; the results are not repeatable and often require a long time to obtain. Therefore, it is meaningful to study the atmospheric corrosion of metals under thin electrolytes by simulating and quantifying the corrosion behaviour in the laboratory.

This research aims to evaluate the impact of solution chemistry and electrolyte thickness on the atmospheric corrosion behaviour of zinc and carbon steel under thin-film electrolytes. In this experiment, a novel atmospheric corrosion cell with a multi-layer structure called the LUNA cell was used to simulate the corrosion under thin-film electrolyte conditions. Compared with other methods that have been used to simulate thin-film electrolyte conditions before, the hydrophilic membrane can break up the surface tension of the aqueous electrolyte so that the electrolyte can evenly be distributed on the surface. In this study, by loading the specific amount and types of electrolytes on the membrane, the effect of electrolyte thickness and electrolyte concentration on thin-film atmospheric corrosion was studied from open circuit potential, polarization, and galvanic coupling electrochemical techniques. The following findings have been proposed:

1. In the case of the bulk electrolyte, extremely low corrosion rates were observed at all concentrations due to the lower oxygen content in the electrolyte. A positive correlation between the chloride ion concentration and corrosion rate was observed.
2. When the thickness of the electrolyte is 320 μm, it is observed that the corrosion rate of carbon steel is almost consistent with the corrosion rate under the bulk electrolyte in all three electrolyte thicknesses. This experimental result is consistent with predictions based on the thickness of the oxygen diffusion layer in water. When the electrolyte thickness is higher than the thickness of the oxygen diffusion layer, oxygen is hard to pass through the electrolyte to participate in the oxygen reduction reaction at the cathode, resulting in a low corrosion rate. However, when the chloride ion concentration in the electrolyte is low enough, a small amount of oxygen still passes through even if the electrolyte thickness is slightly higher than that of the oxygen diffusion layer due to the high vacancies density allowing the transportation. This explains the observed increase in corrosion rate in experiments with electrolyte thickness of 320 μm under 0.01 M NaCl.

3. As the electrolyte thickness decreases, a significant increase in the corrosion rate of carbon steel and zinc was observed due to the participation of more oxygen in the cathodic reaction. The highest corrosion rate was observed at an electrolyte thickness of 40 μm under every electrolyte concentration.
4. Since the concentration of chloride ions in the electrolyte will affect the oxygen solubility, in the case of thin electrolytes, the concentration of chloride ions in the electrolyte exhibits a negative correlation with the corrosion rate. This illustrates the dominated corrosion reaction under thin-film atmospheric corrosion. The corrosion reaction is mainly determined by the oxygen reduction reaction at the cathode rather than the metal dissolution reaction at the anode.

Although LUNA atmospheric corrosion cell provides a good simulation of atmospheric corrosion in the case of thin-film electrolytes, there are still some improvements that can be made in this experimental setup:

1. *Evaporation of electrolyte*. During the experiment, the electrolyte will gradually evaporate into the environment. Due to the large surface area of the membrane, this evaporation will be uniform and rapid. The electrolyte thickness on the metal surface will gradually fall below the pre-set electrolyte thickness, leading to inaccurately measured corrosion rates. According to previous studies, when the thickness of the electrolyte on the metal surface is higher than 30 μm, the reduction of the electrolyte thickness helps oxygen reach the metal surface and finally increases the rate of oxygen reduction reaction at the cathode. But when the thickness of the electrolyte is below the critical thickness, the corrosion rate will decrease rapidly with the decrease of the thickness of the electrolyte. Therefore, this study cannot exclude the effect of electrolyte evaporation on the corrosion rate. Conducting wet/dry cycling tests can help confirm the critical electrolyte thickness at a specific electrolyte concentration. A possible method to minimise the effect of electrolyte evaporation was proposed in the previous study. The experimental setup was placed in an electrolyte reservoir with the same concentration as the experimental electrolyte loaded on the metal, which slowed down the evaporation of the electrolyte on the membrane. Another solution is to perform experiments in a glove box with constant temperature and humidity. When the temperature and humidity were controlled at 25 Celsius degrees and 90% RH, respectively, the effect of electrolyte evaporation on the corrosion rate could be minimized.
2. *Leakage of electrolyte from the bridge tube*. The bridge tube used in this experiment is covered with a 2.8 mm wide Coralpor 1000 tip. The average pore diameter is about 4-10 nm to minimize the leakage of electrolytes from the bridge tube. However, fast water leakage was still observed which resulted in inaccurate electrolyte volumes on the membrane during the experiments. The electrolyte thickness might be too thick if the water leakage rate is high. The

leakage of the electrolyte may help to explain the similar corrosion rate in 320μm thin-film electrolyte and under bulk electrolyte.

3. *Contact method of reference electrode.* In addition to the dynamic polarization experiments, galvanic couple experiments of carbon steel and zinc have also been done during the study. However, under thin-film electrolyte conditions, the corrosion rate and corrosion potential of the galvanic couple cannot be accurately measured. This is because the thickness of the electrolyte is too thin to form an effective water film above the silicone gasket during the experiment. The contact method of the reference electrode with the galvanic couple should be changed in further studies.

7 Reference

1. Isecke, B., M. Schütze, and H.-H. Strehblow, *Corrosion*, in *Springer Handbook of Metrology and Testing*, H. Czichos, T. Saito, and L. Smith, Editors. 2011, Springer Berlin Heidelberg: Berlin, Heidelberg. p. 667-741.
2. Ahmad, Z., *Principles of corrosion engineering and corrosion control*. 2006: Elsevier.
3. Syed, S., *Atmospheric corrosion of materials.* Emirates Journal for Engineering Research, 2006. **11**(1): p. 1-24.
4. Roberge, P.R., R.D. Klassen, and P.W. Haberecht, *Atmospheric corrosivity modeling — a review.* Materials & Design, 2002. **23**(3): p. 321-330.
5. Vernon, W. and W. Patterson, *The relation of the moisture in rust to the critical corrosion humidity. Discussion.* Transactions of The Faraday Society, 1931. **27**.
6. OGAWA, H., et al., *Auger Electron Spectroscopic and Electrochemical Analysis of the Effect of Alloying Elements on the Passivation Behavior of Stainless Steels.* Corrosion, 2013. **34**(2): p. 52-60.
7. Martinez-Lombardia, E., et al., *In Situ Scanning Tunneling Microscopy Study of Grain-Dependent Corrosion on Microcrystalline Copper.* The Journal of Physical Chemistry C, 2014. **118**(44): p. 25421-25428.
8. Fahlman, M., S. Jasty, and A.J. Epstein, *Corrosion protection of iron/steel by emeraldine base polyaniline: an X-ray photoelectron spectroscopy study.* Synthetic Metals, 1997. **85**(1): p. 1323-1326.
9. Thee, C., et al., *Atmospheric corrosion monitoring of a weathering steel under an electrolyte film in cyclic wet–dry condition.* Corrosion Science, 2014. **78**: p. 130-137.
10. Yadav, A.P., A. Nishikata, and T. Tsuru, *Degradation mechanism of galvanized steel in wet–dry cyclic environment containing chloride ions.* Corrosion Science, 2004. **46**(2): p. 361-376.
11. Leygraf, C., et al., *Atmospheric corrosion*. 2016: John Wiley & Sons.
12. Simillion, H., et al., *Atmospheric corrosion modeling.* Corrosion Reviews, 2014. **32**(3-4): p. 73-100.
13. Cai, Y., et al., *Influence of environmental factors on atmospheric corrosion in dynamic environment.* Corrosion Science, 2018. **137**: p. 163-175.
14. Castaño, J.G., D. de la Fuente, and M. Morcillo, *A laboratory study of the effect of NO2 on the atmospheric corrosion of zinc.* Atmospheric Environment, 2007. **41**(38): p. 8681-8696.
15. Shinohara, T., S.-i. Motoda, and W. Oshikawa, *Evaluation of Corrosivity in Atmospheric Environment by ACM (Atmospheric Corrosion Monitor) Type Corrosion Sensor.* Materials Science Forum, 2005. **475-479**: p. 61-64.
16. Wang, X., X. Li, and X.-l. Tian. *Influence of Temperature and Relative Humidity on the Atmospheric Corrosion of Zinc in Field Exposures and Laboratory Environments by Atmospheric Corrosion Monitor*. 2015.

17. LeBozec, N., et al., *Effect of carbon dioxide on the atmospheric corrosion of Zn–Mg–Al coated steel.* Corrosion Science, 2013. **74**: p. 379-386.
18. LeBozec, N., M. Jönsson, and D. Thierry, *Atmospheric Corrosion of Magnesium Alloys: Influence of Temperature, Relative Humidity.* Corrosion, 2004. **60**(04).
19. Lapuerta, S., et al., *The influence of relative humidity on iron corrosion under proton irradiation.* Journal of Nuclear Materials, 2008. **375**(1): p. 80-85.
20. Nyrkova, L., et al., *Investigation of the Atmospheric Corrosion of Carbon Steel under the Conditions of Formation of Adsorption and Phase Moisture Films.* Materials Science, 2013. **48**.
21. Cai, Y., et al., *Atmospheric corrosion prediction: a review.* Corrosion Reviews, 2020. **38**(4): p. 299-321.
22. Van den Steen, N., et al., *An integrated modeling approach for atmospheric corrosion in presence of a varying electrolyte film.* Electrochimica Acta, 2016. **187**: p. 714-723.
23. Kreislova, K. and D. Knotkova, *The Results of 45 Years of Atmospheric Corrosion Study in the Czech Republic.* Materials, 2017. **10**.
24. Walter, G., *Laboratory simulation of atmospheric corrosion by SO2—I. Apparatus, electrochemical techniques, example results.* Corrosion science, 1991. **32**(12): p. 1331-1352.
25. Cao, X., et al., *Electrochemical investigation on atmospheric corrosion of carbon steel under different environmental parameters.* Anti-Corrosion Methods and Materials, 2013.
26. Xian-long, C., et al., *Electrochemical investigation on atmospheric corrosion of carbon steel under different environmental parameters.* Anti-corrosion Methods and Materials, 2013. **60**: p. 199-205.
27. Lin, C.-C. and C.-X. Wang, *Correlation between accelerated corrosion tests and atmospheric corrosion tests on steel.* Journal of Applied Electrochemistry, 2005. **35**(9): p. 837-843.
28. Qu, Q., et al., *Effects of NaCl and SO2 on the initial atmospheric corrosion of zinc.* Corrosion Science, 2002. **44**(12): p. 2789-2803.
29. Allam, I., J. Arlow, and H. Saricimen, *Initial stages of atmospheric corrosion of steel in the Arabian Gulf.* Corrosion Science, 1991. **32**(4): p. 417-432.
30. Ma, Y., Y. Li, and F. Wang, *Corrosion of low carbon steel in atmospheric environments of different chloride content.* Corrosion Science, 2009. **51**(5): p. 997-1006.
31. Thierry, D., D. Persson, and N. Lebozec, *Atmospheric Corrosion of Zinc and Zinc Alloyed Coated Steel*. 2017.
32. Roberge, P.R., *Handbook of corrosion engineering*. 2019: McGraw-Hill Education.
33. Jacobson, M.Z., *Fundamentals of Atmospheric Modeling*. 2 ed. 2005, Cambridge: Cambridge University Press.
34. Lide, D.R., *CRC handbook of chemistry and physics*. Vol. 85. 2004: CRC press.

35. Gupta, D., et al., *Hygroscopic behavior of NaCl–MgCl 2 mixture particles as nascent sea-spray aerosol surrogates and observation of efflorescence during humidification.* Atmospheric Chemistry and Physics, 2015. **15**(19): p. 11273-11290.
36. Escobar, L.A. and W.Q. Meeker, *A Review of Accelerated Test Models.* Statist. Sci., 2006. **21**(4): p. 552-577.
37. Nguyen, M.N., X. Wang, and R.H. Leicester, *An assessment of climate change effects on atmospheric corrosion rates of steel structures.* Corrosion Engineering, Science and Technology, 2013. **48**(5): p. 359-369.
38. Lindström, R., J.-E. Svensson, and L.-G. Johansson, *The Atmospheric Corrosion of Zinc in the Presence of NaCl The Influence of Carbon Dioxide and Temperature.* Journal of The Electrochemical Society, 2000. **147**(5): p. 1751.
39. Cano, H., et al., *Effect of Cu, Cr and Ni alloying elements on mechanical properties and atmospheric corrosion resistance of weathering steels in marine atmospheres of different aggressivities.* Materials and Corrosion, 2018. **69**(1): p. 8-19.
40. Díaz, I., et al., *Five-year atmospheric corrosion of Cu, Cr and Ni weathering steels in a wide range of environments.* Corrosion Science, 2018. **141**: p. 146-157.
41. Liao, J. and M. Hotta, *Atmospheric corrosion behavior of field-exposed magnesium alloys: influences of chemical composition and microstructure.* Corrosion Science, 2015. **100**: p. 353-364.
42. de la Fuente, D., et al., *Long-term atmospheric corrosion of mild steel.* Corrosion Science, 2011. **53**(2): p. 604-617.
43. Kamimura, T., et al., *Mössbauer Spectroscopic Study of Rust Formed on a Weathering Steel and a Mild Steel Exposed for a Long Term in an Industrial Environment.* MATERIALS TRANSACTIONS, 2002. **43**(4): p. 694-703.
44. Leygraf, C., et al., *Atmospheric Corrosion, 2nd Edition.* 2000: p. 292.
45. Morcillo, M., et al., *Atmospheric corrosion of weathering steels. Overview for engineers. Part I: Basic concepts.* Construction and Building Materials, 2019. **213**: p. 723-737.
46. Boulton, L., N. Miller, and M. Sanders, *Atmospheric corrosion performance of welded stainless steels.* British Corrosion Journal, 1988. **23**(2): p. 117-121.
47. Alcántara, J., et al., *Marine atmospheric corrosion of carbon steel: a review.* Materials, 2017. **10**(4): p. 406.
48. Nishikata, A., et al., *Influence of Electrolyte Layer Thickness and pH on the Initial Stage of the Atmospheric Corrosion of Iron.* Journal of The Electrochemical Society, 1997. **144**(4): p. 1244-1252.
49. Cui, Z., et al., *Corrosion behavior of field-exposed zinc in a tropical marine atmosphere.* Corrosion, 2014. **70**(7): p. 731-748.
50. Liu, Y., et al., *Study on corrosion behavior of zinc exposed in coastal-industrial atmospheric environment.* Materials Chemistry and Physics, 2017. **198**: p. 243-249.

51. Prestat, M., et al., *Microstructure and spatial distribution of corrosion products anodically grown on zinc in chloride solutions.* Electrochemistry Communications, 2017. **81**: p. 56-60.
52. Thomas, S., I. Cole, and N. Birbilis, *Compact oxides formed on zinc during exposure to a single sea-water droplet.* Journal of The Electrochemical Society, 2012. **160**(2): p. C59.
53. Svensson, J.E. and L.G. Johansson, *A laboratory study of the initial stages of the atmospheric corrosion of zinc in the presence of NaCl; Influence of SO2 and NO2.* Corrosion Science, 1993. **34**(5): p. 721-740.
54. Falk, T., J.E. Svensson, and L.G. Johansson, *The Role of Carbon Dioxide in the Atmospheric Corrosion of Zinc: A Laboratory Study.* Journal of The Electrochemical Society, 1998. **145**(1): p. 39-44.
55. Falk, T., J.E. Svensson, and L.G. Johansson, *The Influence of CO 2 and NaCl on the Atmospheric Corrosion of Zinc: A Laboratory Study.* Journal of The Electrochemical Society, 1998. **145**(9): p. 2993-2999.
56. Persson, D., et al., *In situ infrared reflection spectroscopy studies of the initial atmospheric corrosion of Zn–Al–Mg coated steel.* Corrosion Science, 2013. **72**: p. 54-63.
57. Hosking, N.C., et al., *Corrosion resistance of zinc–magnesium coated steel.* Corrosion Science, 2007. **49**(9): p. 3669-3695.
58. Prosek, T., et al., *Corrosion mechanism of model zinc–magnesium alloys in atmospheric conditions.* Corrosion Science, 2008. **50**(8): p. 2216-2231.
59. Thierry, D., et al., *Atmospheric corrosion of ZnAlMg coated steel during long term atmospheric weathering at different worldwide exposure sites.* Corrosion Science, 2019. **148**: p. 338-354.
60. Somphotch, C., et al., *Corrosion Behavior of Zinc Covered with Native Oxides Under Thin Solution Films.* Corrosion, 2020. **76**(6): p. 562-569.
61. Cole, I.S., *Recent Progress and Required Developments in Atmospheric Corrosion of Galvanised Steel and Zinc.* Materials, 2017. **10**(11): p. 1288.
62. S Cramer, J.P.C.P.J.L.D.R.F., *Environmental Effects in the Atmospheric Corrosion of Zinc*

Degradation of Metals in the Atmosphere. 1987, West Conshohocken, PA: ASTM International. 247-1987.
63. STRATMANN, M. and H. STRECKEL, *ON THE ATMOSPHERIC CORROSION OF METALS WHICH ARE COVERED WITH THIN ELECTROLYTE LAYERS--I. VERIFICATION OF THE EXPERIMENTAL TECHNIQUE.* Corrosion Science, 1990. **30**(6-7): p. 681-696.
64. STRATMANN, M. and H. STRECKEL, *ON THE ATMOSPHERIC CORROSION OF METALS WHICH ARE COVERED WITH THIN ELECTROLYTE LAYERS--II. EXPERIMENTAL RESULTS.* Corrosion Science, 1990. **30**(6-7): p. 697-714.

65. Chung, K.-W. and K.-B. Kim, *A study of the effect of concentration build-up of electrolyte on the atmospheric corrosion of carbon steel during drying.* Corrosion Science, 2000. **42**(3): p. 517-531.
66. Koushik, B.G., et al., *Review on modelling of corrosion under droplet electrolyte for predicting atmospheric corrosion rate.* Journal of Materials Science & Technology, 2021. **62**: p. 254-267.
67. Li, S. and L.H. Hihara, *Atmospheric-Corrosion Electrochemistry of NaCl Droplets on Carbon Steel.* Journal of The Electrochemical Society, 2012. **159**(11): p. C461-C468.
68. Tait, W.S., *Chapter 5 - Electrochemical Corrosion Basics*, in *Handbook of Environmental Degradation of Materials (Third Edition)*, M. Kutz, Editor. 2018, William Andrew Publishing. p. 97-115.
69. Yamashita, M., et al., *The long term growth of the protective rust layer formed on weathering steel by atmospheric corrosion during a quarter of a century.* Corrosion Science, 1994. **36**(2): p. 283-299.
70. Nishimura, T., K.-i. Tanaka, and Y. Shimizu, *Effect of NaCl on rusting of steel in wet and dry corrosion cycle.* Tetsu-to-Hagane, 1995. **81**(11): p. 1079-1084.
71. Cheng, Y.L., et al., *A study of the corrosion of aluminum alloy 2024-T3 under thin electrolyte layers.* Corrosion Science, 2004. **46**(7): p. 1649-1667.
72. Huang, H., et al., *The effects of Cl− ion concentration and relative humidity on atmospheric corrosion behaviour of PCB-Cu under adsorbed thin electrolyte layer.* Corrosion Science, 2011. **53**(4): p. 1230-1236.
73. Tromans, D., *Modeling Oxygen Solubility in Water and Electrolyte Solutions.* Industrial & Engineering Chemistry Research, 2000. **39**(3): p. 805-812.
74. Schumpe, A., I. Adler, and W.D. Deckwer, *Solubility of oxygen in electrolyte solutions.* Biotechnology and Bioengineering, 1978. **20**(1): p. 145-150.
75. Millero, F.J., F. Huang, and A.L. Laferiere, *Solubility of oxygen in the major sea salts as a function of concentration and temperature.* Marine Chemistry, 2002. **78**(4): p. 217-230.
76. Pascual Marqui, R., *Influencia de la concentración de ion cloruro sobre la corrosión atmosférica de un acero al carbono bajo capa de fase de humedad. Rev.* Corros. Prot, 1980: p. 37-40.
77. Espada, L., et al., *Estudio de la velocidad de corrosión de aceros de bajo contenido de carbono en nieblas salinas de distinta concentración.* Rev. Iberoam. Corros. Prot, 1988. **19**: p. 227-229.
78. Zhao, C. and L. Xu, *Limiting current density in electrochemical micromachining.* Journal of Electrochemical Science and Engineering, 2018. **8**(4): p. 321-330.
79. Tomashov, N.D., *Development of the Electrochemical Theory of Metallic Corrosion.* Corrosion, 2013. **20**(1): p. 7t-14t.
80. Dubuisson, E., et al., *Study of the atmospheric corrosion of galvanised steel in a micrometric electrolytic droplet.* Electrochemistry Communications, 2006. **8**(6): p. 911-915.

81. Han, W., et al., *Characterisation of initial atmospheric corrosion carbon steels by field exposure and laboratory simulation.* Corrosion Science, 2007. **49**(7): p. 2920-2935.
82. Zhang, T., et al., *Corrosion of pure magnesium under thin electrolyte layers.* Electrochimica Acta, 2008. **53**(27): p. 7921-7931.
83. Kelly, R., et al., *Electrochemical Techniques in Corrosion Science and Engineering.* 2003.
84. Zhou, H.R., et al., *Dependence of the corrosion behavior of aluminum alloy 7075 on the thin electrolyte layers.* Materials Science and Engineering: B, 2009. **162**(1): p. 1-8.
85. Neufeld, A.K., et al., *The initiation mechanism of corrosion of zinc by sodium chloride particle deposition.* Corrosion Science, 2002. **44**(3): p. 555-572.
86. El-Mahdy, G.A., A. Nishikata, and T. Tsuru, *Electrochemical corrosion monitoring of galvanized steel under cyclic wet–dry conditions.* Corrosion Science, 2000. **42**(1): p. 183-194.
87. Liu, W., et al., *Corrosion behaviour of AM60 magnesium alloys containing Ce or La under thin electrolyte layers. Part 1: Microstructural characterization and electrochemical behaviour.* Corrosion Science, 2010. **52**(2): p. 627-638.

8 Annex

8.1 The assembling of LUNA corrosion cell

8.1.1 The set-up of LUNA cell for carbon steel/zinc atmospheric corrosion study under thin film electrolyte

The following figures showed the schematic diagrams of the different components in an assembled LUNA cell. The structure of the LUNA corrosion cell was very different from the bottom screw mount corrosion cell used in the bulk electrolyte corrosion study. By sequentially assembling plate electrodes and functional components on a stage consisting of four threaded rods and a square metal substrate, a multi-layer stacking corrosion cell was built up. This multi-layer stacking structure corrosion cell was assembled before each experiment run. The assembly process of LUNA cells will now be explained.

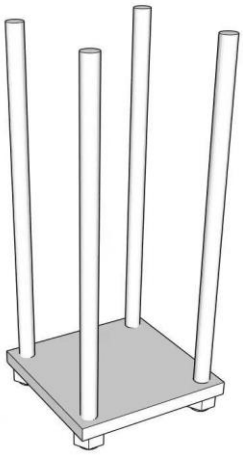

Figure A1. The schematic diagram of the base part of the LUNA cell. The metal base plate was slid over four threaded roads.

First, the base part was assembled. This part was mainly used to support the entire LUNA cell and isolate the corrosion cell from the plane on which it is placed. A 5.08cm*5.08cm squares SS316 metal plate was used as the base plate. Four acorn nuts were installed on the ends of four threaded rods which were inserted into the base plate. All further layers would be slid over on these four threaded rods above the base plate. A 5.08cm*5.08cm PTFE plate was placed on top of the metal base plate as the spacer.

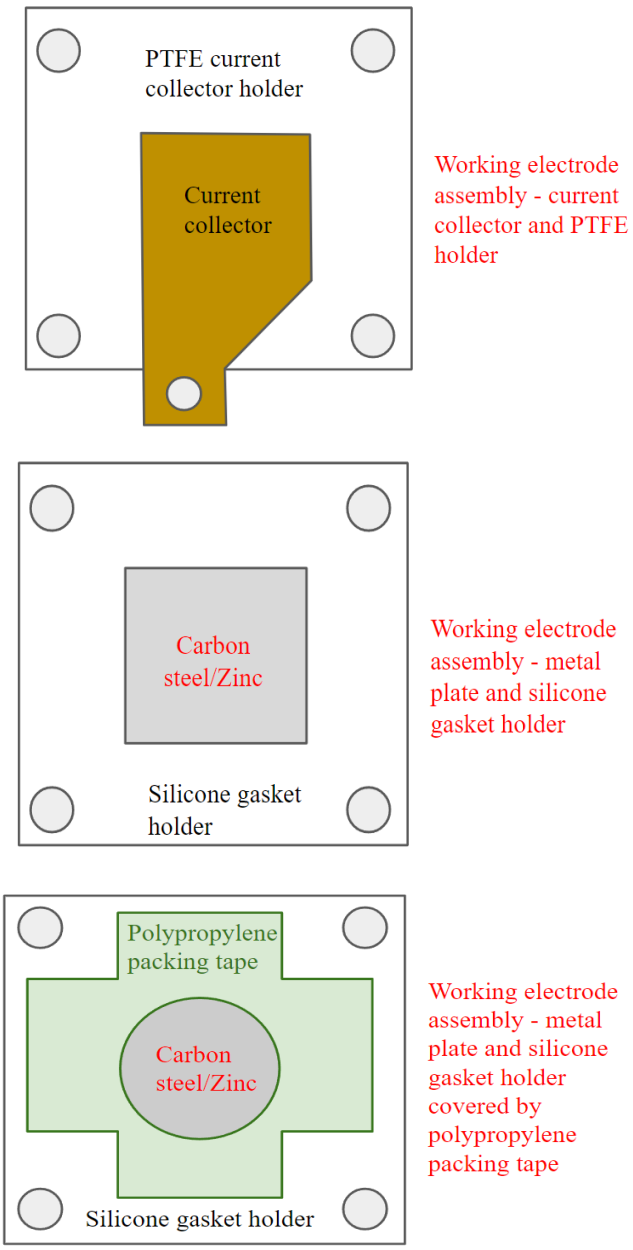

Figure A2. The schematic diagram of working electrode assembly consists of two-layer structures (above) current collector layer (the tab of the current collector will be connected to the alligator clip) and (middle and bottom) the specimen layer. The working electrode will be fixed to the silicone gasket holder with polypropylene packing tape.

Above the base part, the working electrode part of the LUNA cell was assembled next. Another 5.08cm*5.08cm PTFE plate was cut into a shape to fit the brass current collector. The PTFE holder was placed on top of the PTFE spacer and followed by the installation of the current collector into the holder. By controlling the dimensions of the engraved area on the PTFE, the PTFE current collector holder should be able to be tightly fixed to the current collector without external measures. The working electrode would be placed above the current collector layer. A 5.08cm*5.08cm silicone gasket was used as the holder of the working electrode. A 2.54cm*2.54cm hole was cut into the center of a silicone gasket as the place to install the working electrode. In order to

fix the working electrode with a silicon gasket and to control the exposed area of the working electrode, a hole with 2cm diameter was cut from the center of a piece of polypropylene packing tape (or tape of similar rigidity) and center the hole onto the working electrode of choice. The 2.54cm*2.54cm working electrode (carbon steel and zinc metal plate) was then fixed with the silicone gasket holder and the exposed area was controlled to 3.14 cm^2 due to the cover of polypropylene packing tape. It should be noted that the thickness of the silicone gasket holder should refer to the thickness of the working electrode. The top surface of the working electrode should be flush with the top of the selected silicone gasket (or slightly above the top of the gasket). When the working electrode assembly was confirmed, the working electrode assembly was slid along the threaded rods onto the assembled part of the LUNA cell. The bottom surface of the working electrode layer should be in direct contact with the upper surface of the current collector layer.

The layer above the working electrode was the membrane loaded with selected electrolytes. The selection and pre-treatment of the membrane will be mentioned later. The method used to load the electrolyte and control its volume will also be explained. Another thin silicone gasket was placed on the top of the working electrode as the holder of the membrane and the counter electrode, the side cut out should be facing away from the tab of the current collector. A 2.54cm*5.08cm rectangle counter electrode was placed on top of the membrane, the section extending out of the LUNA cell should be in the opposite direction from the tab of the current collector. The top surface of the counter electrode should be flush or slightly above the silicone gasket. Because the thickness of both membrane and the counter electrode is small, the silicone gasket with the lowest thickness was selected. On the side of the counter electrode overlying the working electrode, a hole was cut in the center to allow contact between the reference electrode with the working electrode. The selection and treatment of the counter electrode will also be mentioned later.

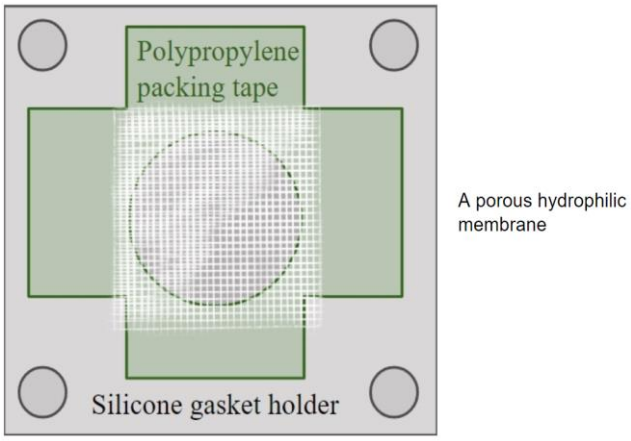

Figure A3. The schematic diagram of the hydrophilic membrane that is covered the top surface of the working electrode. The electrolyte will be loaded on the membrane to create a uniform thin film electrolyte.

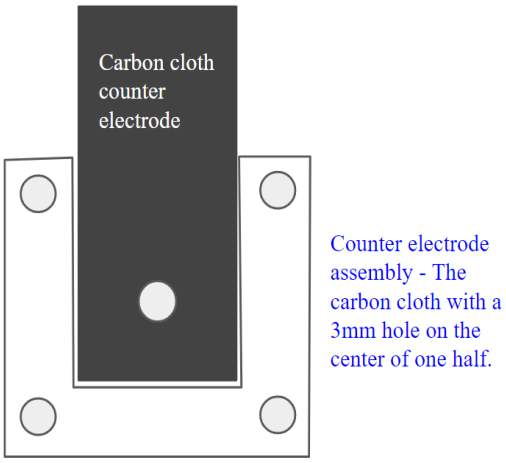

Figure A4. The schematic diagram of the counter electrode assembly. the section extending out of the LUNA cell is in the opposite direction from the tab of the current collector.

The components used to pressurize the contact between the electrodes were then assembled on top of the hydrophilic membrane and the counter electrode layer. A 5.08cm*5.08cm fine plastic mesh was placed above the counter electrode through a slide over the threaded rods. A hole with a 3mm diameter was cut in the center of the fine plastic mesh. It should be made sure that the hole on the fine plastic mesh is centered over the hole on the counter electrode. A coarse plastic mesh was placed above the fine plastic mesh with a hole also cut in the center. The diameter of the hole on the coarse plastic mesh should be slightly larger than the hole on the fine plastic mesh and the counter electrode. The purpose of these two layers of plastic mesh was to apply a uniform compression across the back of the counter electrode. In this way, oxygen in the atmosphere can be transported to the electrolyte and the working electrode through the porous structure of the counter electrode.

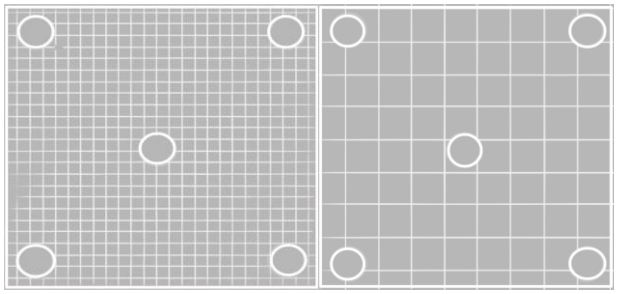

Figure A5. The schematic diagram of the (a) fine plastic mesh and (b) coarse plastic mesh used to apply the uniform compression across the back of the counter electrode.

The first polycarbonate bracket was placed on the coarse plastic mesh. Four bic pen type spacers were slipped over the first polycarbonate bracket, and the second polycarbonate bracket was placed on top of the four bic pen type spacers. The three-layer structure was used to create a stand with a certain height to allow the standing of the reference electrode with the bridge tube. The reference electrode with the bridge tube was placed in the center hole of the polycarbonate bracket, standing vertically

above the multi-layer structure. The probe tip of the bridge tube was touched with the electrolyte and the working electrode through the hole cut on the plastic meshes and counter electrode. The selection of the reference electrode and the role of the bridge tubed will be explained later.
After confirming all layer structure was assembled appropriately, four wing nuts were tightened onto four threaded rods. Over-tightening should be avoided as this may result in over-squeezing of the electrolyte-saturated membrane. The alligator clips were respectively connected to the tab of the current collector (working electrode), the extended out end of the counter electrode and the reference electrode. After checking that the alligator clips were properly connected, the following electrochemical measurements can be performed on the potentiostat and the specialized software.

8.1.2 The selection of electrodes for LUNA cell

The reference electrode was designed to provide a stable referent potential to help accurately measure the potential applied to the working electrode. The appropriate reference electrode selection was depended on the intended environment, cell structure and temperature. Considering both electrolyte chemical properties and the size of the LUNA cell, a small Re-S1 Ag/AgCl reference electrode (52 mm length and 4.5 mm outside diameter) was used in thin film electrolyte experiments at room temperature (25 °C). A bridge tube with a 9.0mm outer diameter was used to connect the reference electrode and the membrane loaded with electrolytes. The bridge tube was filled with the aqueous solution with the same composition and concentration as the membrane electrolyte to ensure it is isotonic with the membrane. The contacting-membrane side of the bridge tube was covered by a 2.8mm wide Coralpor 1000 tip, with a 4-10 nm average pore diameter, to minimize the leakage of electrolyte from the bridge tube.

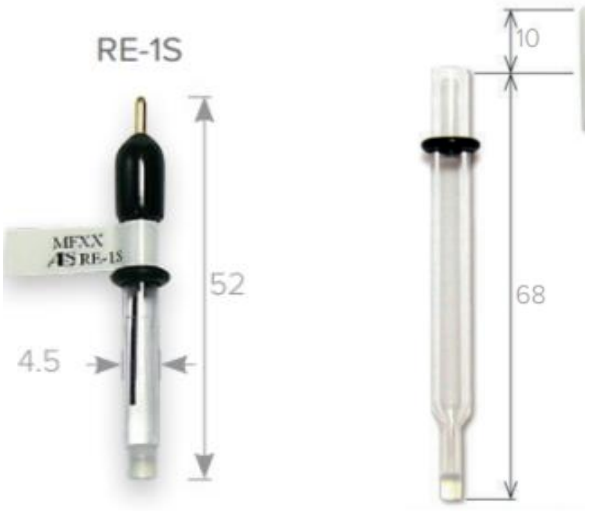

Figure A6. The small Re-S1 Ag/AgCl reference electrode and the bridge tube were used in LUNA cell experiments. In the experiment, the reference electrode was placed into the bridge tube which had already been filled with the same electrolyte loaded on the membrane. The tip of the bridge tube was passed through the hole to contact the electrodes.

The counter electrode was used to provide the applied current thereby inducing the occurrence of corrosion and other electrochemical reactions. The corrosion of the counter electrode itself might undergo since it provides all current in the system during the electrochemical experiment, therefore, a highly corrosion resistant/inert material was generally used. A common counter electrode selection was platinum metal mesh, while in this thin film electrolyte atmospheric corrosion experiments, woven carbon fiber cloth was used as the counter electrode material. A Nafion Post Coat was applied to improve the water resistance and adhesion to the membrane. The carbon cloth could establish high-density contact points with the electrolyte membrane and promotes both the cathodic and the anodic reaction. The advantages of using carbon cloth as the counter electrode include good air permeability, conductivity and inexpensiveness. Corrosion of the counter electrodes during the electrochemical experiments can significantly alter the electrolyte chemical properties, complicating and potentially ineffective the measurements. The low cost of the carbon cloth facilitates the non-reuse of the counter electrode to ensure the best performance and repeatability in the experiments. In general, the size of the counter electrode should be proportional to the amount of current it is intended to provide, usually equal to or larger than the size of the working electrode. The typical counter electrode size in this study was a 2.54cm*5.08cm rectangle, which is completely covered on the 2.54cm*2.54cm square membrane and extended out from one side of the cell to connect with the potentiostats through a steel alligator clip. A 3 mm diameter hole was cut into the center of the 2.54cm*2.54cm side which covers the working electrode. The hole was used to allow direct contact between the bridge tube tip (with reference electrode) and the membrane.

*Figure A7. The 0.03 mg/cm² 20% Platinum on Vulcan - carbon cloth counter electrode was used in LUNA cell experiments. The carbon cloth was cut into 2.54cm*5.08cm rectangles size with a hole for electrodes contact.*

8.1.3 The pre-treatment of membranes and electrolyte loading methods

A highly porous hydrophilic membrane was covered on the surface of the working electrode to control the formation of a thin film aqueous electrolyte. The atmospheric electrolyte membrane used in the LUNA cell is based on a woven glass fiber fabric. The fiberglass fabric was pre-treated with 50% w/v NaOH for 1 hour at room temperature and then soaked in deionized water several times to remove residual NaOH contamination. This pre-treatment was mainly to increase the hydrophilicity of the membrane.

Because the surface tension of the aqueous electrolyte would be broken by the hydrophilic membrane, the electrolyte could be evenly distributed on the surface to form a thin film with a thickness above 30μm. A micropipette was used to dispense a specific volume of a known amount of corrosive electrolyte on the hydrophilic membrane. The dry hydrophobic membrane was laid on top of the working electrode in advance instead of applying the electrolyte droplets before placing the membrane can ensure the uniform distribution of the electrolyte thin film to the greatest extent. The thin film electrolyte with a specific thickness could be created by controlling both the dimensions and thickness of the membranes. One typical setting for an atmospheric corrosion experiment was to use an 80μm membrane loaded with a 4μL/cm^2 aqueous solution. The volume of the loading solution in this setup approximately corresponds to a 40μm thick electrolyte membrane. The electrolyte should fully and evenly wet the entire membrane also the area over the tape-masked off portions of the working electrode.

In this study, 26μL aqueous solution was loaded on each 80μm thick 2.54cm*2.54cm hydrophilic membrane to form a 40μm-thick thin film electrolyte. By stacking the

hydrophilic membrane, a thicker electrolyte film could reach up to 320μm. Four 80μm thick hydrophilic membranes were stacked on each other for experiments in 160μm electrolyte, and eight membranes were used for 320μm electrolyte experiments. For the experiments of these two thicknesses settings, the volume of the electrolyte loaded was changed to 104μL and 208μL. The size of the pores on membranes was relatively larger compared to the size of oxygen molecules, oxygen could still reach the metal surface through the stacked membranes and participate in the reaction.

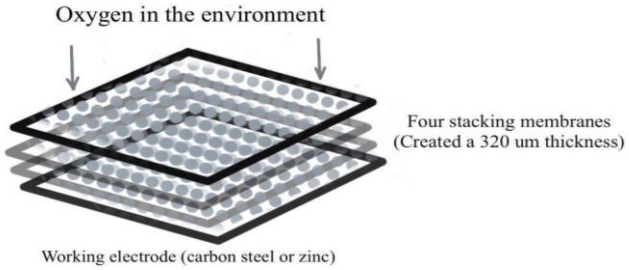

Figure A8. The schematic diagram of the stacked four membranes. A thick membrane was created to support a 160μm thick electrolyte.

8.1.4 LUNA cell - the set-up for carbon steel-zinc galvanic coupling study under thin film electrolyte

A 5.08cm*5.08cm PTFE plate was cut into a shape to fit the carbon steel specimen and zinc specimen together. It should be noted that the exposed areas of carbon steel and zinc specimens placed on the PTFE plate need to be consistent with each other. This could be achieved by adjusting the rectangular cutouts carved into the PTFE and covering the unwanted area with polypropylene packing tape. To avoid direct contact, the sides of carbon steel and zinc specimens were separated by insulation. In this study, the insulating property of PTFE itself was used to separate two specimens with a one-millimeter gap.

The current collector layer and counter electrode assembly were no longer necessary in the LUNA cell. Instead, two copper tapes were attached to both carbon steel and zinc which will be connected to the counter electrode alligator clip and working electrode alligator clip respectively. The assembled electrode layer was placed just above the PTFE spacer at the base part. The treated hydrophilic membrane was placed just above the electrode layer, covering both carbon steel and zinc specimens. A silicon gasket could be used as the holder to restrict the potential movement of the hydrophilic membrane during the experiments. The shape of the silicon gasket holder shape could be referred to in the schematic diagram in figure 11. Since the thickness of the hydrophilic membrane was very thin, the contact between the electrodes should be considered when choosing the appropriate thickness of the silicone gasket. The fine

plastic mesh and coarse plastic mesh were directly placed on the top of the hydrophilic membrane and then followed by the first polycarbonate bracket, bic pen type spacers and second polycarbonate bracket. The selection and placement of the reference electrode were set to be the same as in the previous experimental setup.

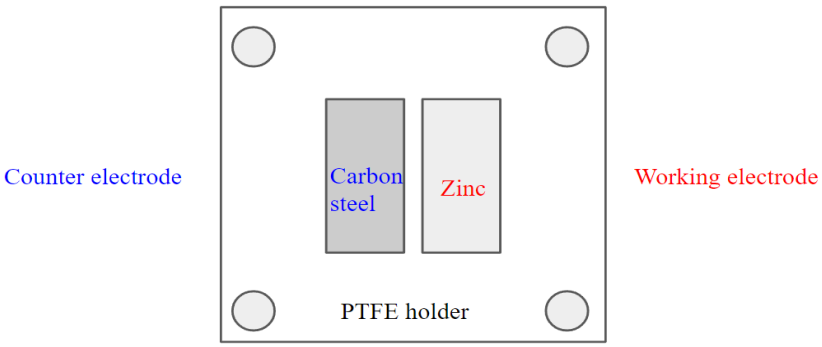

Figure A9. The schematic diagram of the electrodes assembly used in galvanic coupling experiments. The carbon steel metal plate will be connected as the counter electrode and zinc will be connected as the working electrode. The exposure area of the two electrodes should be controlled to the same size.

8.2 Experimental results

8.2.1 Carbon steel

8.2.1.1 Bulk electrolyte experiments

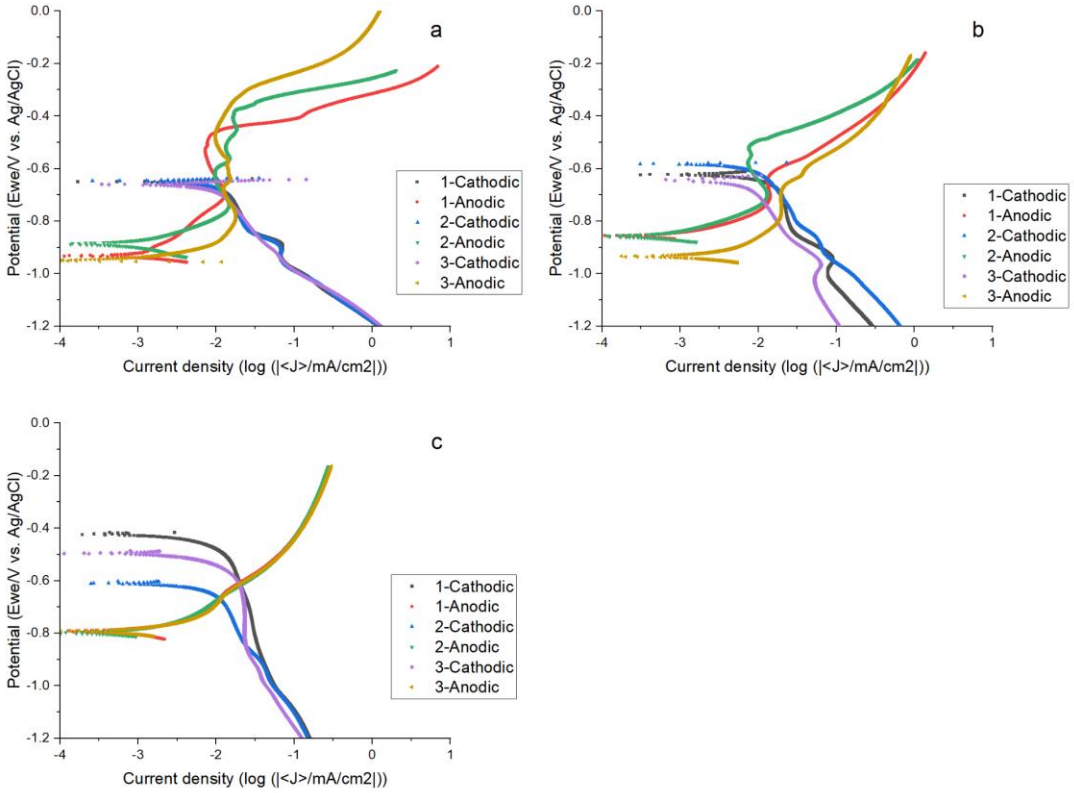

Figure A10. The polarization curves of carbon steel in (a) 1.0M, (b) 0.1M and (c) 0.01M NaCl when the electrolyte is a bulk solution. The anodic and cathodic branches are polarized separately.

Table A1. The corrosion potential and corrosion rate of carbon steel under 1.0M NaCl bulk electrolyte.

	β_a (mV)	β_c (mV)	Corrosion potential (mV)	Current density ($\mu A/cm^2$)	Limiting current density ($\mu A/cm^2$)
1	/	122.3	-951.9	9.5	NaN
2	/	111.8	-940.9	9.9	NaN
3	/	111.8	-918.4	8.5	NaN
Average	/	115.3	-937.1	9.3	NaN
Standard Deviation	/	6.1	17.1	0.7	NaN

Table A2. The corrosion potential and corrosion rate of carbon steel under 0.1M NaCl bulk electrolyte.

	β_a (mV)	β_c (mV)	Corrosion potential (mV)	Current density ($\mu A/cm^2$)	Limiting current density ($\mu A/cm^2$)
1	/	135.6	-866.4	4.2	NaN
2	/	148.7	-905.5	8.4	NaN
3	/	139.4	-896.2	8.5	NaN
Average	/	141.1	-889.3	6.7	NaN
Standard Deviation	/	6.7	20.4	2.5	NaN

Table A3. The corrosion potential and corrosion rate of carbon steel under 0.01M NaCl bulk electrolyte.

	β_a (mV)	β_c (mV)	Corrosion potential (mV)	Current density ($\mu A/cm^2$)	Limiting current density ($\mu A/cm^2$)
1	2212	188	-800	2.8	15.4
2	195	214	-782	2.9	13.9
3	247	176	-811	2.9	20.9
Average	221	193	-798	2.9	16.7
Standard Deviation	26	19	15	0.0	3.7

8.2.1.2 Thin-film electrolyte experiments

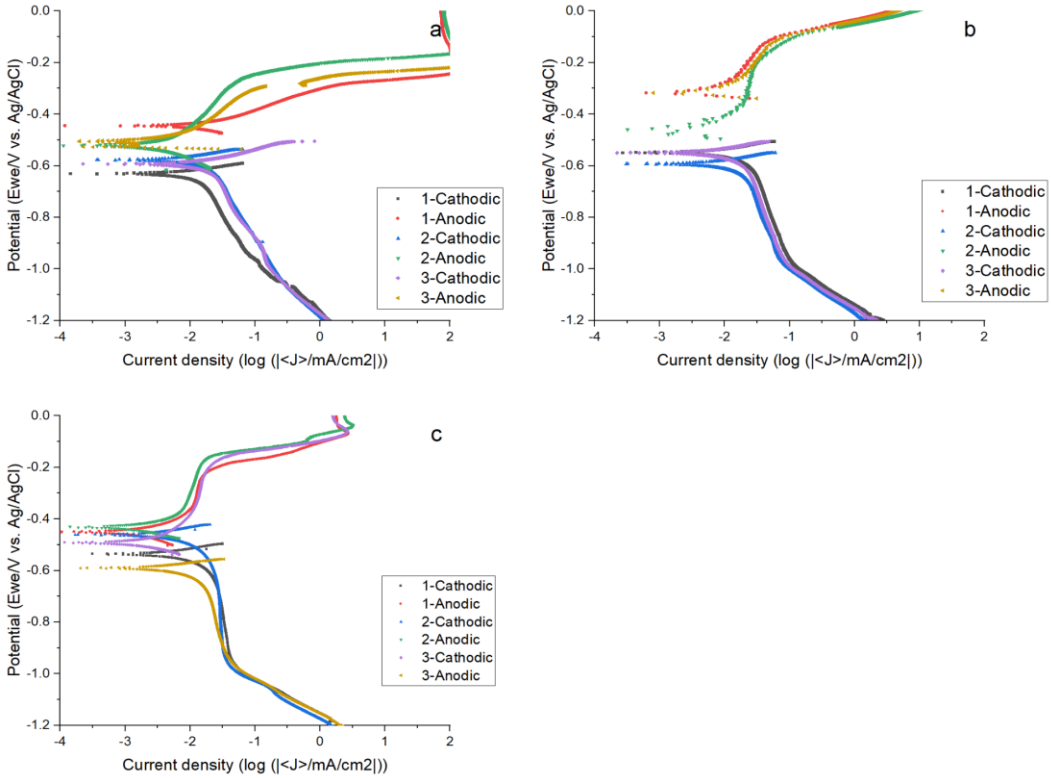

Figure A11. The anodic and cathodic polarization curves of carbon steel in (a) 1.0M, (b) 0.1M and (c) 0.01M NaCl when the electrolyte thickness is 320μm. The anodic and cathodic branches are polarized separately.

Table A4. The corrosion potential and corrosion rate of carbon steel in 320μm 1.0M NaCl electrolyte.

	β_a (mV)	β_c (mV)	Corrosion potential (mV)	Current density ($\mu A/cm^2$)	Limiting current density ($\mu A/cm^2$)
1	81	367	-492	5.4	26.5
2	199	407	-438	8.2	31.6
3	158	402	-465	8.7	32.4
Average	146	392	-465	7.4	30.2
Standard Deviation	60	22	27	1.8	3.2

Table A5. The corrosion potential and corrosion rate of carbon steel in 320μm 0.1M NaCl electrolyte.

	β_a (mV)	β_c (mV)	Corrosion potential (mV)	Current density ($\mu A/cm^2$)	Limiting current density ($\mu A/cm^2$)
1	212	/	-268	9.2	33.1
2	236	/	-385	8.9	27.5
3	200	/	-330	8.7	37.2
Average	216	/	-328	8.9	32.6
Standard Deviation	18	/	59	0.3	4.9

Table A6. The corrosion potential and corrosion rate of carbon steel in 320μm 0.01M NaCl electrolyte.

	βa (mV)	βc (mV)	Corrosion potential (mV)	Current density ($\mu A/cm^2$)	Limiting current density ($\mu A/cm^2$)
1	/	/	-262	14.8	37.2
2	/	/	-239	13.5	31.6
3	/	/	-366	9.1	26.9
Average	/	/	-289	12.5	31.9
Standard Deviation	/	/	68	3.0	5.2

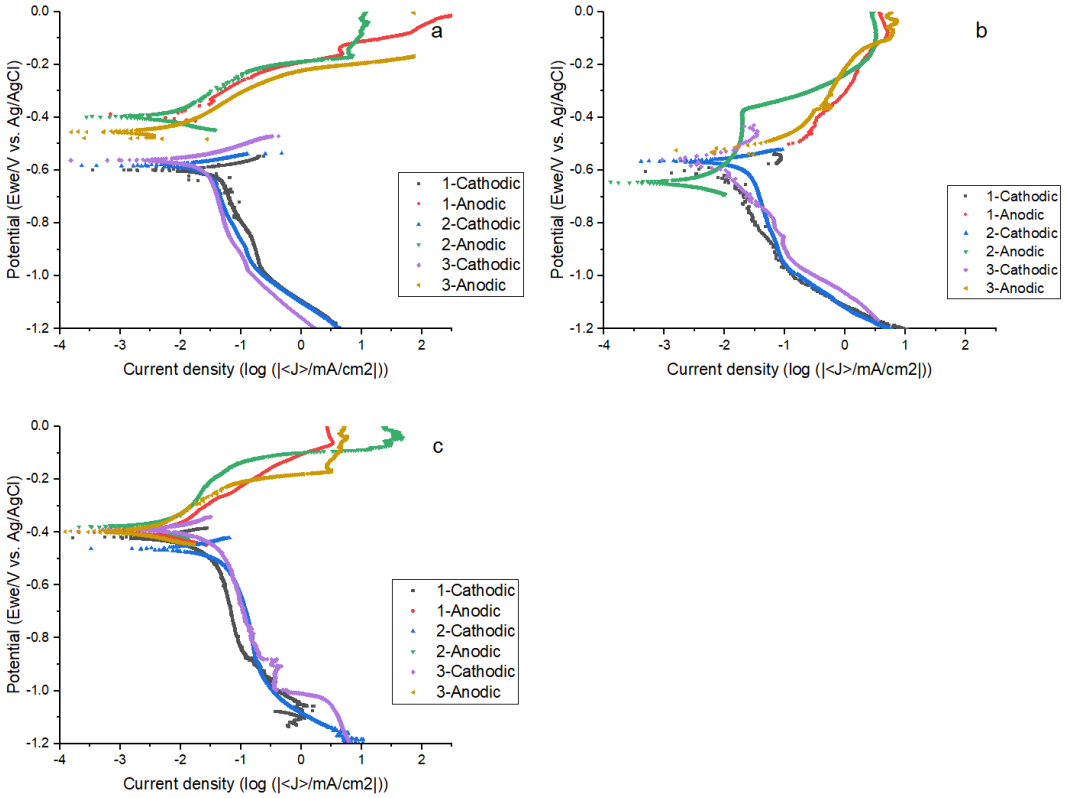

Figure A12. The anodic and cathodic polarization curves of carbon steel in (a) 1.0M, (b) 0.1M and (c) 0.01M NaCl when the electrolyte thickness is 160μm. The anodic and cathodic branches are polarized separately.

Table A7. The corrosion potential and corrosion rate of carbon steel in 160μm 1.0M NaCl electrolyte.

	β_a (mV)	β_c (mV)	Corrosion potential (mV)	Current density (μA/cm^2)	Limiting current density (μA/cm^2)
1	135	/	-385	14.8	49.0
2	104	/	-416	10.6	39.8
3	123	/	-421	12.3	50.1
Average	121	/	-407	12.6	46.3
Standard Deviation	15	/	19	2.1	5.7

Table A8. The corrosion potential and corrosion rate of carbon steel in 160μm 0.1M NaCl electrolyte.

	β_a (mV)	β_c (mV)	Corrosion potential (mV)	Current density ($\mu A/cm^2$)	Limiting current density ($\mu A/cm^2$)
1	313	377	-571	17.2	67.6
2	181	645	-536	17.5	51.9
3	328	395	-559	20.9	66.1
Average	274	472	-555	18.5	61.9
Standard Deviation	81	150	18	2.1	8.7

Table A9. The corrosion potential and corrosion rate of carbon steel in 160μm 0.01M NaCl electrolyte.

	β_a (mV)	β_c (mV)	Corrosion potential (mV)	Current density ($\mu A/cm^2$)	Limiting current density ($\mu A/cm^2$)
1	130	810	-309	22.7	68.5
2	166	754	-223	28.2	112.9
3	104	703	-270	26.3	106.8
Average	133	756	-267	25.7	96.1
Standard Deviation	31	54	43	2.8	24.1

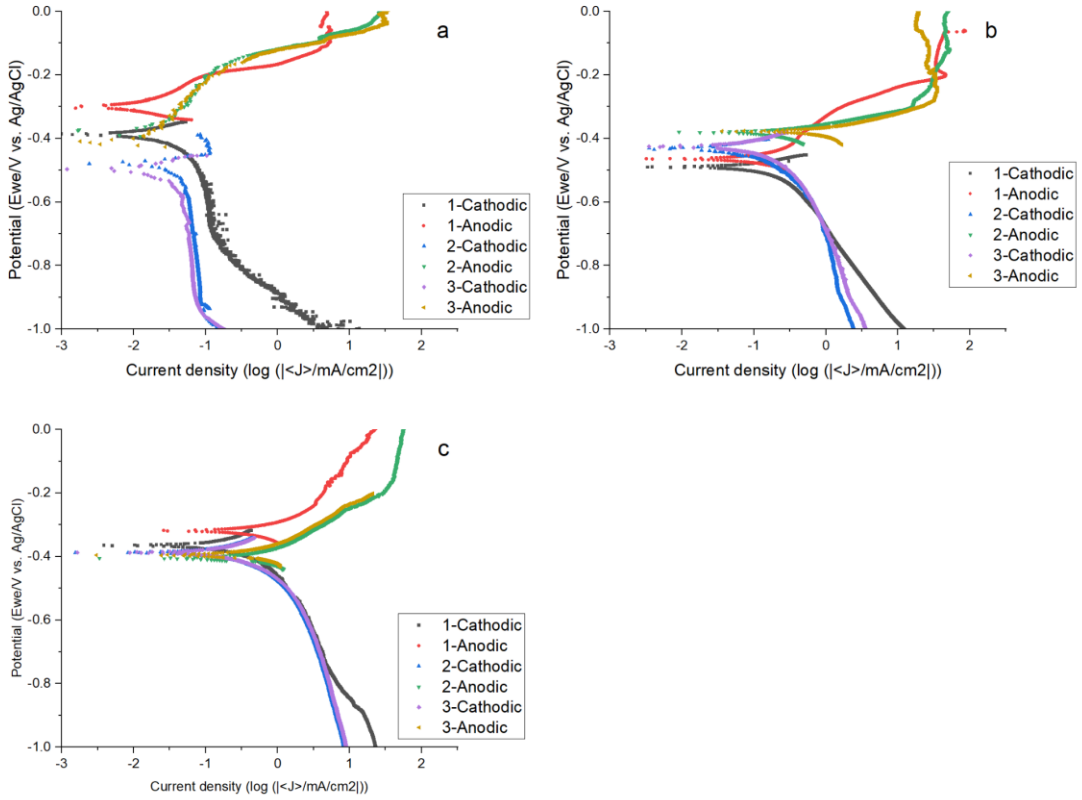

Figure A13. The anodic and cathodic polarization curves of carbon steel in (a) 1.0M, (b) 0.1M and (c) 0.01M NaCl when the electrolyte thickness is 40μm. The anodic and cathodic branches are polarized separately.

Table A10. The corrosion potential and corrosion rate of carbon steel in 40μm 1.0M NaCl electrolyte.

	β_a (mV)	β_c (mV)	Corrosion potential (mV)	Current density (μA/cm^2)	Limiting current density (μA/cm^2)
1	77	/	-329	54.1	107.2
2	190	/	-305	43.9	79.4
3	164	/	-314	37.2	63.1
Average	143	/	-316	45.1	83.2
Standard Deviation	59	/	12	8.5	22.3

Table A11. The corrosion potential and corrosion rate of carbon steel in 40μm 0.1M NaCl electrolyte.

	β_a (mV)	β_c (mV)	Corrosion potential (mV)	Current density ($\mu A/cm^2$)	Limiting current density ($\mu A/cm^2$)
1	125	319	-442	190.5	NaN
2	43	584	-383	249.5	1273.5
3	67	479	-381	261.0	1256.0
Average	78	461	-402	233.7	1264.8
Standard Deviation	42	133	35	37.8	12.4

Table A12. The corrosion potential and corrosion rate of carbon steel in 40μm 0.01M NaCl electrolyte.

	β_a (mV)	β_c (mV)	Corrosion potential (mV)	Current density ($\mu A/cm^2$)	Limiting current density ($\mu A/cm^2$)
1	274	441	-414	880.7	4079.2
2	126	493	-379	783.0	4390.5
3	124	503	-377	776.2	4466.8
Average	175	479	-390	813.3	4312.2
Standard Deviation	86	33	21	58.5	205.4

8.2.2 Zinc

8.2.2.1 Bulk electrolyte experiments

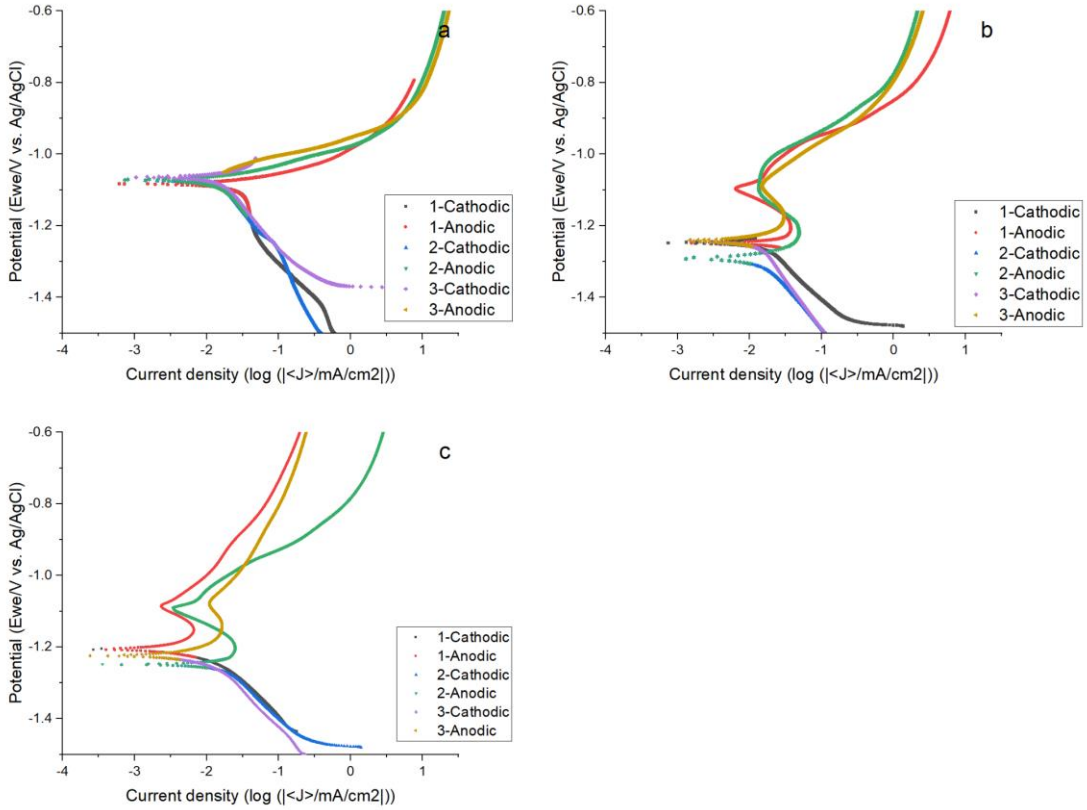

Figure A14. The polarization curves of zinc in (a) 1.0M, (b) 0.1M and (c) 0.01M NaCl when the electrolyte is bulk solution. The anodic and cathodic branches are polarized separately.

Table A13. The corrosion potential and corrosion rate of zinc under 1.0M NaCl bulk electrolyte.

	βa (mV)	βc (mV)	Corrosion potential (mV)	Current density ($\mu A/cm^2$)	Limiting current density ($\mu A/cm^2$)
1	110	253	-1154	27.3	NaN
2	116	332	-1096	25.1	NaN
3	87	320	-1108	27.8	NaN
Average	104	301	-1119	26.7	NaN
Standard Deviation	15	35	25	1.2	NaN

Table A14. The corrosion potential and corrosion rate of zinc steel under 0.1M NaCl bulk electrolyte.

	βa (mV)	βc (mV)	Corrosion potential (mV)	Current density ($\mu A/cm^2$)	Limiting current density ($\mu A/cm^2$)
1	/	266	-1201	8.4	NaN
2	/	239	-1234	8.7	NaN
3	/	179	-1155	12.5	NaN
Average	/	225	-1197	9.7	NaN
Standard Deviation	/	36	32	1.9	NaN

Table A15. The corrosion potential and corrosion rate of zinc under 0.01M NaCl bulk electrolyte.

	βa (mV)	βc (mV)	Corrosion potential (mV)	Current density ($\mu A/cm^2$)	Limiting current density ($\mu A/cm^2$)
1	/	199	-1097	3.3	NaN
2	/	184	-1158	5.0	NaN
3	/	208	-1172	6.0	NaN
Average	/	197	-1142	4.8	NaN
Standard Deviation	/	10	33	1.1	NaN

8.2.2.2 Thin-film electrolyte experiments

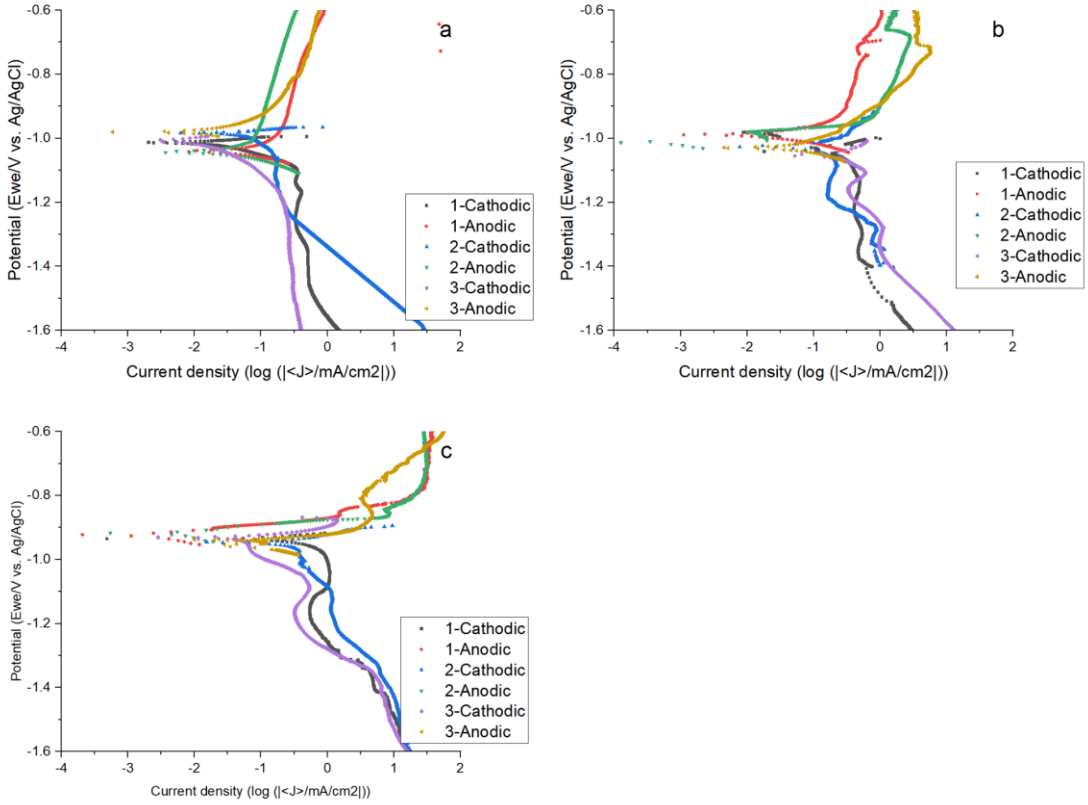

Figure A15. The anodic and cathodic polarization curves of zinc in (a) 1.0M, (b) 0.1M and (c) 0.01M NaCl when the electrolyte thickness is 40μm. The anodic and cathodic branches are polarized separately.

Table A16. The corrosion potential and corrosion rate of zinc in 40μm 1.0M NaCl electrolyte.

	βa (mV)	βc (mV)	Corrosion potential (mV)	Current density (μA/cm^2)	Limiting Current density (μA/cm^2)
1	594	1038	-984	213.3	338.8
2	667	814	-999	105.9	213.8
3	512	1119	-972	119.9	269.2
Average	631	926	-991	159.6	276.3
Standard Deviation	51	158	11	75.9	88.4

Table A17. The corrosion potential and corrosion rate of zinc in 40μm 0.1M NaCl electrolyte.

	βa (mV)	βc (mV)	Corrosion potential (mV)	Current density ($\mu A/cm^2$)	Limiting Current density ($\mu A/cm^2$)
1	445	766	-951	263.0	457.1
2	414	484	-1065	257.0	346.7
3	273	495	-991	223.7	501.2
Average	377	581	-1002	247.9	435.0
Standard Deviation	92	160	58	21.2	79.6

Table A18. The corrosion potential and corrosion rate of zinc in 40μm 0.01M NaCl electrolyte.

	βa (mV)	βc (mV)	Corrosion potential (mV)	Current density ($\mu A/cm^2$)	Limiting Current density ($\mu A/cm^2$)
1	61	529	-924	378.9	822.2
2	102	498	-928	413.9	1122.0
3	159	406	-916	296.8	524.8
Average	107	478	-923	363.2	823.0
Standard Deviation	50	64.	6	60.1	298.6